Master Thesis in Geosciences

Palaeogene depositional environments of the Frysjaodden and Hollendardalen formations in central Spitsbergen

Florin Burcă

UNIVERSITY OF OSLO

FACULTY OF MATHEMATICS AND NATURAL SCIENCES

Palaeogene depositional environments of the Frysjaodden and Hollendardalen formations in central Spitsbergen

Florin Burcă

Master Thesis in Geosciences

Discipline: Petroleum Geology and Geophysics

Department of Geosciences

Faculty of Mathematics and Natural Sciences

UNIVERSITY OF OSLO

June, 1st, 2008

ABSTRACT

The current study reveals the transgressive-regressive sequences and depositional environments of Paleogene Frysjaodden and Hollendardalen formations recorded in the Central Tertiary Basin of Spitsbergen. In addition, the most rapid and significant climatic perturbation of the Cenozoic era, known as PETM (Paleocene-Eocene Thermal Maximum) is discussed using mineralogical data. The paleoenvironment has been reconstructed using a combination of sedimentary field data, XRD, micropaleontology and detailed analyses of clay minerals.

The results display a shallowing upward succession developing from offshore shales into a distinct offshore-transition zone with storm-generated sand beds including hummocky cross stratification and fragments of fossil wood. The succeeding sediments reveal shoreface and foreshore deposits characterized by low angle cross stratified sandstones. The upper most part of the section is interpreted as beach-ridge strandplains with coal seams and roots structures in an inferred lagoonal or marsh setting.

Key words: lithofacies, sedimentology, Paleogene, PETM, Svalbard, XRD, thin sections, clay minerals

TABLE OF CONTENT

1 INTRODUCTION

This master thesis constitutes part of an international project (pACE - http://www.wun.ac.uk/pACE/index.html), where scientists and students from seven different Universities analyze the Paleocene and Eocene beds of Svalbard. The main purpose of the project is to offer a better understanding of the dramatic climatic changes which took place during Paleogene. Of particular interest is the Palaeocene/Eocene Thermal Maximum (PETM). The project started in august 2007 and so far data from outcrops and cores have been collected and analyzed by using palynological, biostratigraphycal, geochemical and mineralogical methods.

The University of Oslo contribution presently mainly focuses on sedimentological, stratigraphical, mineralogical and micropalaeontological analysis of the shallow marine to deltaic facies which are represented by the Frysjaodden and Hollendardalen formations.

The field work was carried out August 2007 in cooperation with master student Denise Rüther, supervised by professors Henning Dypvik and Jenö Nagy in the Nordenskiöldfjellet localities, circa 5 km south-east of Longyearbyen (Figure 1-1).

The primary goal of this thesis is constituted by the integration of detailed sedimentary logs, mineralogical data and natural gamma radiation measurements in the attempt of reconstructing depositional environments. XRD analysis and optical petrography were the main laboratory methods used. In addition results from field measurements of natural gamma ray radiation are included. Secondly, the results from clay mineralogical analysis were applied with particular respect to possible climatic discussions of Paleocene-Eocene series.

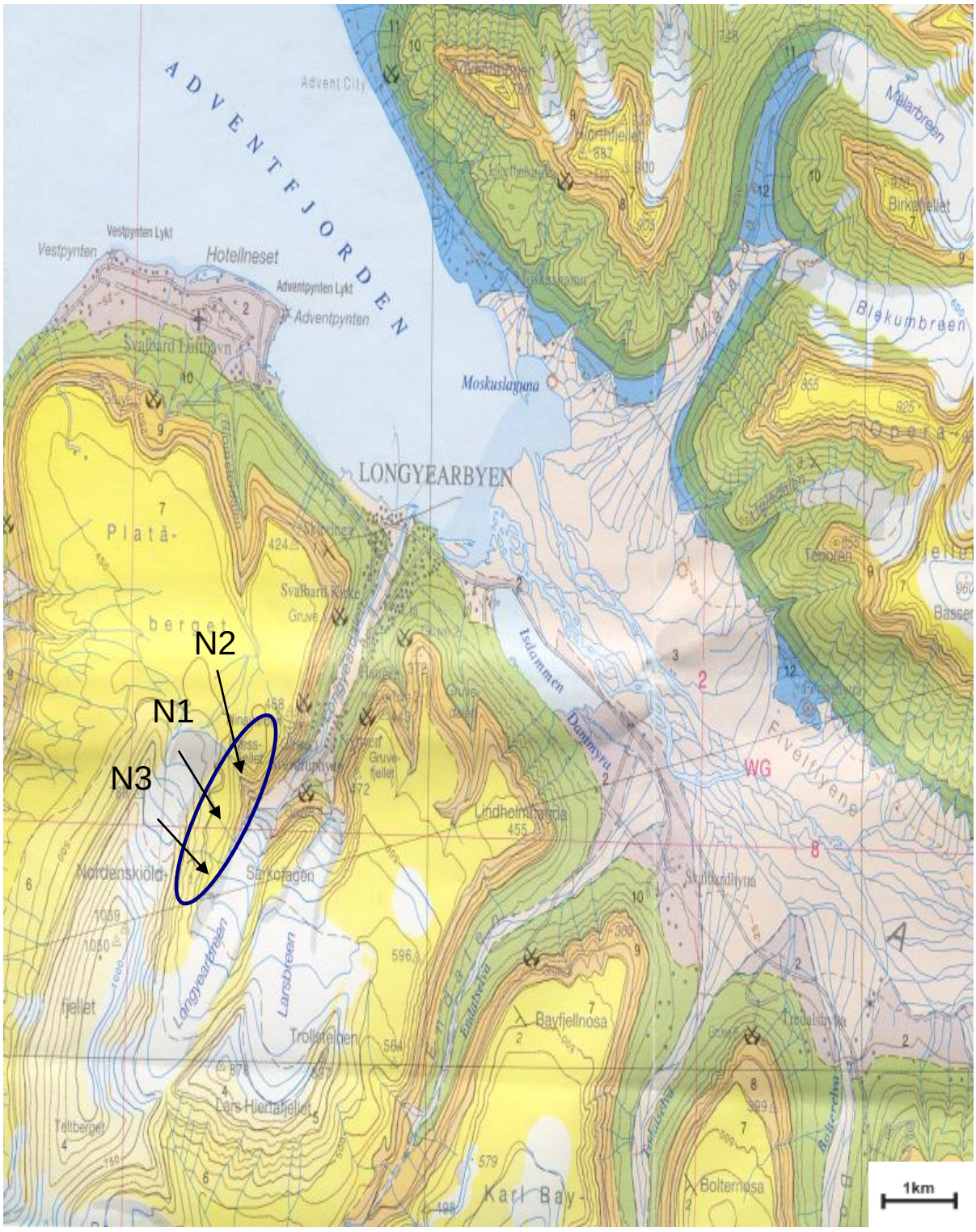

Figure 1-1: Location of outcrops N2, N1 and N3 in Adventalen area, Spitsbergen. Modified from Dallmann et al. (2001).

2 GEOLOGICAL BACKGROUND

The studied formations are located within the Palaeogene Central Basin successions of Spitsbergen and according to Dallmann et al. (1999) belong to the Van Mijenfjorden Group (Figure 2.4). This chapter summarizes several published theories regarding genesis and evolution of Central Tertiary Basin and presents the lithostratigraphical setting of the studied section. The PETM (Paleocene-Eocene Thermal Maximum) subchapter is presented at the end of this chapter.

2.1. REGIONAL SETTING

The occurrence of sedimentary basins and an orogenic mountain chain of Tertiary age in Spitsbergen have been subject of many discussions in the last decades. Harland (1969) was among the first to suggest a relation between 'West Spitsbergen orogeny' and large-scale transcurrent movement between Greenland and Eurasia.

Talwani and Eldholm (1977) proposed a model for an opening of the Norwegian-Greenland Sea and of the north-eastern Atlantic region based on the sea-floor magnetic anomalies and the major structural elements. They identified two distinct phases of tectonic development: 1) north northwesterly motion of Greenland from Euroasia which produced a strike slip regime from latest Paleocene to early Eocene and 2) west northwesterly plate movement from early Oligocene to present which create a rift regime, off western Svalbard. The Paleogene transform boundary has been called the De Geer Line (Harland, 1969), whereas the later plate boundary has been named Hornsund fault zone (Myhre et al., 1982). According to Myhre et al. (1982) the Hornsund fault zone is located at or near the continent-ocean boundary.

Hinz and Schlüter (1979) identified a series of deep basins between the Knipovich Ridge and the Hornsund fault zone. Myhre et al. (1982) and Spencer et al. (1984) proposed three tectonic events in the history of the Central Tertiary basin (Figure 2-1): (1) sea floor spreading south of the Senja Fracture Zone from about 58 Ma; (2) sea-floor spreading between the Senja Fracture Zone and the southern end of the Hornsund fault zone (48 Ma; mid-Eocene); and (3) sea floor spreading opposite the Hornsund fault zone (37 Ma; early oligocene) (Steel et al. 1985).

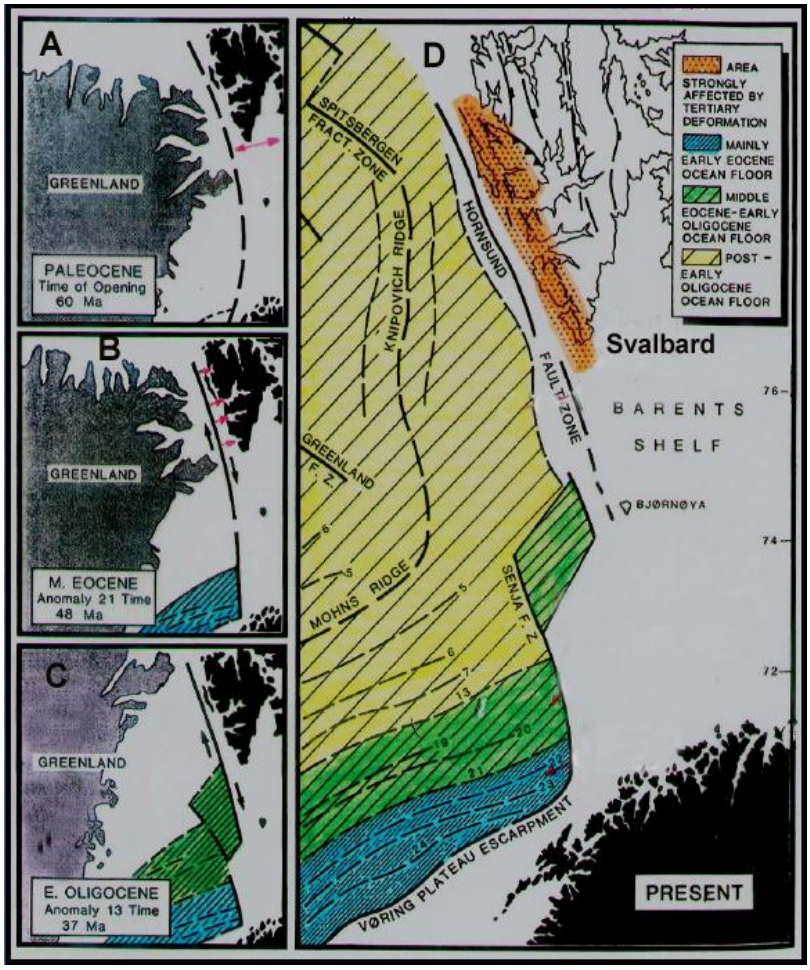

Fgure 2-1: Outline of Tertiary displacement of Svalbard from Greenland during the opening of the Norwegian-Greenland Sea (A-C), and present-day map of ocean floor generated by seafloor spreading (D). Modified from Steel et al., (1985).

The general accepted scenario for development of the Central Tertiary Basin of Spitsbergen involves a two-stage evolution of the basin from a series of strike-slip Paleocene subbasins into an Eocene compressional or transpressional basin (Steel et al. 1981; Steel et al. 1985; Müller and Spielhagen 1990). The observed change in sediment supply from eastern area (Firkanten, Basilika and Grumantbyen formations) to western regions (Frysjaodden, Hollendardalen, Battfjellet and Aspelintoppen formations) has been interpreted as a change from transtensional to transpressional regime along the sheared Western Spitsbergen margin (Steel et al. 1981).

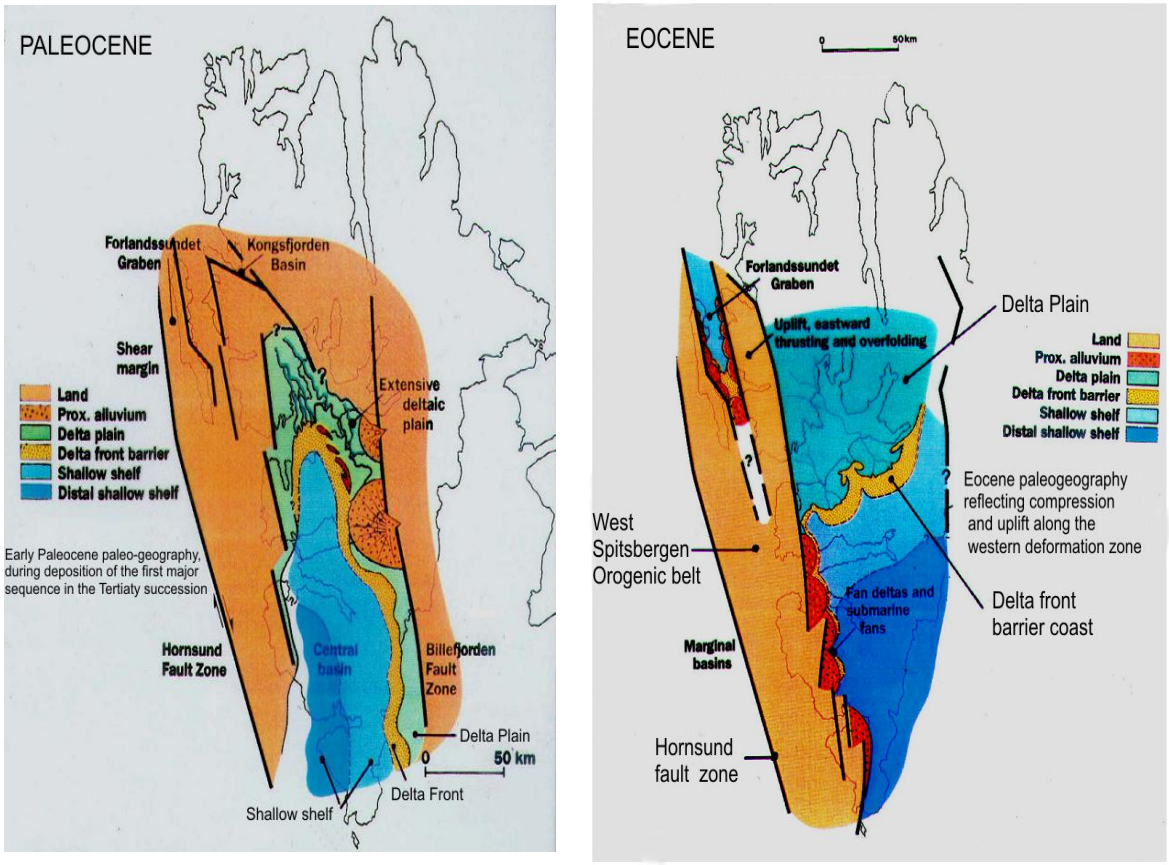

Figure 2-2: Strike-slip plate movements controling the development of Tertiary basin in Spitsbergen and on its Atlantic margin. Modified from Worsley and Aga (1986).

Based on time constraints on Late Cretaceous and Paleogene sea-floor spreading, tectonic activity in the Norwegian–Greenland and Arctic seas and analysis of sedimentary succession in the Central Basin, Bruhn and Steel (2003) incorporated the entire Svalbard Paleocene–Eocene into a foreland-basin scenario. They conclude that the Paleocene and Eocene segments of the basin fill represent the effect of complementary landward-stepping and basinward-stepping parts of an eastward-migrating foreland basin. The Paleocene, overall landward-stepping, eastward-migrating succession of coastal-plain-to-shelf deposits was derived from the peripheral bulge east of the present basin margin, and the Eocene basinward-stepping, also east-migrating succession of clastic wedges was derived from the West Spitsbergen Orogen to the west of the basin (Figure 2-3).

In this conjuncture the deposition was controlled by the position and height of a thrust-load-generated peripheral bulge, implying that compression along West Spitsbergen began in Late Cretaceous or early Paleocene times (Bruhn and Steel 2003).

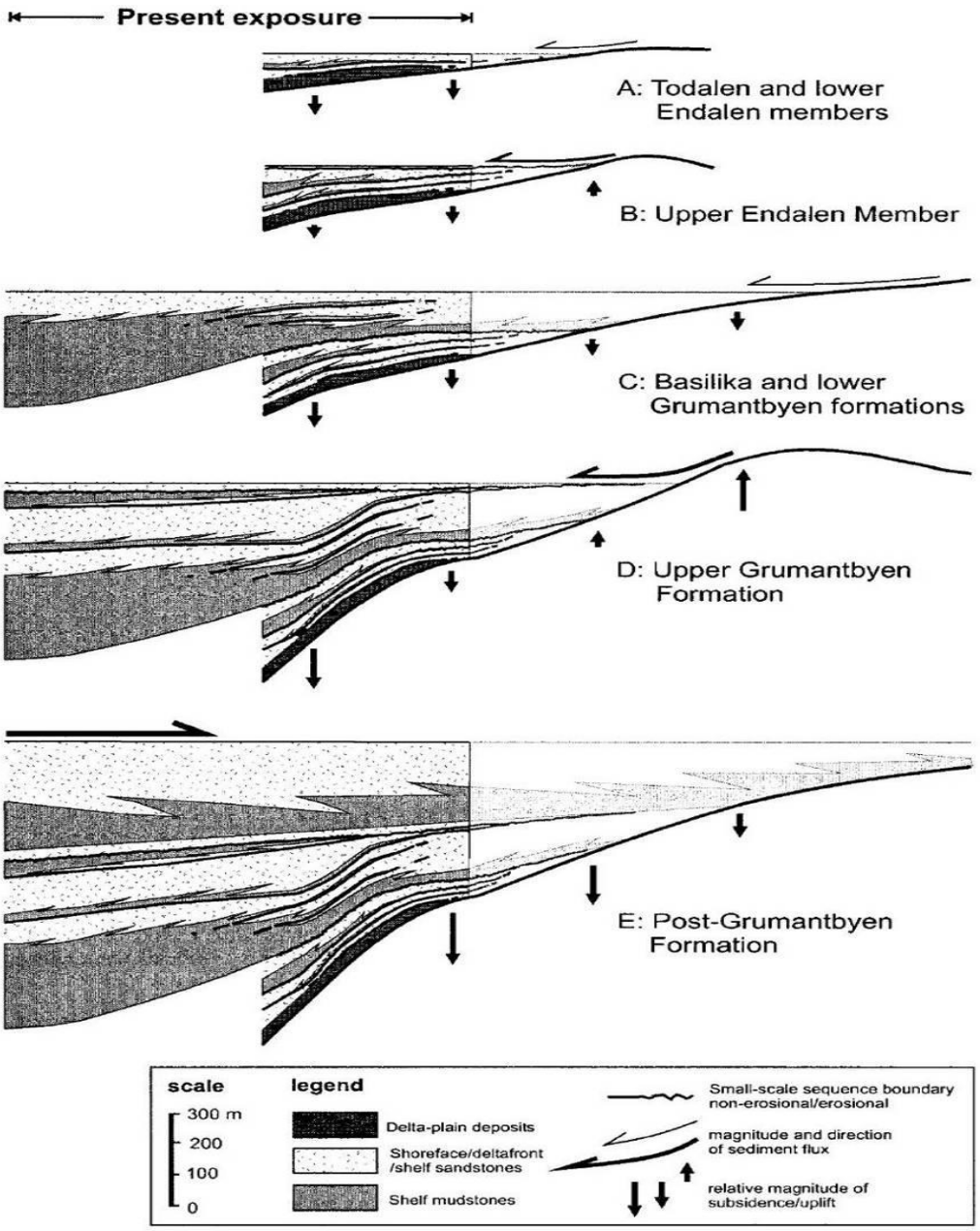

Figure 2-3: Depositional model for the Palaeogene Central Basin as suggested by Bruhn and Steel (2003).

2.2 LITHOSTRATIGRAPHY

The Svalbard and Barents shelf were subjects of an uplift regime in mid-Cretaceous to Early Tertiary, when no sediments were deposited in the Svalbard region (Dallmann et. al., 2001). After this period, development of foreland depressions with respect to the Tertiary fold and thrust belt created adequate accommodation space for the sediment infill.

Based on studies of individual basin developments and history infill, Dallmann et al. (1999) suggest that the deposition of the Tertiary sedimentary succession of Svalbard is confined to five distinct basins: Bellsund, Forlandsundet, Kongsfjorden, Central Tertiary Basin and N. Spitsbergen (Figure 2-4).

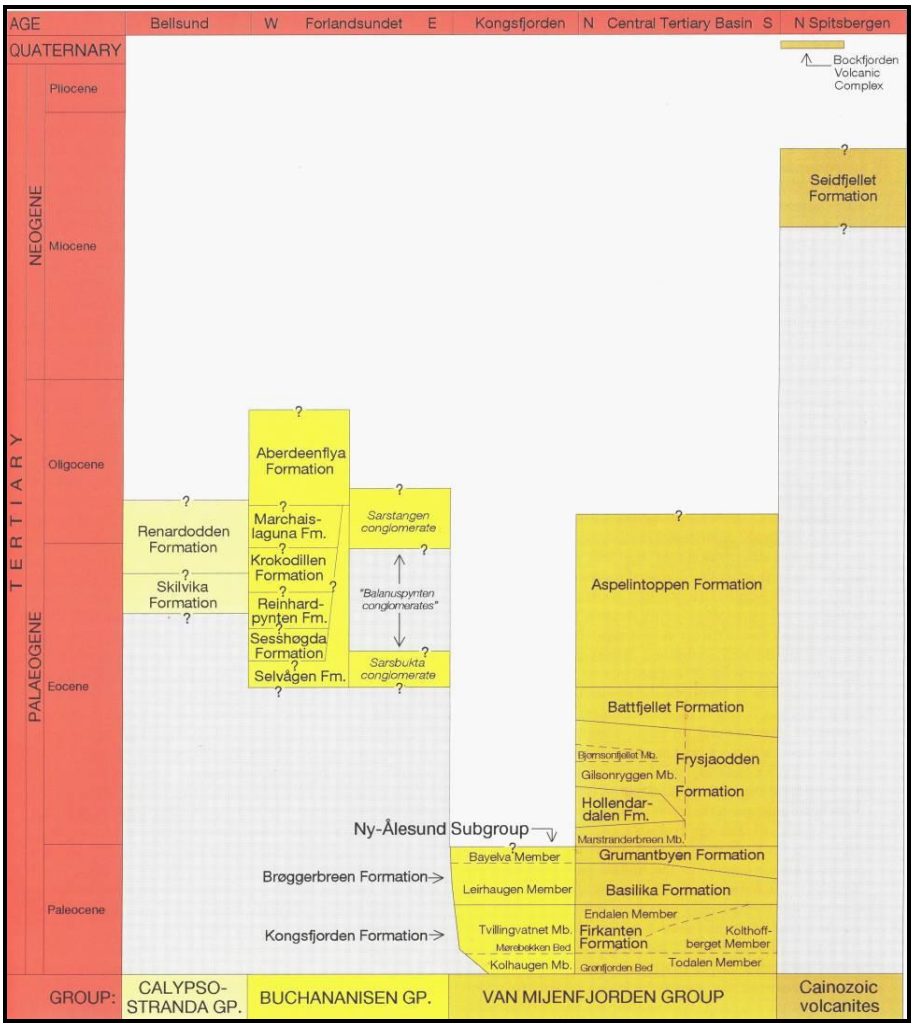

Figure 2-4: Lithostratigraphic subdivision of the Tertiary of Svalbard as compiled by Dallmann et al. (1999).

(1) Bellsund

This basin is located in south west of Spitsbergen and comprises Calypsostranda Group with its two formations: Renardodden and Skilvika. If Renardodden Formation was deposited in late Eocene to early Paleocene, the Skilvika Formation most likely belongs to late Eocene.

(2) Forlandsundet Graben

The Eocene-Oligocene Buchananisen Group is exposed within the Forlandsundet Graben on the western coast of north-central Spitsbergen and on northeastern Prins Karls Forland. It is composed of seven formations with unknown interval relations, overlying the Precambrian basement (Dallmann et. al., 1999).

(3) Kongsfjorden area

This sub-basin is located on the southwestern shore of Kongsfjorden. The sedimentary package belongs to the Ny Ålesund Subgroup, deposited in a tectonic block within the Tertiary fold-and-thrust belt. The subgroup overlies Triassic and Permian rocks (Dallmann et. al., 1999).

(4) Central Tertiary Basin/ Palaeogene Central Basin

The Central Tertiary Basin forms a NNW-SSE trending synclinorium located in southern and central parts of Spitsbergen (Dallmann et. al., 2001). According to the lithostratigraphic scheme proposed by Dallmann (1999), the Central Tertiaty Basin comprise seven formations which belong to Van Mijenfjorden Group. The sequence stratigraphy of Van Mijenfjorden Group is discussed in chapter 2.3.

(5) N. Spitsbergen

North Spitsbergen sub-basin comprises Seidfjellet formation which represents Tertiary plateau basalts, overlying Precambrian and Devonian formations.

2.3 LITHOSTRATIGRAPHIC SUBDIVISIONS OF VAN MIJENFJORDEN GROUP

Van Mijenfjorden Group constitutes the whole Paleogen sedimentary package of Central Tertiary Basin which covers an area of approximately 60 by 200 km (Bruhn and Steel, 2003) (Figure 2-5).

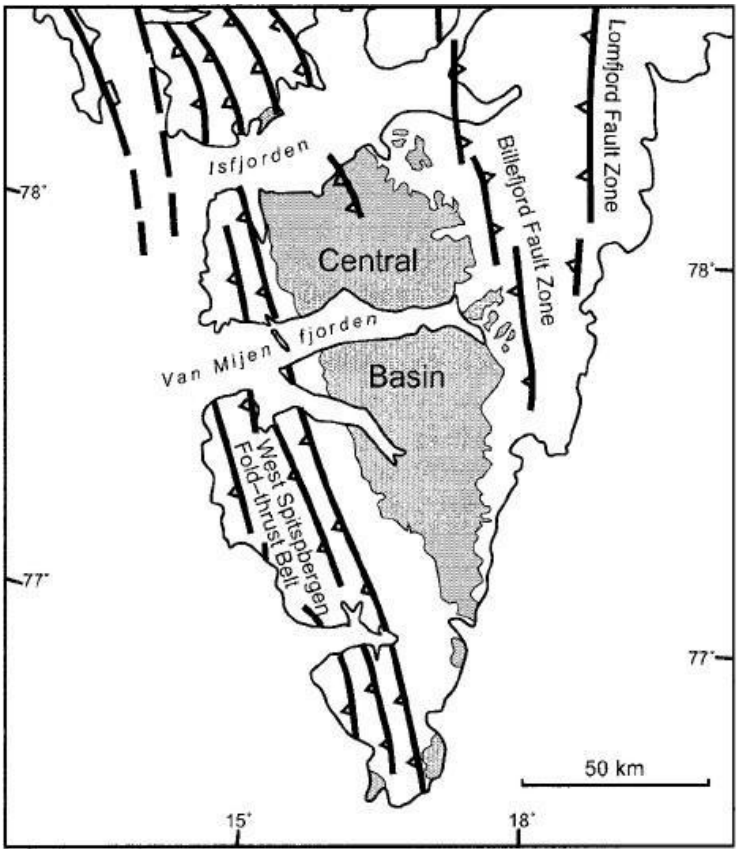

Figure 2-5: South-western Spitsbergen, showing present day outcrop of the Palaeogene Central Basin in grey (Bruhn and Steel 2003).

The present thickness of the Van Mijenfjorden Group varies from 1500m north to 2500m south of Van Mijenfjorden fiord. This variation reflects the prevalence of sediment influx from north and northeast and the maximum downwarp of the basin south of Van Mijenfjorden (Steel et al. 1981).

Two stratigraphical subdivisions of Van Mijenfjorden Group have been presented in the literature: a Russian version (Livšic 1967, 1974) and Norwegian/British subdivision

(Major & Nagy 1964; Major & Nagy 1972). In this study the Norwegian/British subdivision of Van Mijenfjorden Group is used.

Based on the description made by Steel et al. (1981), Dallmann et al. (2001) and Bruhn and Steel (2003), the Van Mijenfjorden Group is presently divided in seven formations (Figure 2-6).

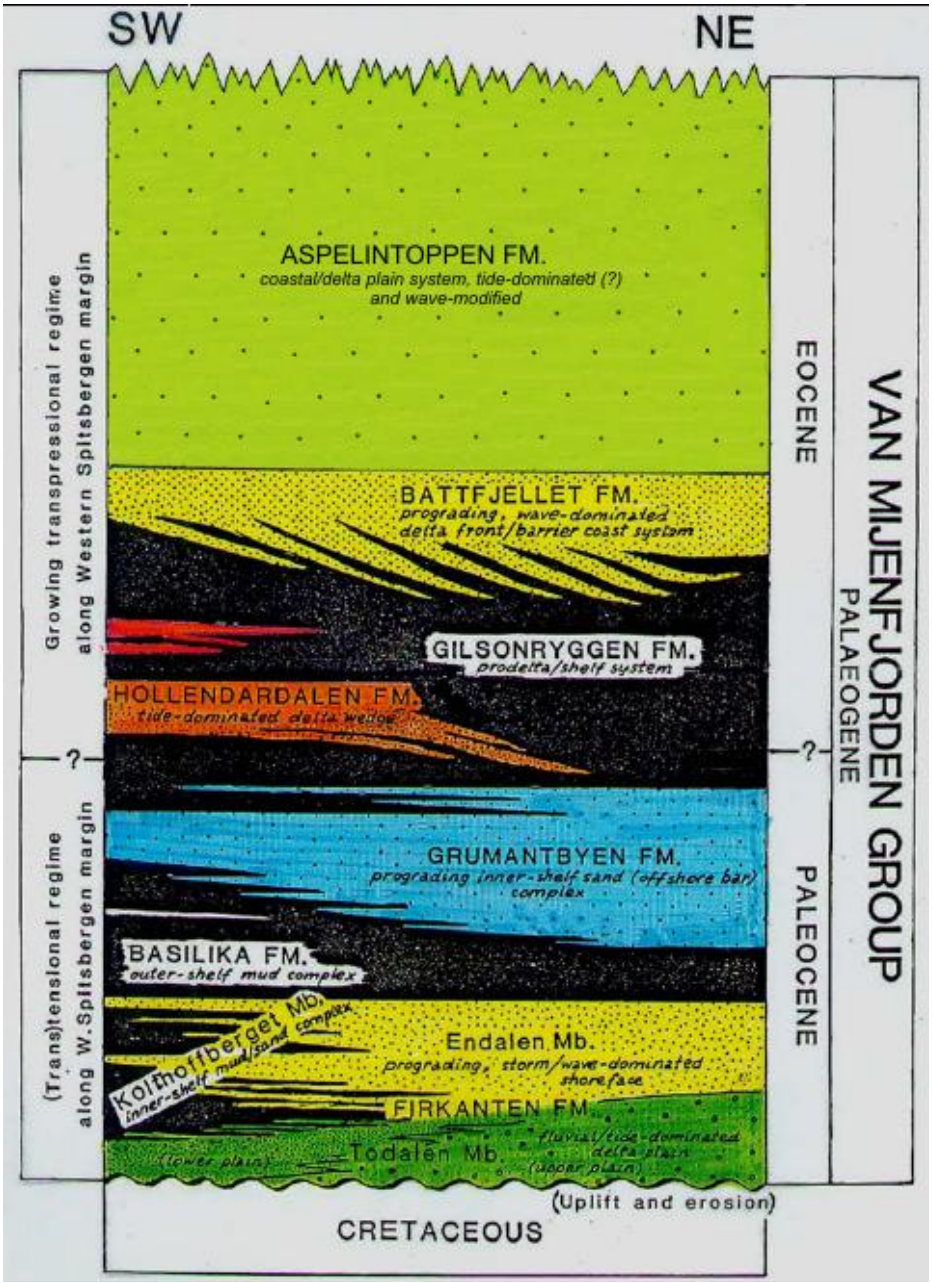

Figure 2-6: Palaeogene stratigraphy along the tectonic interpretations of Steel et al. (1985) and revised tectonic interpretations of Bruhn and Steel (2003). Modified from Bruhn and Steel (2003).

1. Firkanten Formation (Figure 2.6) (Barentsburg Formation – Livšic 1967) is the basal unit which rests with a low-angle unconformity above the Lower Cretaceous Carolinefjellet Formation. It comprises coal-bearing delta-plain, paralic and shoreface sediments deposited in an overall transgressive basin infilling phase (Steel et al. 1981). Firkanten Formation is divided in three members: Todalen, Endalen and intermediary Kolthoffberget. The Todalen Member contains the most important productive coal deposits of Svalbard while the Endalen Member is mainly constituted by stacked sand beds which often show an upward-coarsening trend (Dallmann et al. 2001). The Kolthoffberget Member consists of interbedded shales, siltstones and sandstones deposited in a transitional delta front - prodelta environment (Nagy et al. 2000).
2. Basilika Formation (Figure 2.6) (Colesbukta Formation - Livšic 1967), is a shelf mudstone unit overlying Firkanten Formation. It is constituted mainly by black and grey shales, claystone and siltstones occasionally interbeded by very fine sandstones. The formation disclose a general coarsening upward succession (Dallmann et al. 2001) and like Firkanten formation is considered a part of the same transgression phase of basin infilling Steel et al. (1981).
3. Grumantbyen Formation (Figure 2.6) is a highly-bioturbated sandstones unit and a contrast to the underlying Basilika shale. The origin of this unit is still not very clear, but based on the high content of glauconite, its massivity and presence of bioturbation Steel et al. (1985) suggested a submarine shelf-related origin. Steel et al. (1981) attributed to a regressive basin infilling phase.
4. Hollendardalen Formation (Figure 2.6) consists of several wedges of well-laminated sandstones displayed in a general coarsening upward succession. A mudstone unit (Marstranderbreen Member) separates the sand formations of Grumantbyen and Hollendardalen. This mud unit is continuous with the above lying Frysjaodden Formation and therefore, the Hollendardalen sandstone is considered an eastward clastic wedge within the Frysjaodden shale Formation. (Dallmann et al. 2001).
5. Frysjaodden Formation (Figure 2.6) comprises deep-water marine shales, intercalated with deep-water sand-rich turbidite intervals derived from the West

Spitsbergen Fold belt. The formation shows clear evidence of sediment input from the west, and an eastwards migration of the basin depocenter (Steel et al. 1985). Marstranderbreen and Gilsonryggen members compose the Frysjaodden Formation and are separated by Hollendardalen sand-wedge. The Marstranderbreen and Gilsonryggen members consist of grey and black shales, occasionally with interbedded siltstone and bentonites layers. The bentonites beds are present only in Gilsonryggen.

6. Battfjellet Formation (Figure 2.6) (Collinderodden Formation - Livšic 1967) consists of sandstones, silty shales containing clay-ironstone nodules and coal lenses. The formation represents a late phase of coastal progradation and infill in the foreland basin, a phase when sediment input finally exceeded subsidence and the basin was filled to sea level (Steel et al. 1985).
7. Aspelintoppen Formation (Figure 2.6) (Storvola Formation - Livšic 1967) consists of alternating grey and greenish sandstones and grey to brownish siltstones, along with calcareous and thin coal beds. (Dallmann et al. 2001). The abundant presence of plant remains, especially tree leaves as well as distributary channels, crevasse splay areas and swamps, indicate strong terrestrial depositional influence, most probably a coastal plain environment. (Steel et al. 1985).

2.4 PALEOCLIMATE

As specified in the introductory chapter, the main objective of the pACE project is to get more information and paleogeographical understanding of the Paleogene period. The studied succession which includes sedimentary packages from both Paleocene and Eocene epochs may constitute a possible element in paleoclimate understanding. We can study changes from greenhouse situations with higher levels of carbon dioxide, methane and water vapor to cooler climates, eventually ending in icehouse conditions. The most rapid and significant climatic perturbation of the Cenozoic Era was recorded at Paleocene/Eocene boundary, 55.8 million years ago and represents one of the key elements in our project (PETM).

2.4.1 THE PALEOGENE PALEOCLIMATE BACKGROUND

During last decades evidence has accumulated to demonstrate that the Paleogene represents one of the most dynamic climatic periods in the Earth's history. Rapid climate changes often culminated in ephemeral episodes with more extreme conditions than subsequent long term variations (Zachos et al. 1993). Based on δ^{13}C isotope distributions Zachos et al. (1993) suggested two such climatic episodes. One in the middle of a warming trend (early Eocene) was first known as Late Palaeocene Thermal Maximum [LPTM]. It is presently called the Palaeocene/Eocene Thermal Maximum (PETM). The second was formed in the global cooling trend from early/middle Eocene to earliest Oligocene (Oligocene Glacial Maximum (EOGM) (Zachos et al. 1993) (Figure 2-7).

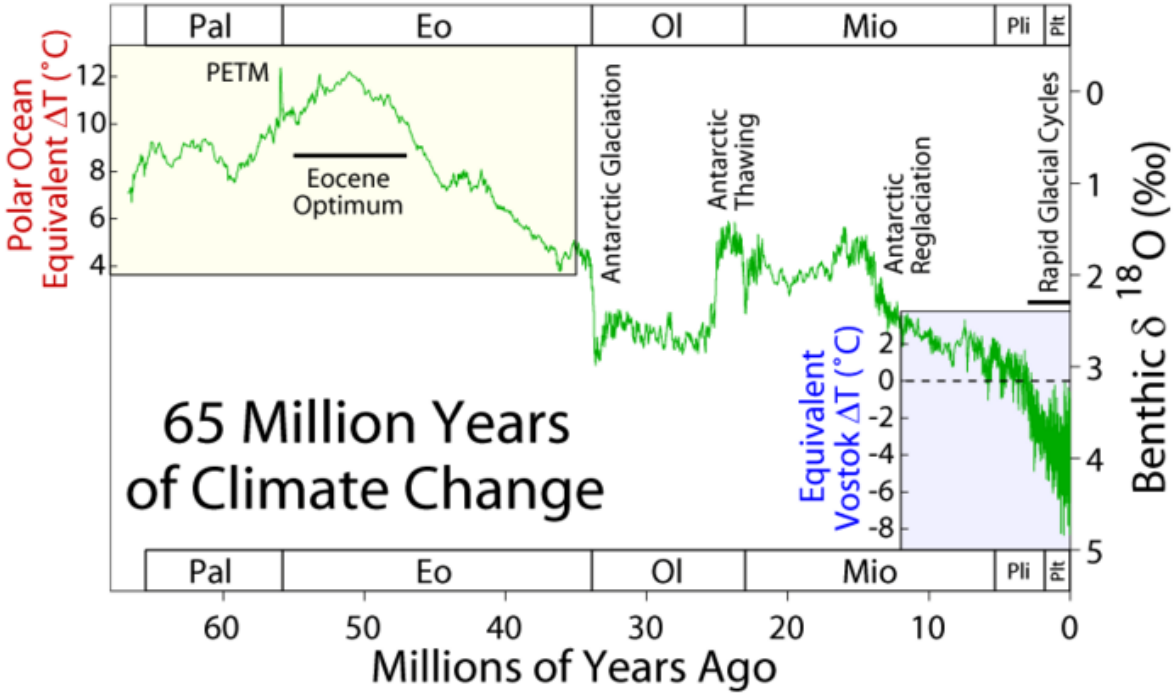

Figure 2-7: Climate change over the last 65 million years based on a compilation of oxygen isotope measurements (δ^{18}O) and benthic foraminifera. Modified from Zachos et al. (2001).

In spite of these evidences, so far, few related studies have been carried out on Svalbard's Tertiary climate. The low productivity and poor preservation of dynocysts and the virtually agglutinated nature of foraminiferal assemblages represent a problem in climate reconstruction. Nagy (2005) summarizes the environmental conditions of the Tertiary

Central Basin of Svalbard to be highly influenced by low salinities, reduced carbonate contents and probably reduced oxygen concentrations.

The first information about Paleogene climate of Svalbard were published by Dalland (1976), based on studies of clasts distribution (randomly scattered or occurred in horizons), he suggested the idea that shore-ice was the rafting agent of the clasts. The climate that controlled such processes was probably more continental than today with hot summers and cold winters.

Schweitzer (1980), based on floral assemblages, summarizes the lowermost and uppermost part of the Palaeogene Central Basin succession (Firkanten and Aspelintoppen formations) to have been deposited during terrestrial conditions and a warm to temperate climate. Based on the comparison of predominant megafossil conifers (*Metasequoia occidentalis*) present in the Central Tertiaty Basin with modern species (*M. glyptostroboides*) from border of the Chinese provinces Szechuan and Hupeh, Schweitzer (1980) attributes a climate characterized by rainfall that is moderate to absent in winter and heavy in summer season. Mean annual temperatures were probably of 15 to 18° C.

2.4.2 PETM

The Paleocene Eocene thermal maximum (PETM) is one of the most abrupt and ephemeral climatic events documented in the geologic record. The event was characterized by pronounced warming of the oceans and atmosphere, changes in ocean chemistry, and reorganization of the global carbon cycle (Röhl et al. 2007). The temperature of the sea surface water increased with 5-8^{o}C in a very short period of time (few thousands of years). This resulted in extinction of 30–50% of deep-sea benthic foraminiferal species (Thomas and Shackleton, 1996) and to changes in planktonic biota in surface water habitats (Kelly et al. 1996) (Figure 2-8). Global warming also may have led to a pulse of speciation or migration among mammalian groups (Koch et al.1992).

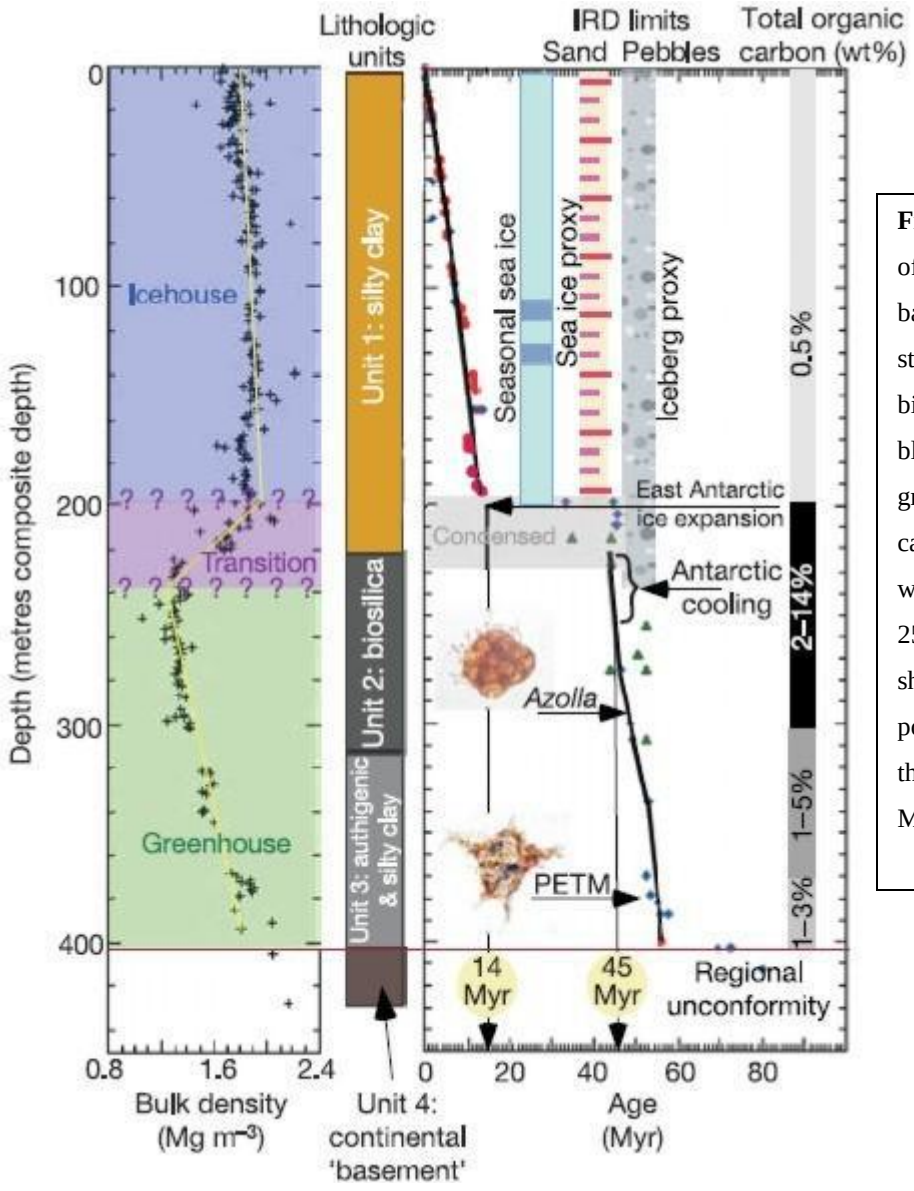

Figure 2-8: Schematic "Synthesis of the ACEX coring results. Age based on: palaeomagnetic stratigraphy shown as red circles; biostratigraphic data (dinocysts, blue diamonds; silicoflagellates, green triangles; and a few calcareous microfossils, squares which only occur in the upper 25m). Two micrographs are shown in their stratigraphic position; the upper is *Azolla* and the lower is *Apectodinium*." Modified from Moran et al. 2006

The PETM corresponds to a significant (~3.5–4.5%) negative carbon isotope excursion (CIE) recorded in marine and terrestrial sections (Sluijs et al. 2008; Smith et al. 2007). This rapidly released mass of ^{13}C depleted carbon and its massive injection into the earth's geosphere, was quantified by Zachos et al. (2007) as being in the order of 2000Gt or greater. Pagani et al. (2006) claimed that PETM might be the best ancient analogue for future anthropogenically causes increases in atmospheric CO_2. The PETM isotopic and sedimentological data suggest that atmospheric CO_2 was the primary greenhouse gas responsible for the PETM as has been claimed in the present situation.

Different opinions have been presented as the causes of this catastrophic PETM event (Cramer & Kent 2005, Panchuk et al. 2008). The major challenge in analyzing the causes of PETM is the large decrease in $\delta^{13}C$ concentrations. It seems too large and too fast to be explained within the context of standard carbon cycle models (Cramer & Kent 2005). This resulted in to the proposal of alternative theories; Dickens et al. (1995) suggested the input of substantial quantities of isotopically light methane from thermal dissociation of seafloor clathrate deposits. Kurtz et al. (2003) explained the increasing terrestrial organic carbon-rich deposition as a result of the burning of large peat deposits. Cramer & Kent (2005) presented evidence that only an extraterrestrial impact may provide a trigger of sufficiently large energy to develop such short and intense event. Other possible explanations have been discussed attempting to of elucidate the causes of PETM; they include volcanic activity, orbital forcing or intense flood basalt magmatism and generating of metamorphic methane from sill intrusion into possible carbon-rich sedimentary rocks related with the opening of the North Atlantic (Katz M., et al. 1999, Panchuk et al. 2008, Farley & Eltgroth 2003, Thomas et al. 2002, Storey et al. 2007).

3. METHODS AND MATERIAL

The pACE group is using various methods and materials in the reconstruction of paleoenvironmental and paleoclimatic record of Paleogene in Svalbard archipelago. This master thesis was carried out by studying sedimentological, mineralogical and natural gamma log data. The field work was carried out in Svalbard, august 2007 (Figure 1-1).
In 1997 Jenö Nagy collected series of sediment samples and compiled sedimentological logs of the Upper Grumantbyen, Frysjaodden and Hollendardalen formations; the N1 and N2 sections. The shortcut "N" comes from the name of the area (Nordenskiöldfjellet) and the numbers (1, 2, 3) represent the chronological sequence of gathering sedimentological log information. Due to poor exposures, two adjacent gullies were used in the logs of 1997. In August 2007, a new and detailed sedimentological log (N3) was measured and sampled. Gamma ray measurements were mainly carried out along section N3. In addition, new samples and updates of the old logs were done in sections N1 and N2. GPS

measurements for the distances between the three sections (N1, N2 and N3) are the following: 648 m between N1 and N2 and 349 m between N1 and N3 (Rüther, 2007). Section N3 is located ~ 5km south west from Longyerbyen (Figure 1.1).

3.1 SEDIMENTOLOGICAL FIELD LOGGING

In the logging process a clinometer-compass, a two meter wood pliant, a hand-lens and a grain size checking tool were used for measurements and grain size estimation. Sedimentary data like grain shape, degree of sorting, color, bed, lamina thickness and so on were recorded on sheets with millimetric column (Appendix 1). This operation was conducted hand in hand with sampling for both sections N3 and N1+2. For the latter combined section the old logs by Jenö Nagy was updated with additional sedimentary data, especially focused on the Hollendardalen Formation.

3.2 SAMPLING

In this study 74 samples have been investigated. 44 samples were collected in August 2007 and the others in 1986 (8) respectively 1997 (22) by Jenö Nagy. From the samples of August 2007 collection, 14 were taken from sections N1 and N2 and 30 from section N3. However, for mineralogical analyses only 59 samples were used (Table 3-1). The samples cover all types of lithologies encountered: shale, claystone, siltstone and sandstone.

Samples were collected from different sections, by different people and in different periods of time and therefore they have unfortunately different IDs. A simplified sample ID is being used in the present study. Short IDs for samples collected from sections N1 and N2 have the prefix „n" for north, while short IDs from N3 section samples the prefix „s" for south (Table 3.1).

Table 3-1: Simplified sample renaming in section N1+2 and N3.

N1+N2		N3	
Short IDs	**Original IDs**	**Short IDs**	**Original IDs**
n1	N-1-2-97	s1	N-3-1
n2	N-1-4-97	s2	N-3-2
n3	N-1-5-97	s3	N-3-3
n4	N-1-6-97	s4	N-3-4
n5	N-1-07-1	s5	N-3-5
n6	N-1-07-2	s6	N-3-6
n7	N-1-07-3	s7	N-3-7
n8	N-1-07-6	s8	N-3-8
n9	N-1-07-7	s9	N-3-9
n10	N-1-07-8	s10	N-3-10
n11	N-1-07-9	s11	N-3-11
n12	N-1-07-10	s12	N-3-12
n13	N-1-07-11	s13	N-3-13
n14	N-2-07-3	s14	N-3-14
n15	N-2-3-97	s15	N-3-15
n16	N-2-07-1	s16	N-3-16
n17	N-2-07-2	s17	N-3-17
n18	P4	s18	N-3-18
n19	N-2-8-97	s19	N-3-19
n20	N-2-9-97	s20	N-3-20
n21	N-2-11-97	s21	N-3-21
n22	N-2-12-97	s22	N-3-22
n23	N-2-13-97	s23	N-3-23
n24	P8-86	s24	N-3-24
n25	P11-86	s25	N-3-25
n26	P14-86	s26	N-3-26
n27	P19-86	s27	N-3-27
n28	P21-86	s28	N-3-28
n29	P24-86	s29	N-3-29
n30	P28-86		

3.3 NATURAL GAMMA RADIATION

Natural gamma radiation measurements have been carried out in section N3, mainly with respect to evaluation of the clay/shale content of the formation using a portable combination radiagem2000-CSP (Canberra Smart Probes) connected via a 1.5 meter cable. The radiagem2000 is a survey meter (host) that includes an energy-compensated Geiger-Müller instrument which measures Dose-rate equivalent $H^*(10)$ from 0.1 μSv/h to 100 μSv/h and which can be used both in measurement mode and in source finder mode. The CSP used is a probe designed for gamma measurements used for high sensitivity with a dose-range going from 1 μR/h to 5 μmR/h. Its unit measure is counts/second. 75 data points were picked along the whole N3 section with an average distance of 20-30 cm.

3.4 FACIES DESCRIPTION AND FACIES ASSOCIATIONS

On the basis of structures, textures, geometries, palaeo current indicators and gamma ray data, sedimentary facies were identified and described. Thirteen facies have been distinguished in section N3 and studied in detail during field work in 2007. They are presented in chapter 4. Facies used to define a particular sedimentary environment and have been grouped into associations.

3.5 MINERALOGICAL ANALYSIS

Mineralogical analysis involving combined optical studies, XRD (X-ray diffraction), and SEM (Scanning Electron Microscopy) analysis have been carried out using different preparation methods and/or different instruments. These are briefly described in the following subchapters.

3.5.1 THIN SECTIONS

A total number of 49 thin sections have been used for optical mineralogy analysis using several polarizing microscopes. Thin sections were prepared by both Naturhistorisk Museum Geo-Laboratoriene in 1997 and at Department of Geology, University of Oslo in 2007. They were made from small slabs of the rock samples, glued to a glass slide (2.5

by 4.5 cm), and then grounded to a specified thickness of 0.03mm (30 μm). At this thickness most minerals become more or less transparent and can then be studied by a microscope using transmitted light.

3.5.1.1 THIN SECTION DESCRIPTION

The analyses of the thin section have been effectuated using both PPL (plain polarized light) and cross polarized microscope. The main features of interest are related with the framework, structure, texture and mineralogical composition of the samples. A few thin sections coated with carbon conductor (Polaron SEM coating unit E 150) were examined morphologically under JEOL JSM 6400 (with Link EXL, EDS) Scanning Electron Microscopy (SEM). The thin sections of representative samples were SEM analyzed for identification of matrix minerals.

3.5.1.3 COUNTING OF MINERALS

48 samples have been counted covering both sections (N3 and N1+2) using petrographic microscopes both in PPL (plain polarized light) and in cross polarized by using of a point counting equipment. 400 counts were picked for each sample. For a correct as possible result of the mineralogical composition, the whole area was generally counted. Where possible, the counting process has been made across lamination (Appendix 2, 3).

3.5.2 XRD ANALYSIS

Crushed bulk samples and clay fraction analysis were executed by a PHILIPS X'Pert Automated Powder Diffractometer System 5000 X-Ray diffractometer with a θ-θ goniometer and automatic divergent slit connected to a Philips X'Pert software program. Samples were X-rayed using Ni-filter monochromatic copper radiation with a scan range from 2 to 40º 2θ, a step size of 0.06º and a dwell time of 3s per step.

3.5.2.1 BULK ANALYSIS

Prior to XRD bulk process, samples were crushed manually to an acceptable grain size (not bigger than 2-3 mm in diameter) and then, an automatic ball mill has been used for 30-60 seconds depending on the rock. The fine powder obtained was packed into

aluminum holders by using a compaction machine and run on X-ray diffractometer (XRD) for bulk analysis. The process was carried out using both normal and slow scan. Slow scan recording has been done in the interval 26 - 28.5 $^{o}2\theta$ and 4 sec sampling time in order to determinate K-feldspar and plagioclase reflections. The identification of minerals by X-ray diffraction analysis is based on reflection of X-rays by the characteristic atomic lattice planes within the minerals crystals (Thorez, 1976). The minerals were identified by using X-ray diffraction patterns (diffractograms or diffraction tracing) of oriented aggregates that enhanced the basal, or *00l,* reflections (Moore and Reynolds 1989). After identification of minerals, quantification of data was carried out with the help of reports made in X-pert software program and by direct measurements on the diffractograms.

3.5.2.2 CLAY SEPARATION

In order to run XRD only for the clay fraction, clay separation method has been applied. Samples were crushed to a size of 1-2 mm in diameter. Roughly 5-10 grams of each sample was placed individually in graded glass. In each recipient 300 ml of distillated water was added and mixed for 1 min. The mixed composition underwent a 10 minutes ultrasound treatment in a Bandelin Sonorex RK102 transistor. The reason was to accelerate dispersion of clay particles (<2μm). After this step, samples were left for sedimentation for one night. Thereafter 100 ml of distillated water was added in each recipient and the composition mixed again for 1-2 minutes. Samples were left in suspension for 3.5 hours. Prior to filtering, for samples with flocculation problems, 15 ml of Calgon (dispersing agent) by a concentration of 1g/l was added, mixed and left for more 3.5 hours. In some cases this process was repeated 2-3 times. The upper 200ml of the solution was then removed and transferred in new recipients, stirred for 10 seconds and filtered in a vacuum suction through millipore filter. In the filtering process, samples were treated with $MgCl_2$ (0.1M) and washed with distillated water. The resulted clay fractions were placed on silica glass sides and mounted in aluminum holders.

The clay fraction has been first run in the XRD as air-dried (untreated). Three treatments were applied and they were all analyzed by XRD. To separate different clay minerals and in particular to identify swelling clay, the samples were treated with

ethylene glycol vapor (EG) into an exsicator for 12 hours. They were heated two times for 2 hours at 300 and 550^{o}C respectively. For identification of kaolinite and chlorite from overlapping peaks located at ~25^{o} 2θ, the slow scan method was applied for the 24-26^{o} 2θ areas with a goniometer velocity of 1/80/min.

A problem in the XRD analysis was the presence of iron oxides and hydroxides in the samples, partially acting as cementing agents, blocking the XRD peaks of clay minerals. In order to remove this effect the proposed method of Mehra and Jackson (1960) has been applied with success. A short description of the method follows:

- 40 ml of 0.3 M Na-Citrate solution and 5 ml of 1M $NaHCO_3$ solution were added to 1 g of sample in each 100 ml plastic recipient.
- one gram of solid $Na_2S_2O_4$ was added and the mixture stirred for 1 minute.
- samples were place in a water bath for 15 minutes at 80^{o}C.
- thereafter, 10 ml of saturated NaCl solution and 10 ml of acetone, was added to the tube to promote flocculation.
- the suspensions were centrifuged for 5 min at 1600-2200 rev/min.
- the clay fraction was separated at the bottom of the tube after removing the liquid solution and prepared for filtering as described above.

Initially, for saving time, a simplified method was tried but without good results. After this method, samples were filtered and treated once more before the XRD runs.

The identification of clay minerals was conducted based on methods suggested by Moore and Reynolds (Moore and Reynolds, 1989). The quantification was carried out on ethylene glycolated peaks where the identification of clay minerals is most complete. In the case of overlapping vermiculite and chlorite peaks at 14.2Å, for the quantification of vermiculite, a combination of ethylene glycolated and low heated (300^{o}C) runs were applied. Two samples were tested by treatment with K^{+} to confirm the identification of vermiculite at 14.2Å peak, which clearly shifted in air dry run to 10.5Å (Moore and Reynolds, 1989).

4 SEDIMENTOLOGICAL DESCRIPTION OF STUDIED SECTIONS

Field logs were collected at sections Nordenskiöldfjellet 3 (N3) and N1+2 in August 2007 and they form the foundation for sedimentological analysis. The composite field logs from Nordenskiöldfjellet 1 and 2 made by Nagy in 1997 were updated and supplemented with new sedimentological details (for location see Figure 1-1). Furthermore the same section was extended stratigraphicaly upward, with 28 meters, in order to comprise the samples above PETM collected by Nagy in 1986. The presented logs are modified versions of those presented by Rüther (2007). The characteristic facies of the resulting seven facies associations in section N3 are presented in chapters 4.3. The most important sedimentary features of sections N1+2 are described in chapter 4.4. Results from mineralogical analyses by XRD and thin section are illustrated in chapter 5.

4.1 SEDIMENTOLOGICAL LOGS

Detailed facies analysis have only been done on section N3 which was measured by Rüther and Burcă. A simplified description of the Nagy's sections N1+2 follows in chapter 4.4.

Two sedimentological logs (Figure 4-1 and 4-2) were compiled and are presented in the following chapters 4.2 and 4.4; figure 4-1 emphasizes section N3, while figure 4-2 represents an updated version of sections N1+2 with details on Hollendardalen and Frysjaodden formations. Both logs comprise the upper part of Grumantbyen Formation, entire Hollendardalen Formation and Frysjaodden Formation including two members (Marstranderbreen and Gilsonryggen). By comparing the two logs, one can easily notice the differences in formations thickness between N3 and N1+2. Marstranderbreen Member is about 1.2m thicker in N3 than in section N1+2, while Hollendardalen Formation is about 4m thicker in N1+2 compared to N3 (Figure 6-2).

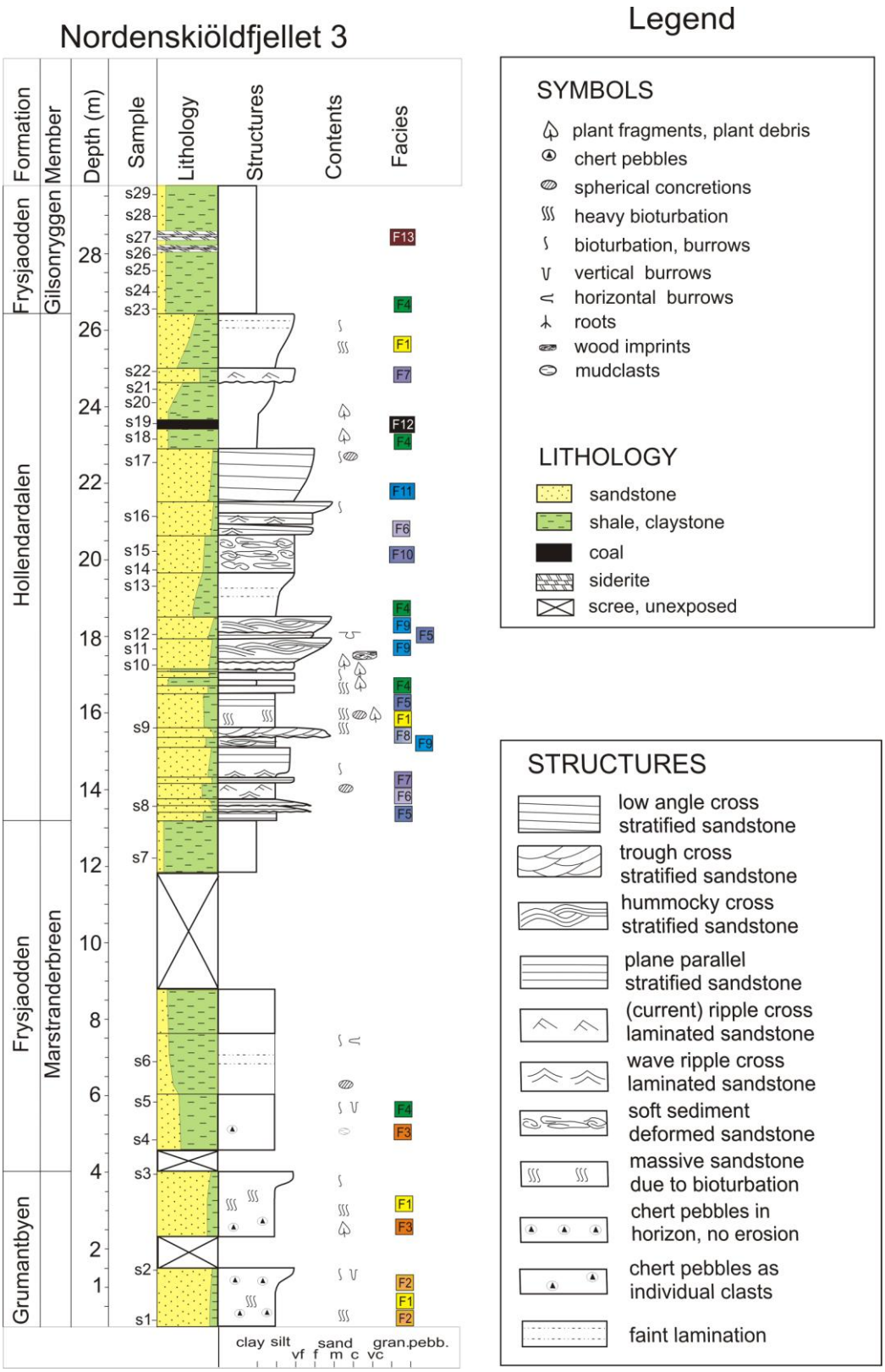

Figure 4-1: Sedimentological log of section N3 (Facies descriptions are presented in table 4-2).

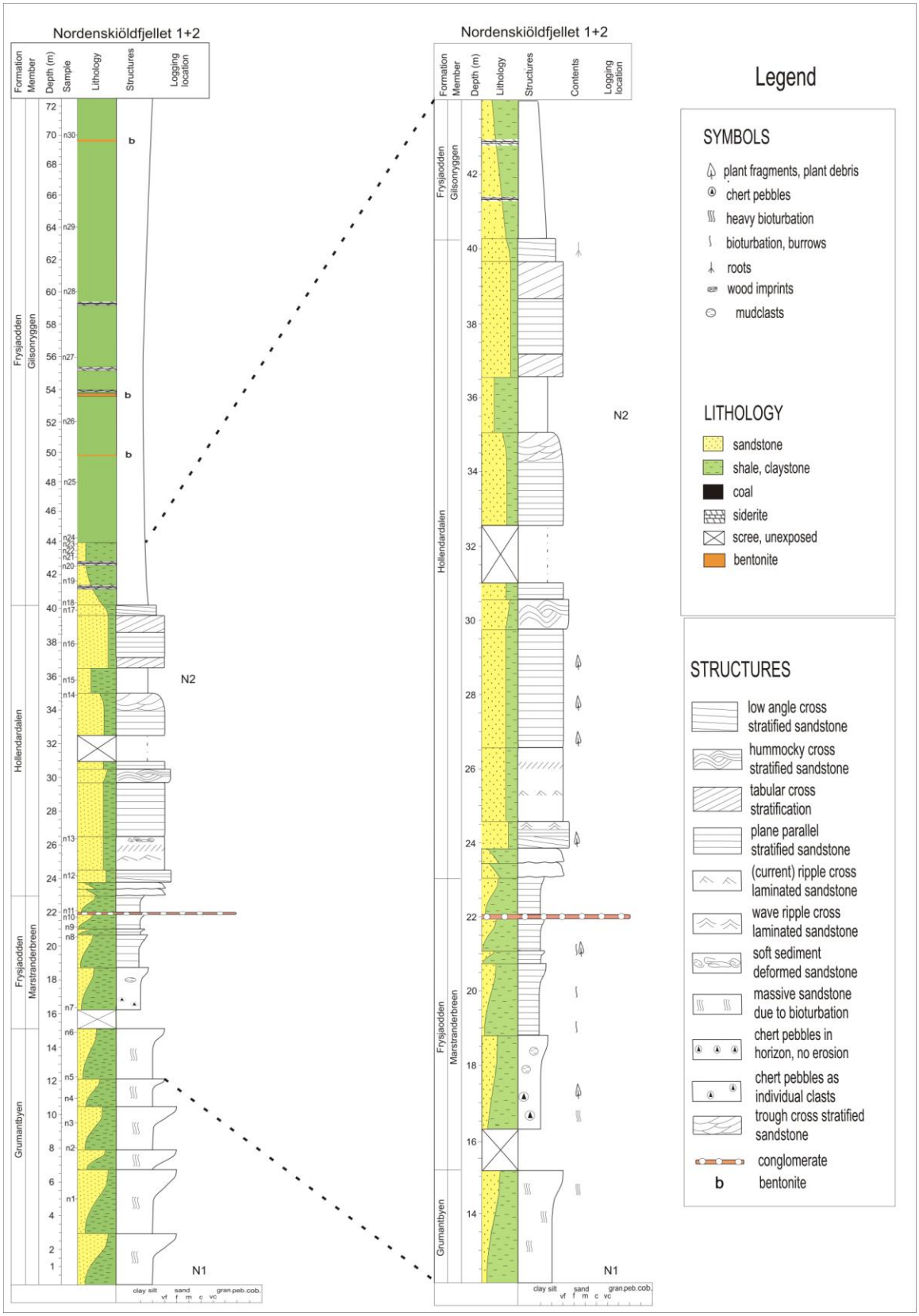

Figure 4-2: Sedimentological log of section N1+2

4.2 FACIES DESCRIPTION OF NORDENSKIÖLDFJELLET 3

Lithology, texture, sedimentary structure, palaeocurrent direction indicator, and geometry form the base of facies identification and description. Based on these characteristics, at Nordenskiöldfjellet section 3, thirteen facies have been distinguished and recorded. The facies and their characteristic features are summarized in Table 4.1.

4.2.1 F1 HIGHLY BIOTURBATED SANDSTONES AND SILTSTONE

In log N3 (Figure 4-1) the highly bioturbated facies is present in three intervals. First occurrence is in the Upper Grumantbyen Formation and the other two are in Lower and Upper Hollendardalen Formation, respectively.

The Upper Grumantbyen highly bioturbated sandstones comprises about 4m of silty sandstone sediments disposed in two coarsening upward successions. They are massive and characterized by lack of sedimentary structures. The colour is olive grey for both intervals and the thickness is about 150cm for each. Roughly 1m of scree is covering the section on top of the first coarsening upward succession. The grain size indicates silt deposits at the base which quite rapidly change to very fine sandstone towards the top.

The Hollendardalen siltstone deposits, located at ~15.5-16m in log N3 represent the second occurrence of this type of facies. It contains cemented nodules, plant debris and fossil plant fragments along bedding planes. The grains are poorly sorted, without evidence of graded bedding. Succeeding these deposits (at 16.5m in log N3), two 59cm tick mudstone beds are rich in plant debris and interbedded with very fine, highly bioturbated sandstone.

The third bioturbated facies is present at level 26.3m in Upper Hollendardalen sandstones. A very fine sandstone interval, with a total thickness of ~180cm comprises in its first 40cm occasionally non-symmetric ripple lamination, while only faint lamination is visible in the upper part. The absence of sedimentary structures is probably the effect of bioturbation.

Table 4-1 Characteristic features of sedimentary facies of Nordenskiöldfjellet section N3

Facies	Occurrence in section N3 (Depth-m)	Grain-size	Paleo-transport direction	Sedimentary structures	Geometry (thickness)	Bounding surfaces
F1. Highly bioturbated siltstone and sandstones	0, 2.2, 15.5, 26.3	silt to very fine sand	non-identifiable	mud clasts, chert pebbles, bioturbation	3-125cm	conformable
F2. Chert pebbles in bed without erosional surface	0.60, 1.5	medium to very coarse pebbles	330°, 352°, 360°	indication of imbrication	5-10 cm	non-erosional
F3. Chert pebbles as individual clasts	2.6	fine to medium pebbles	non-identifiable	very rounded	2-5 cm	non-identifiable
F4. Moderate to non-bioturbated mudstone	5.7, 16.5, 18.5, 26.4	clay to silt	non-identifiable	spherical concretions, mud clasts, burrows, sometimes rich in plant debris	1-90 cm	sharp planar
F5. Plane parallel-stratified sandstones (PPS)	13.2, 16.4, 18	fine sand	non-identifiable	poorly sorted, sometimes organic rich	3-16cm	erosional
F6. Wave ripple cross laminated sandstones and siltstone	13.7, 20.7	silt to very fine sand	40°, 180°	symmetrical ripples	3-40cm	conformable

Table 4-1, continuation.

Facies	Occurrence in section N3 (Depth-m)	Grain-size	Paleo-transport direction	Sedimentary structures	Geometry (thickness)	Bounding surfaces
F7. Current ripple cross laminated sandstones and siltstone	14, 24.5	silt to very fine sand	40^o 76^o	large-scale bulging of sedimentary layers, mud clasts, bioturbation	8cm	conformable
F8.Trough cross stratified sandstone	15.3	very fine to medium sand	147^o	cross beds	14cm	erosional
F9.Hummocky cross stratified sandstone and siltstone	15, 17.2, 18	silt to medium sand	360^o, 36^o, 216^o, 180^o	Groove casts, plant fragments, bioturbation	16-80 cm	erosional, conformable
F10. Soft sediment deformed sandstones	19.6	silt to very fine sand	non-identifiable	large-scale bulging of sedimentary layers, contorsion	100cm	conformable
F11. Low angle cross stratified sandstone	20.7	very fine to medium sand	126^o	spherical concretions, bioturbation, ripple bedds	24-140cm	conformable
F12. Coal	23.5	mud	non-identifiable	plant debris in mudstone below and above	20cm	sharp
F13. Siderite beds and concretions	28, 28.3	mud	non-identifiable	bed forming concretions, some separate nodules	2-20cm	sharp

4.2.2 F2 CHERT PEBBLES IN BEDS WITHOUT EROSIONAL SURFACE

In the first coarsening upward interval of the upper Grumantbyen Formation, two chert pebble beds located at level 60cm and 105cm are of particular interest. The pebbles are 2-5cm in diameter, well rounded, black in colour, and show indications of imbrications. Palaeoflow directional measurements indicate north-westerly to northerly flow direction (Table 4-1). Almost spherical to elongate mud clasts of 2-8cm diameter occur at the top interval. The beds do not display any erosional base (Figure 4-1a).

a **b**

Figure 4-1 Pebble occurrences in the Grumantbyen Formation: **a)** horizon without erosional base in lowermost coarsening-upwards interval (at level 0.6m in log N3); **b)** individual chert pebbles occurring in second coarsening- upwards interval (at 2.6m in log N3).

4.2.3 F3 CHERT PEBBLES AS INDIVIDUAL CLAST

In the second coarsening upward interval of the Upper Grumantbyen Formation, black or whitish-grey chert pebbles occur as individual clasts. They are very well rounded and of smaller dimension (0.5-1.5cm) and located at level 2.6m (Figure 4-1b). A second occurrence of individual chert pebble clast with similar characteristics takes place at ~5m in Marstranderbreen Member

4.2.4 F4 MODERATE TO NON-BIOTURBATED MUDSTONES

This mudstone facies comprises the entire Marstranderbreen and Gilsonryggen members as well as parts of lower and middle Hollendardalen Formation.

The clay and silt deposits of Marstranderbreen Member compose a gradual fining upward succession. Vertical and horizontal bioturbation traces may disclose possible original variations in deposition environments. This part contains occasionally mud clasts and individual pebbles of about 1-2cm diameter. The colour of basal siltstone is grey to olive grey. The degree of bioturbation decreases upwards and simultaneously, the identification of lamination was possible. Vertical burrows of 1mm in diameter and 1-2cm length are present in the first 200-300cm, while horizontal bioturbation dominates the next 160 cm. The entire association is heavily fractured with a fracture spacing of 3-5cm. The presence of spherical concretions or cemented nodules is one of particular interest in the lowermost part of succession.

Figure 4-2: Spherical concretions in Mastranderbreen siltstone at 6.2m in log N3

In the Hollendardalen Formation at 16.7m in log N3, the mudstone beds are rich in plant debris and interbedded with very fine and highly bioturbated sand. Another mudstone layer present at level 18.5m in log N3, comprises 115cm of heavily fractured siltstones showing faint traces of parallel lamination. It contains some thin mud laminae and fossil imprints at mm-scale. A gradual transition into very fine sandstones characterized by soft sediment deformation marks the upper border of facies F4.

4.2.5 F5 PLANE PARALLEL-STRATIFIED SANDSTONES AND SILTSTONES

Very fine, plane parallel lamination siltstone (PPS) of 20cm thickness is located at level 13.2m in log N3, overlying the upper part of Marstranderbreen mudstones (Figure 4-1). On the top of this unit, two fining-upwards developments from medium to very fine and silt grain size were observed. Each of them is poorly sorted at the base and develops into plane parallel lamination towards top. They display erosional surfaces at the base and lack of bioturbation rate.

Plane parallel-stratified sandstones were also identified at the base of HCS deposits ~15m, while at level 16.4m plane parallel-lamination becomes visible in a siltstone unit concomitant with a decrease in bioturbation.

At level 18m in log N3, two prominent coarsening-upward sandstone packages of 80cm and 71cm thickness are separated by ~20cm of plane parallel laminated fine sandstone (Figure 4-3).

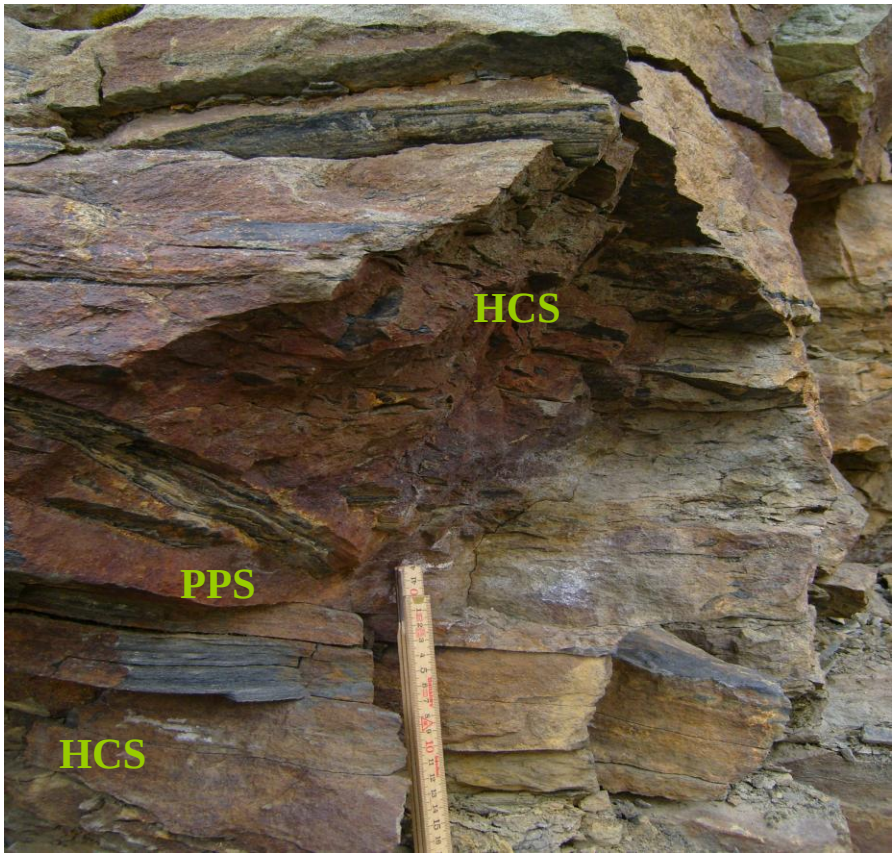

Figure 4-3: Plane parallel stratification (PPS) separating two hummocky cross stratified (HCS) units at level 18m in log N3.

4.2.6 F6 WAVE RIPPLE CROSS LAMINATED SANSDSTONES AND SILTSTONES

At ~14m in log N3 wave ripple cross laminated and moderate bioturbated siltstones of 20cm thickness are found. The bioturbation is seems as horizontal burrows of 3-10 cm length and black spots. The wave generated ripples have a wave length of 10-15cm and amplitude of 1-3cm. At 14.2m in log N3 similar wave ripples were observed. At 20.7m in log N3, a moderate extensive wave ripple cross lamination forms the lowermost 58cm of the well sorted and homogeneous thick interval of low angle cross stratified, fine sandstone. The symmetrical ripples have wave lengths of ~30cm and amplitudes of ~1cm, and indicate a south-north palaeoflow direction (Figure 4-4).

Figure 4-4: Wave ripples and low angle cross stratification in fine sandstone bed (at 20.9m in log N3).

4.2.7 F7 CURRENT RIPPLE CROSS LAMINATED SANDSTONE AND SILTSTONE

Current ripple structures occur both in silt and sand fractions (Figure 4-1). Current ripple traces were observed at level 14m in log N3 and indicate easterly to north easterly palaeoflow directions. Spherical concretions are present along bedding planes and occur in the middle part of the interval. The thickness of this interval is about 15cm and the wavelength is of 5 to 6cm (Figure 4-5). A very fine sandstone bed of 30cm thickness is located in the Upper Hollendardalen Formation (level 24.5m in log N3) and contains also asymmetrical ripple lamination.

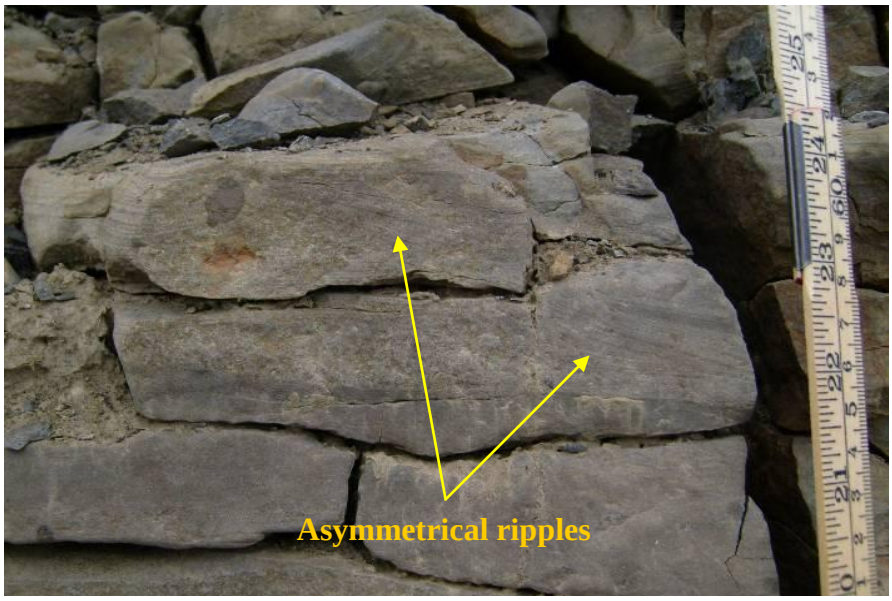

Figure4-5: Asymmetrical ripples in a very fine sand bed at level 14.25m in log N3.

4.2.8 F8 TROUGH CROSS STRATIFIED SANDSTONES

Presence of trough cross stratified sandstone was observed only in one location (level 15.3m in log N3), comprising 12cm of medium sand in the Lower Hollendardalen Formation (Figure 4-6). Its development is fining upward and the palaeoflow direction was identified as beeing towards south-east (Table 4-1).

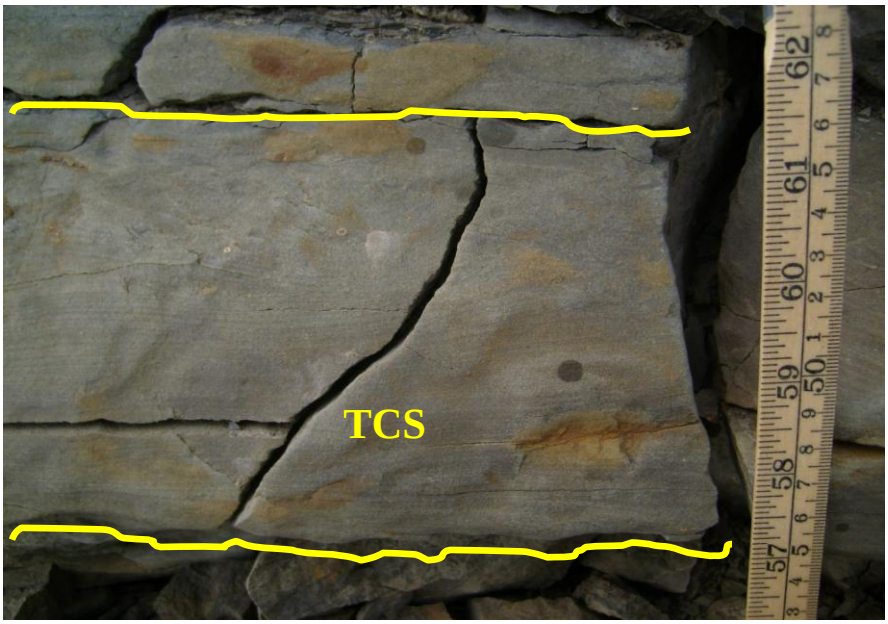

Figure 4-6 Trough cross stratification sandstones (TCS) with erosional bases (indicated in yellow) at level 15.4m in log N3.

4.2.9 F9 HUMMOCKY CROSS STRATIFIED SANDSTONES AND SILTSTONES

The first HCS structure encountered in log N3 was found in a siltstone bed at level 15.5m (Figure 4-1). Its thickness is about 30cm. 3D ripples of 6cm wavelength with organic rich mud lamina were observed. Plant fragments and debris on bedding planes are present. It is separated by an erosional surface towards a trough cross stratified sandstone bed above. The second and much more prominent hummocky cross stratified sandstone unit starting at 17.2m in log N3 comprises two prominent coarsening-upwards sandstone packages of 80cm and 71cm thickness, separated by ~20cm of plane parallel laminated fine sandstone.

In the lower HCS bed, at level 17.2 m it was observed an interval of low angle hummocky cross stratification with wavelengths of 10 to 40cm and amplitudes of 1 to 2cm which overlie a plane parallel-stratified sandstone bed. Each HCS interval has an erosional surface and the coarsening upward trend is developed from very fine to medium sand. The upper part of first HCS interval is poorly sorted with high contents of organic matter, fossil plant leaves, wood imprints, and plant debris along bedding planes (Figure 4-3). Hummocky cross stratification, up to about 50cm wavelength, becomes more pronounced upwards.

Along the erosional base of the second coarsening-upwards unit, the groove cast indicate a palaeoflow direction roughly north-south (Figure 4-7a).

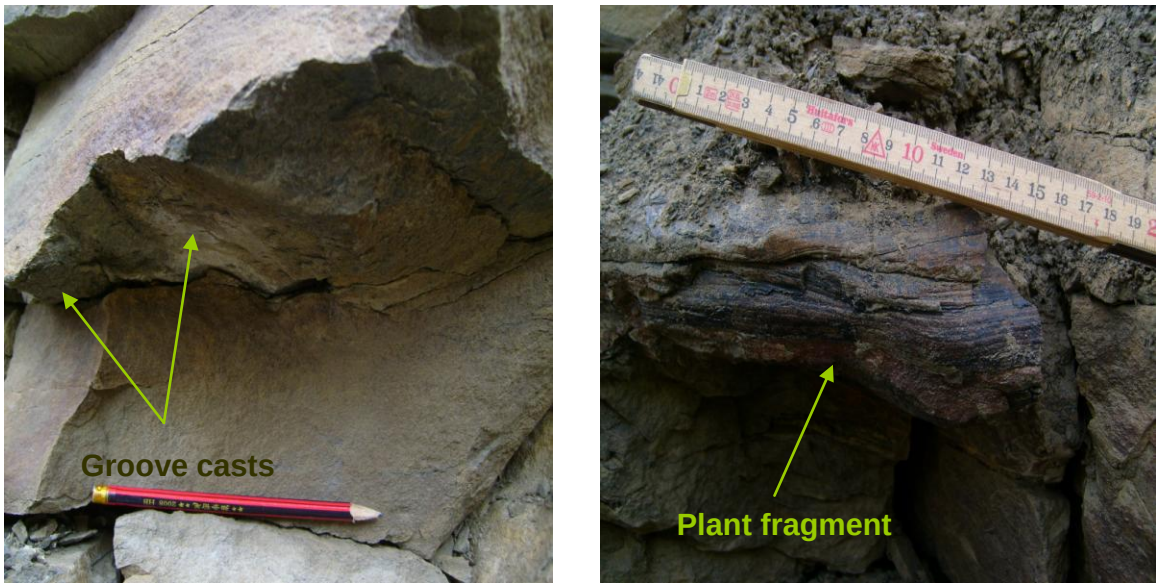

a b

Figure 4-7a: Groove casts and **b:** plant fragment at level 17.7m (Figure 4-1) in section N3.

At level 18m in section N3 an unsorted mica-rich sandstone sediment and the presence of very fine lamination (1mm) suggests a plane parallel stratification facies. Upwards, like in the underlying HCS bed, hummocky cross stratifications of comparable dimensions are developing. In contrast with previous HCS bed, the upper one has less organic matter content and its coarsening-upwards development can be traced from fine to medium sand.

4.2.10 F10 SOFT SEDIMENT DEPORMATION SILTSTONES

From level 19.6m to 20.6m in log N3 soft sediment deformation was observed in a siltstone interval. The unit thickness is about 100cm and presents convolute laminations (Figure 4-8).

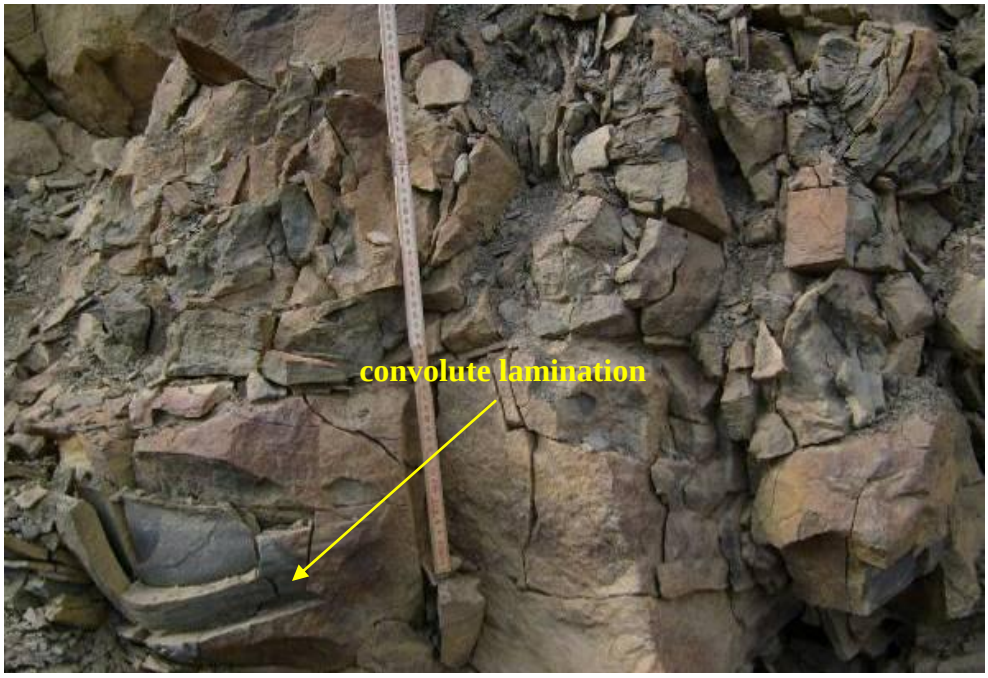

Figure 4-8: Siltstone with soft sediment deformation (at level 19.65m in log N3).

4.2.11 F11 LOW ANGLE CROSS STRATIFIED SANDSTONES

Between 20.7 and ~ 23m in log N3, a well sorted and homogeneous thick interval of low angle cross stratified fine sandstones forms the first 58cm of the interval. At the base it is characterized by the presence of wave ripple cross lamination. Next, two coarsening-upwards beds of low angle cross stratified sandstone are developing upwards from very fine to medium sand. The first interval is moderately bioturbated, includes fine lamina and its coarsening-upward trend develop from fine to medium sand. The thickness is

about 30cm. The upper interval is thicker (140cm) and also comprises low angle cross stratification. In contrast to the underlying interval the upper one is coarsening upwards from very fine to fine sand, moderately sorted and shows occasionally spherical concretions and horizontal bioturbation.

4.2.12 F12 COAL

In the upper part of Hollendardalen Formation, mud was deposited on top of the low angle cross stratified sandstone at 22.9m in log N3. A sharp boundary separates the two lithological units. The coal seam located at level 23.5m is 20cm thick. No root structures have been observed at its base. The reddish sediment below the coal seam might be a paleosol or just recent weathering surface (Figure 4-9).

Figure 4-9: Mudstones with a 20cm thick coal seam at 22.9m in log N3

4.2.13 F13 SIDERITE BEDS AND CONCRETIONS

Siderite units occur both in the upper Hollendardalen Formation and at the base of Gilsonryggen Member. First, 100cm of siltstone at level 23.3m in section N3, rich in plant debris is alternating with sideritic horizons in thinner lamina in the Hollendardalen

Formation below the coal seam. The overlying Gilsonryggen shales contain siderite beds and concretions with thickness up to 20cm (Figure 4-10).

Figure 4-10: Siderite bed at the base of Gilsonryggen Member in section N3

4.3 FACIES ASSOCIATIONS OF SECTION N3, NORDENSKIÖLDFJELLET

Based on features that potentially define particular sedimentary environments and especially on the stratigraphical development of the formations and members, the facies presented above have been grouped into seven facies associations. The section cover the upper part of Grumantbyen Formation to lower part of Gilsonryggen Members and the facies associations are as follows:

FA1. Offshore bars (?) - Upper Grumantbyen sandstones

FA2. Offshore shelf - Marstranderbreen mudstones

FA3. Offshore transition to shoreface - Lower Hollendardalen silt and sandstones

FA4. Foreshore - Mid Hollendardalen sandstones

FA5. Coastal marsh - Upper Hollendardalen mudstones and coal

FA6. Transgressive sands - Upper Hollendardalen sandstones

FA7. Shelf to offshore - Basal Gilsonryggen mudstones

The facies description has been presented in chapters 4.2.1 to 4.2.11. The facies associations and their corresponding facies are summarized in table 4-2.

Table 4-2: Facies associations and facies of section N3.

Facies association	Included facies
FA1. Upper Grumantbyen sandstones	highly bioturbated siltstone and sandstone facies (F1), chert pebbles in bed without erosional surface (F2), chert pebbles as individual clasts (F3).
FA2. Offshore Marstranderbreen mudstone	chert pebbles as individual clasts facies (F3), moderate or non-bioturbated mudstones (F4).
FA3. Lower Hollendardalen silt- and sandstones – offshore transition to shoreface	plane parallel- stratified sandstones (PPS) (F5), wave ripple cross laminated sandstones and siltstones (F6), current ripple cross laminated sandstones and siltstones (F7), trough cross stratified sandstones (F8), hummocky cross stratified sandstones and siltstones (F9), highly bioturbated siltstones and sandstones facies (F1), soft sediment deformed sandstones (F10), moderate to non-bioturbated mudstones (F4).
FA4 Mid- Hollendardalen sandstones – foreshore	low angle cross stratified sandstone (F11), wave ripple cross laminated sandstones and siltstones (F6).
FA5 Upper Hollendardalen mudstone and coal – costal marsh	moderate or non-bioturbated mudstones (F4), coal (F12) siderites beds and concretions (F13).
FA6 Upper Hollendardalen sandstones – transgressive sands	current ripple cross sandstones and siltstone (F7), highly bioturbated siltstones and sandstones (F1).
FA7 Basal Gilsonryggen mudstone - offshore	moderate or non-bioturbated mudstone (F4), siderite beds and concretions (F13).

4.1.2 FA1 UPPER GRUMANTBYEN SANDSTONES – POSSIBLE OFFSHORE BARS (0-4m in log N3)

The Upper Grumantbyen sandstone association forms the lowermost part of log N3. Its lithology comprises highly bioturbated siltstone and sandstones facies (F1), chert pebbles in bed without erosional surface (F2) and chert pebbles as individual clasts (F3). The grain size indicates silt deposits at the base, which change quite abruptly to very fine sandstones towards the top of the successions.

4.1.3 FA2 OFFSHORE MARSTRANDERBREEN MUDSTONES (4-13m in log N3)

The clay and siltstone deposits of Marstranderbreen facies association include the chert pebbles as individual clasts facies (F3) and moderate or non-bioturbated mudstones (F4). The succession shows a fining upward development from silt to clay. The entire association is heavily fractured with a fracture spacing of 3-5cm.

4.1.4 FA3 LOWER HOLLENDARDALEN SILT AND SANDSTONES – OFFSHORE TRANSITION TO SHOREFACE (13-20.7m in log N3)

This facies association comprises the largest number of facies: plane parallel- stratified sandstones (PPS) (F5), wave ripple cross-laminated sandstones and siltstones (F6), current ripple cross laminated sandstones and siltstones (F7), trough cross-stratified sandstones (F8), hummocky cross-stratified sandstones and siltstones (F9), highly bioturbated siltstones and sandstones facies (F1), soft sediment deformed sandstones (F10) and moderate or non-bioturbated mudstones (F4).

4.1.5 FA4 MID-HOLLENDARDALEN SANDSTONES – FORESHORE (20.7-22.8m in log N3)

Two facies are grouped together in this association: low angle cross stratified sandstones (F11) and wave ripple cross laminated sandstones and siltstone (F6).

4.1.6 FA5 UPPER HOLLENDARDALEN MUDSTONES AND COAL – COASTAL MARSH (22.8-24.6m in log N3)

This facies association is entirely composed of mudstones disposed in a gradually coarsening upwards development from clays to siltstones. A coal seam of 20cm thickness separates the lower claystone interval from the upper one, dominated by siltstones. It compriseses three facies: moderate or non-bioturbated mudstones (F4), coal (F12) and siderites (F13).

4.1.7 FA6 UPPER HOLLENDARDALEN SANDSTONES – TRANSGRESSIVE SANDS (24.6-26.4m in log N3)

Current ripple sandstones and siltstones (F7) and highly bioturbated siltstones and sandstones facies (F1) are grouped together in this facies association

4.1.8 FA7 BASAL GILSONRYGGEN MUDSTONES – OFFSHORE (26.4 to top in log N3)

Homogeneous mudstone deposits with occasionally siderite beds mark the abrupt change from Hollendardalen sandstones to Gilsonryggen shale. This facies association constitutes two facies: moderate or non-bioturbated mudstone facies (F4) and siderite (F13).

4.4 SIMPLIFIED FACIES DESCRIPTION OF NORDENSKIÖLDFJELLET 1+2

Section N1+2 were logged (Figure 4-2) by Nagy in 1997 along two gullies (for their location see Figure 1-1). During field work carried out in August 2007 both sections were quickly measured to confirm and update the 1997-log. Particular attention was given to the Hollendardalen Formation, where a sedimentary log was measured. In addition, based on Nagy's field observations, the log N1+2 was extended 28m upwards, in order to include samples located within and above located PETM. In this context detailed facies description and discussion will not be done due to lack of sufficient data.

The 2007 updated log at location N1 (Figure 4-2) started in the uppermost Grumantbyen Formation coarsening-upwards unit at level 12.2m. A detailed log is illustrated in Figure 4-2. The sedimentary unit (Grumantbyen Formation) is similar to

corresponding one from log N3, where high degree of bioturbation probably resulted in the absence of physical sedimentary structures.

The Marstranderbreen Member mudstones contain five coarsening upwards parasequences disposed in a general upward fining succession. The lower part of the Marstranderbreen Member contains chert pebbles as well as occasional mud concretions. Plane parallel lamination becomes increasingly visible upwards, as the degree of bioturbation decreases. A 5 to 10.5cm thick conglomerate bed was observed in the upper Marstranderbreen Member at level 22m in log N1+2 (Figure 4-11).

Figure 4-11: Conglomerate bed (c) in the Marstranderbreen Member at level 22m in log N1+2.

It is matrix supported, poorly sorted with chert clast sizes ranging from less than 1mm to 3cm. The grain shapes vary from angular to well rounded. Several thin fining upwards intervals of very fine sandstones with erosional bases mark the start of the Hollendardalen Formation in log N1+2 at level 23m. The sandstone beds are 1-5cm thick and contain fine mud laminae. On the top of this, 80cm of low angle to parallel bedded very fine to fine sandstones with occasional indications of current ripples are present (Figure 4-12). Wave ripple interval located on the top of this sand unit indicates north-westerly palaeo-transport directions.

Figure 4-12: Parallel bedded, occasionally ripple cross laminated sandstone of the Hollendardalen Formation at level 24.3m in log N1+2.

The overlying 2m of very fine sandstone (Figure 4-2) contains sedimentary structures like ripples cross laminated sandstone, tabular cross stratification and soft sediment deformation with convolute lamination at the top. In the succeeding 3.80m, at level 26.5 in log N1+2, very fine parallel bedded sandstones are preceding a 0.80m bed of hummocky cross stratified very fine to fine sandstone. The top of this, 40cm parallel bedded fine sandstone is followed by 1.6m interval covered by recent scree. The scree is probably covering mudstone beds. Parallel bedded fine sandstones of 1.5m thick developing into 0.80cm of through cross stratified very fine sandstone marks the end of section N1 (Figure 4-2).

From level 35m the N1+2 log was measured at Nordenskiöldfjellet 2 which is located 650m north of Nordenskiöldfjellet 1 (Figure 6-2). After correlation of the hummocky cross stratified interval located in N3 at level 18.5m with the top of N1 section, a ~1.40m claystone deposits occurs in section N2. This suspected low energy interval is followed by ~70cm of tabular cross bedded fine sandstones. The palaeoflow direction indicates transportation to north-west at the base, and to north-east in the upper part of the bed. The top of Hollendardalen Formation is marked by ~2m of plane parallel stratified sandstone at level 38m, 80cm of tabular cross stratified sandstones at level 39m and 60cm interval at level 40m of low angle cross stratified very fine sandstone with distinct rootlets of ~10 cm long at the top (Figure 6-2).

From level 44m up to 72m the log was compiled based on the logs of Nagy from 1997. In the homogeneous shale dominated deposits of Gilsonryggen five siderite beds located at 41.2m, 42.7m 54m, 55.2m and 57.2m are present. The first two siderite beds are 12cm and 14cm in thickness, while the upper three are 10cm, 15cm and 10cm respectively. The presence of three bentonite beds located at 50m, 53.3m and 69.5m in Gilsonryggen Member with various thicknesses (10cm, 2cm and 10cm) should be mentioned.

5. MINERALOGICAL ANALYSIS

The present chapter comprises the mineralogical results and description of data from thin sections, XRD and natural gamma ray. The applied methods were described in chapter 3.5.

5.1 THIN SECTIONS ANALYSIS

Optical microscopy was carried out on polished thin section for both mineralogical description and quantification. From a total number of 49 thin sections, 35 were selected for mineralogical description. In order to get a complete overview the thin sections were selected from all major formations covering N3 and N1+2 sections. These results of the thin section description are briefly summarized in Tables 5-1 and 5-2. The point counting was carried out for all 49 thin sections, but only 35 have been utilized in this study. The data base is presented in appendix 2 and 3.

Table 5-1: Mineralogical description of the thin sections in section N3

Formation / Member	Sample	Lithology from sedimentary logs	Dominating framework configuration	Predominant structures	Average grain size, (mm)	Most common grain shape	Sorting	Comments
Grumantbyen Fm.	s1	siltstone	grain supported	bedding, highly bioturbated	0.10	subangular	moderate	large grains (0.67mm)
	s2	sandstone	grain supported	lamination, bioturbation	0.09	subangular to angular	moderate to well sorted	agglutinated foraminifera
	s3	sandstone	grain supported	thin lamina, moderate bioturbated	0.12	angular	moderate to well sorted	polycrystalline quartz with sutured contacts, high amounts of glauconite
Marstranderbreen Mb.	s4	siltstone	grain supported	moderate bioturbated	0.07	subangular	poorly sorted	-
	s5	siltstone	grain supported	highly bioturbated	0.06	subangular to subrounded	poorly sorted	rich in plagioclase and glauconite, agglutinated foraminifera
	s6	siltstone	grain supported	bedding, lamination, moderate bioturbated	0.09	subangular	moderate to well sorted	rich in glauconite and occasional agglutinated foraminifera
	s7	claystone	matrix supported	bioturbation, bedding	<0.01	rounded	moderate to well sorted	quartz clusters (0.95 mm)
Hollendardalen Fm.	s8	sandstone	grain supported	ripple lamination, moderate bioturbated	0.15	angular	poorly sorted	inhomogeneous, high content of organic matter, plant debris
	s9	sandstone	grain supported	lamination, bioturbation	0.10	subangular	moderate	occasionally clay clasts
	s10	sandstone	grain supported	lamination, bioturbation	0.17	subangular to angular	poorly sorted	polycrystalline quartz with sutured contacts, plant fragments

Table 5-1, continuance.

Formation / Member	Sample	Lithology from sedimentary logs	Dominating framework configuration	Predominant structures	Average grain size, (mm)	Most common grain shape	Sorting	Comments
Hollendardalen Fm.	s11	sandstone	grain supported	parallel lamination	0.27	subangular to angular	moderate	polycrystalline quartz with straight contacts, chert
	s12	sandstone	grain supported	parallel lamination	0.15	angular	poorly sorted	clay clast
	s13	siltstone	grain supported	highly bioturbated	0.05	subangular to subrounded	moderate	rootlets
	s15	sandstone	grain supported	-	0.10	subangular	moderate	bended grains, high amount of biotite
	s16	sandstone	grain supported	bedding	0.14	subangular to subrounded	moderate	clay clasts of larger size than quartz, precipitated iron oxides
	s17	sandstone	grain supported	bedding, lamination	0.13	subangular to angular	poorly to moderate	high concentration of chert and polycrystalline quartz
	s18	claystone	matrix supported	bedding	<0.02	-	-	framboidial pyrite, clay particles mixed with coarser ones
	s19	claystone	matrix supported	fine lamination	-	-	-	coal bed
	s20	siltstone	matrix supported	graded beds, lamination	<0.03	-	-	agglutinated foraminifera
	s22	sandstone	grain supported	bedding	<0.10	subangular	poorly sorted	clay clast bended by coarser grains, alternating beds of fine and coarse sediments
Gilson. Mb.	s24	claystone	matrix supported	bioturbation	<0.02	-	poorly sorted	alternating beds of fine and coarse sediments, large quartz grains floating into matrix
	s28	claystone	matrix supported	-	0.01	-	-	-

Table 5-2: Mineralogical description of the thin sections in section N1+2

Formation/ Member	Sample	Lithology from sedimentary logs	Dominating framework configuration	Predominant structures	Average grain size, (mm)	Most common grain shape	Sorting	Comments
Grumantbyen Fm.	n1	sandstone	grain supported	moderate bioturbated	0.09	subangular to subrounded	moderate	high amounts of glauconite
	n2	sandstone	grain supported	bedding	0.07	subangular to angular	poorly sorted	weathered quartz grains floating into matrix
	n3	sandstone	grain supported	highly bioturbated	0.10	angular	poorly sorted	-
	n4	siltstone	grain supported	highly bioturbated	0.05	subangular to rounded	poorly sorted	whethered quartz grains, occasional pyrite
Marstranderbreen Mb.	n8	siltstone	matrix supported	moderate bioturbated	0.07	subangular	poorly sorted	feldspar and quartz heavily affected by weathering
	n9	siltstone	matrix supported	highly bioturbated	0.06	subangular	poorly sorted	glauconite and agglutinated foraminifera
	n10	siltstone	matrix supported	highly bioturbated, bedding	0.06	rounded	moderate to well sorted	quartz clusters (0.95 mm)
	n11	conglomerate	grain supported	-	0.32	angular	poorly sorted	large grains (0.50->1mm) alternating with smaller ones
Hollendardalen Fm.	n12	claystone	matrix supported	bedding	<0.01	-	moderate to well sorted	heterogeneous, clay beds alternating with coarser ones
	n13	sandstone	grain supported	bedding, bioturbation	0.09	subangular	poorly sorted	quartz grains affected by weathering
	n14	sandstone	grain supported	bedding	0.08	subangular to angular	poorly sorted	very homogeneous, fine sand
	n15	siltstone	matrix supported	bedding	0.05	subrounded to rounded	moderate to well sorted	quartz clusters
	n16	sandstone	grain supported	fine lamina	0.16	subangular to angular	moderate	clay clasts, possible pellets
Gilson. Mb.	n17	sandstone	grain supported	-	0.15	subangualar	moderate to well sorted	homogeneous, polycrystalline quartz with straight crystal boundaries, quartz with inclusions
	n19	claystone	matrix supported	highly bioturbated	<0.01	-	moderate to well sorted	quartz clusters (0.20mm)
	n21	claystone	matrix supported	bedding	<0.01	-	moderate to well sorted	heterogeneous as possible result of bioturbation

The thin section description was focusing on the following features: mineralogical composition, lithology, structure, texture and framework. The following minerals were identified and quantified: quartz (monocrystalline, polycrystalline and chert), feldspar (plagioclase and K-feldspar), muscovite, biotite, pyrite, chlorite, illite and glauconite. Organic matter content, iron oxides and/or hydroxides, forams and clay minerals, as part of the matrix, were also identified and quantified (Appendix 2, 3). The identification of clay minerals from the matrix was challenging, scanning electron microscope (SEM) was used for detailed analysis. In most of the cases, however, clay minerals from the matrix were counted as part of the matrix and not as separate clay minareals. Structure features such as lamination, layering and bioturbation or texture parameters like grain size, grain shape and roundness were subject of investigation. Average grain size was calculated by measuring ten different grains picked randomly from the sample. The thin sections were firstly analyzed individually and thereafter they were grouped according to formation. The petrographical descriptions of the formations in both sections N3 and N1+2 will follow in subchapters 5.1.2 to 5.1.

5.1.2 PETROGRAPHICAL DESCRIPTION OF UPPER PART OF GRUMANTBYEN FORMATION.

The Upper Grumantbyen unit in section N1+2 and N3 is under microscope commonly seen to be composed of grain supported, moderate to highly bioturbated sandstones and siltstones. The average grain size is measured to be around 0.10mm. The sample display large variations in grain shape and sorting, from angular to subrounded and from poorly to well sorted. The mineralogical composition is dominated by quartz which is ~62% in section N3 and only 31% in section N1+2 (Appendix 2 and 3). In both sections monocrystalline quartz is the predominant type of quartz. It can be also noticed a high content of clay matrix; ~16% in section N3 and (46%) in section N1+2. The difference between the two section mineral compositions is related to the different lithologies from where the samples were taken. In section N3, the analyzed samples belong more to sandy units, while in section N1+2 more fine grained rocks were sampled, originally for micropaleontological studies. High amounts of iron oxides, feldspars, organic matter and glauconite were also identified and quantified in the two sections (Figures 5-1 b).

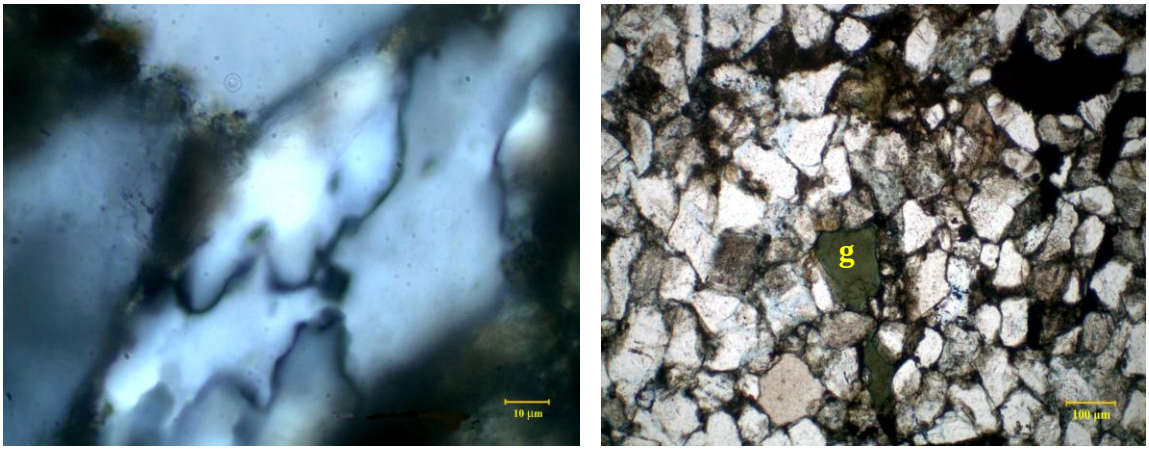

a **b**

Figure 5-1 a): Polycrystalline quartz with sutured contacts in sample s6 and **b):** glauconitic (g) sandstone in sample s6.

The thin section analysis show differences between the mineralogical composition of the two sections (N3 and N1+2). In both sections (N3, N1+2), large individual quartz grains (0.67mm) were present in the matrix and several agglutinated foraminifera were observed. The feldspar grains from siltstone beds of section N1+2 (n2, n3, n4) are heavily weathered and their contact with the matrix is undecipherable. Most polycrystalline quartz observed in thin sections seems to have sutured crystal boundary contacts (Figure 5-1a.).

5.1.3 PETROGRAPHICAL DESCRIPTION OF THE MARSTRANDERBREEN MEMBER.

In thin sections from section N3, Marstranderbreen mudstone deposits show mainly grain supported framework. Common observed features are thin laminae, fine sediments beds containing quartz clusters in alternation with coarser beds and moderate degree of bioturbation (Figure 5-2a). Large quartz grains up to 1mm, are floating in the fine grained matrix. The grains are poorly sorted at the base of the succession but gradually change to moderate and well sorted towards the top of the member. The normal grain shape is from subangular to subrounded, while the size is oscillating from 0.09mm in the siltstones to <0.01mm in the upper most claystones. Some thin sections are rich in plagioclase (albite), while others contain high amounts of glauconite and agglutinated foraminifera, indicating a marine environment (Figure 5-2b). From the selected thin

sections, mineralogical composition is mainly made up of quartz (~50%), feldspar (~5%) mica (~2.5%) and clay minerals (~33%).

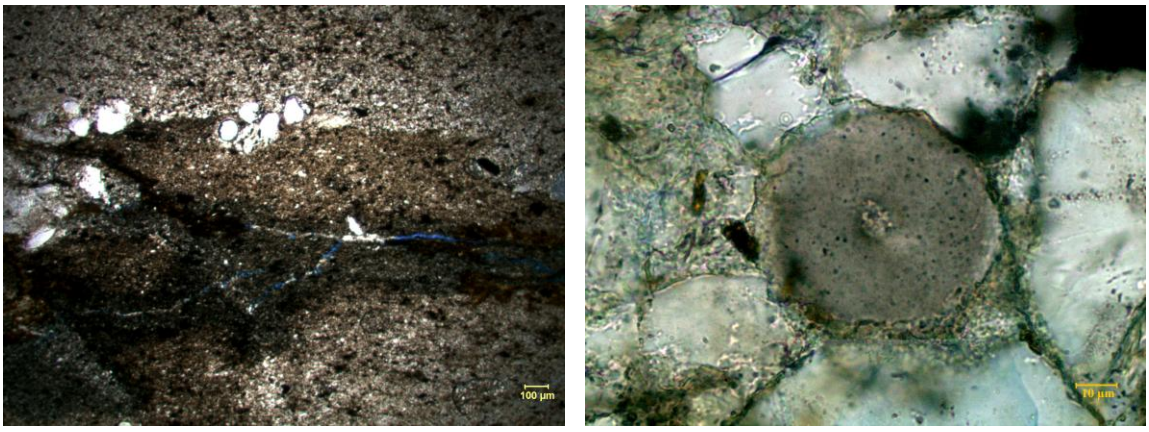

a **b**

Figure 5-2 a): Bedding with quartz clusters in Marstranderbreen siltstone in sample s6 and **b):** agglutinated foraminifer (?) in sample s7 at level ~7m and ~12m respectively in section N3.

Glauconite, pyrite and chlorite are also common minerals observed in this formation (Appendix 2, 3). Organic matter represents ~6.% while iron oxides ~1.8% of total composition. By checking the chemical iron oxides composition under SEM analysis it was determined that hematite is the main iron oxide.

In the samples from section N1+2, in contrast to those from section N3, the framework is mainly constituted of matrix. The average grain size is about 0.06mm with large variations in grain shape; from angular to rounded. The samples are generally poorly sorted. In some samples quartz and especially feldspar grains show traces of weathering. Individual quartz grains (>1mm) or quartz clusters are also common in section N1+2. Large amounts of glauconite and occasionally agglutinated foraminifera were also observed and quantified in the Marstranderbreen Member of section N1+2. In the upper part of Marstranderbreen Member in section N1+2 is present a conglomerate layer (Figure 4-2, 4-11). Under microscope it is seen to be grain supported, with angular grains, poorly sorted and most grains larger than 1.5mm. No structures were visible in the conglomerate.

5.1.4 PETROGRAPHICAL DESCRIPTION OF HOLLENDARDALEN FORMATION

Based on the predominant lithology, the petrographical description of Hollendardalen Formation can be divided in two distinctive lithological units: mudstones and sandstones.

5.1.4.1 HOLLENDARDALEN FORMATION MUDSTONES

Four thin sections have been analyzed from mudstones in section N3; only s13, located at 19.3m depth, in log N3 is from the middle part of the succession, while the other three samples are located at the top of formation (levels 23-25m) (Figure 4-1). The framework generally seems to be matrix supported for the upper clay unit (s18, s19 and s20), while the lower silty unit (s13) is grain supported. The average grain size is slightly higher (~0.05mm) in the lower part (s13) than in the upper one (s18, s19, s20) with values <0.02mm. The quartz concentration also varies; it is ~35% in s13, while only ~19% in the upper most samples. The content of organic matter is generally high, from 16% in s13 to >80% in s19. The amounts of clay minerals are found in higher concentrations than quartz or feldspar (Appendix 2, 3).

The mudstones of Hollendardalen Formation in section N1+2 have been analyzed in thin section only in one sample (n15). It is matrix supported with common grain sizes of ~0.07m. The grains are subrounded to rounded and moderate to well sorted. It is occasionally constituted by quartz clusters which are floating in the matrix. The clay matrix represent >80%, while the quartz, feldspar and mica represent less than 10% of total composition (Appendix 2, 3).

5.1.4.1 HOLLENDARDALEN FORMATION SANDSTONES

Nine thin sections were analyzed from the sand fraction of Hollendardalen Formation in section N3 (Appendix 2 and 3). Approximate 45% of the mineralogical composition is made up of quartz. The clay matrix forms ~39%, while the feldspar concentration is 2.6%, in great contrast to the underlying Grumantbyen Formation (6.9%) and Marstranderbreen Member (~4.9%). The quartz fraction mainly consists of monocrystalline quartz (30.9%), but large amounts of chert (8.1%) are also present. The polycrystalline quartz make up 6.7% of the Hollendardalen sandstones in section N3.

The framework is entirely grain supported with a variety of microstructures observed; fine parallel and ripple lamination, moderate and highly degree of bioturbation and rootlet traces. The heterogeneous composition is illustrated in bedding, where fine grained beds are alternating with coarser ones (Figure 5-3).

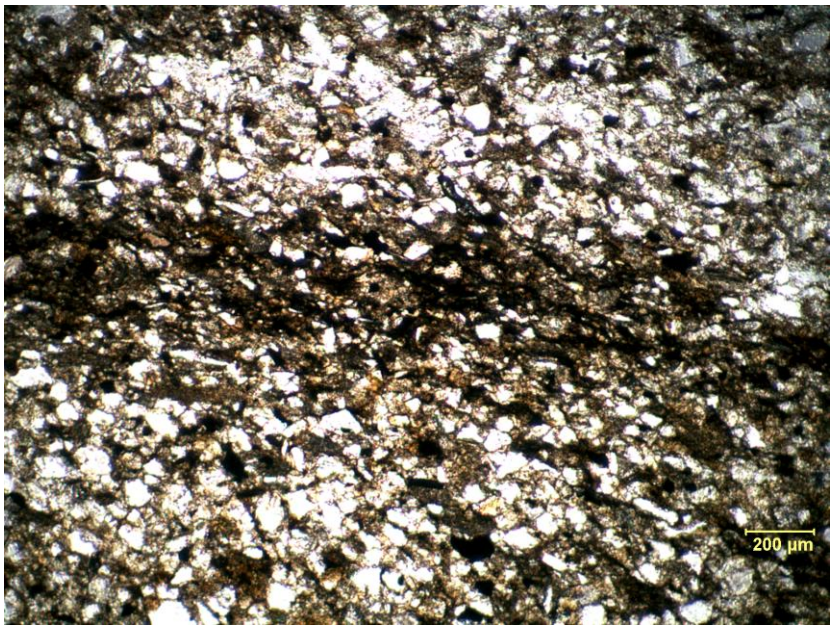

Figure 5-3: Heterogeneity expressing fine and coarse laminae of the Hollendardalen Formation sandstone in s8.

The grain size distribution of the sandstones from Hollendardalen Formation show slight variations with general sizes of 0.10mm or larger. The grains are subangular to subrounded and they are generally moderate sorted. The sandstones are characterized by soft clay clasts occasionally larger than the quartz grains, moderate to high content of organic matter and diagenetically precipitated iron oxides. The clay clasts are generally elongated and subangular to subrounded, and seem to be oriented along the lamination (Figure 5-4a). Wood clasts are also commonly found in some samples, indicating a possible terrestrial influence (Figure 5-4b).

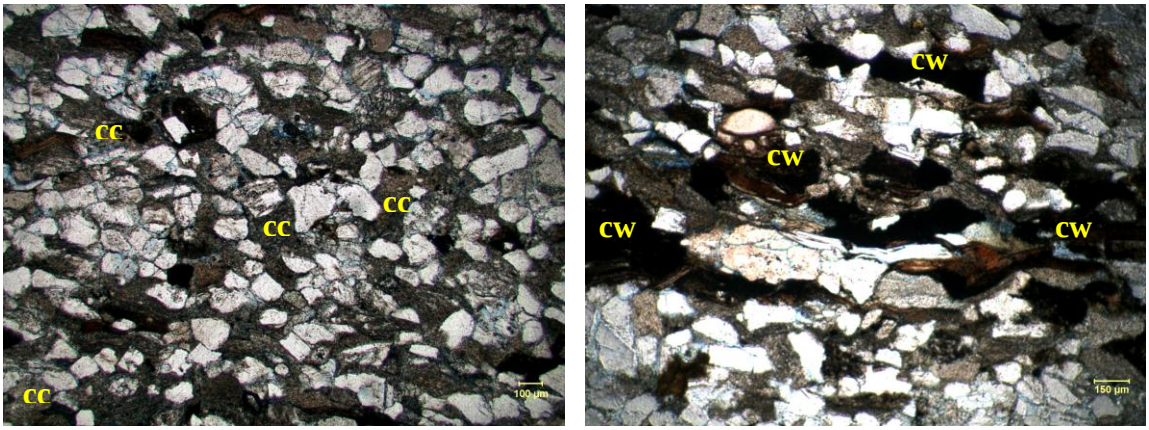

a **b**

Figure 5-4 a): Oriented clay clast (cc) along lamination and **b):** coalified wood (cw) in sample s12.

The presence and preservation of soft clay clasts in the sandstones indicates that the Hollendardalen Formation has only been subject of mild compaction with shallow burial depths and no significant lithostatic stresses. Under the scanning electron microscope (SEM), the matrix composition has been identified as being enriched in iron rich chlorite. Diagenetic kaolinite and high concentration of christalobite (high-temperature polymorph of quartz) are also parts of the matrix according to the SEM analysis (Figure 5-5a and b).

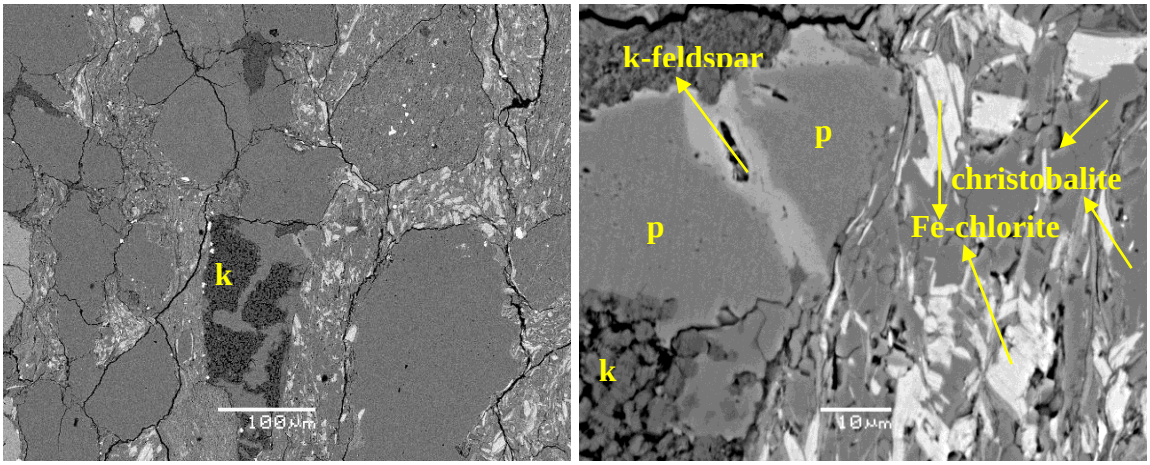

a **b**

Figure 5-5 a): Diagenetic kaolinite (k) general view and **b):** booklets of kaolinite replacing a plagioclase grain (p) in sample s12 (SEM).

In section N1+2 four thin sections were analyzed under the petrographical microscope. They are rich in quartz (52%) and the framework, type of structures, sorting, grain shape and size are generally comparable to those from section N3 (Appendix 2 and 3).

5.1.5 PETROGRAPHICAL DESCRIPTION OF MUDSTONES OF GILSONRYGGEN MEMBER

Totally five thin sections from Gilsonryggen Member have been analyzed from the two sections N3 and N1+2 (Appendix 2 and 3). The framework is entirely matrix supported and the grain sizes mainly less than 0.02mm. Fine graded beds alternate with coarser ones along the base of the member reflecting changes in the energy of the environment. Towards the top of the studied section, lack of bioturbation explain the very homogeneous deposits. (Figures 5-6a and b).

Scanning electron microscope analyses reveal the presence of detrital illite, composed of irregular flakes in the matrix (Figure 5-7). Clay minerals of the matrix represent more than 60% of the thin sections, followed by quartz (~22%) and organic matter (~6%). The quartz grain shape is difficult to distinguish because of their reduced size, but is normally considered angular if are finer than 63μm.

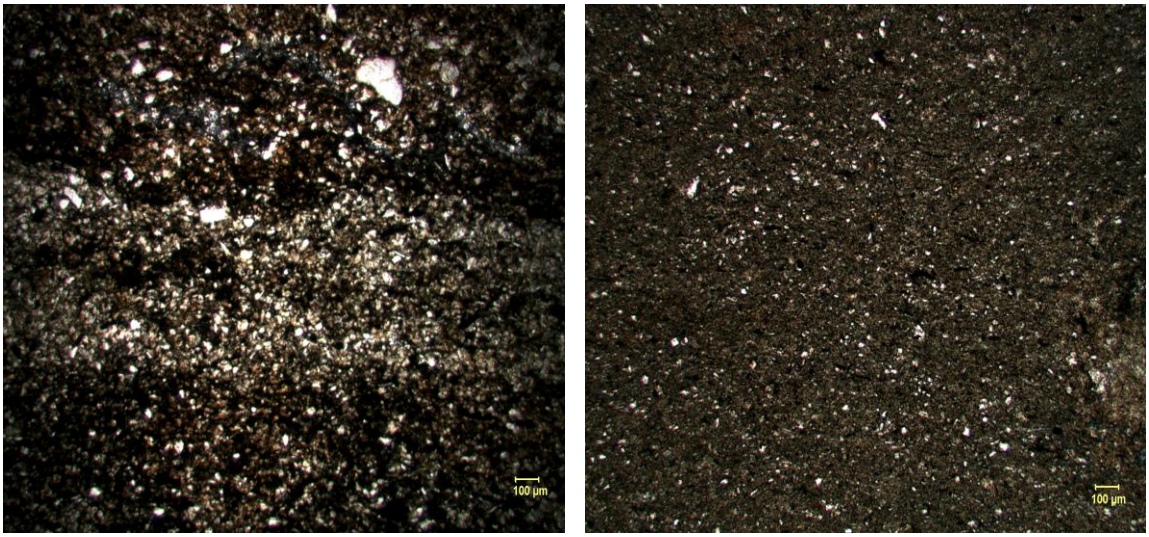

a **b**

Figure 5-6 a): laminated mudstsone in sample s24, **b):** homogeneous mudstone in sample s28.

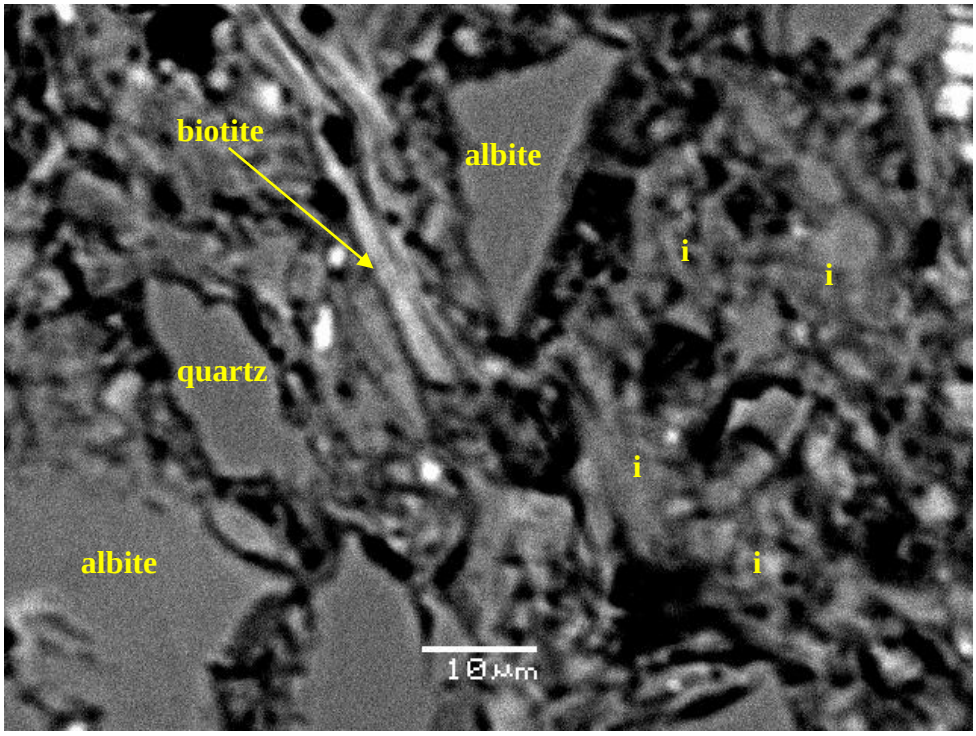

Figure 5-7: Detritital illite (i) identified in basal Gilsonryggen in sample n22 (N1+2) (SEM).

5.2 MINERALOGICAL ANALYSIS BY XRD

Bulk X-ray diffraction analyses were carried out on random powder preparations in order to determine the qualitative and quantitative variations of the mineralogical content of the studied sections. This chapter presents the results of X-ray diffraction analysis (XRD) of both bulk and clay separation analysis ran on totally 56 samples selected both from N3 and N1+2 sections.

5.2.1 XRD - BULK ANALYSIS

In the bulk analysis the following minerals have been identified and quantified: illite (10Å), chlorite and kaolinite peak (7Å), kaolinite (3.58Å), quartz (4.25Å), K-feldspar (3.24Å), plagioclase (3.19 Å), calcite (3.03Å), dolomite (2.89Å), siderite (2.79Å) and pyrite (2.71Å). However, the values of peak reflections represents XRD% and are not real volume percentages. The d-spancing (Å) used in quantification has been selected based on the strongest mineral peak occurrence. Only in the case of quartz, because of the many mineral occurrences at 3.34Å, the second strongest peak (4.25Å) has been used. The detailed results are presented in Appendix 4 and 5. The clay fractions were X-rayed individually after clay separation process and the results are presented in the 5.3

chapter. A short mineralogical description of the two sections (N3 and N1+2) based on the bulk X-ray diffraction percentages follow this paragraph. The summarized mineralogical composition of N3 and N1+2 sections is presented in tables 5.3, 5.4 and figure 5.8 and 5.9.

Table 5.3: Summarized bulk mineralogical values (XRD%) for the studied stratigraphical units in section N3. Raw data in Appendix 4.

Formation & Member	10.0Å	7.0Å	3.6Å	4.3Å	3.2Å	3.2Å	3.0Å	2.9Å	2.8Å	2.7Å	Total
Grumantbyen Fm.	4.1	3.0	1.3	32.1	15.4	40.1	0.6	2.0	0.9	0.6	100
Marstranderbreen Mb.	9.6	11.1	2.0	34.2	10.6	28.8	0.5	1.2	1.2	0.7	100
Hollendardalen Fm. mudstone	15.9	15.3	5.0	40.8	6.0	11.8	1.1	1.5	1.6	1.1	100
Hollendardalen Fm. sandstone	14.4	18.7	5.4	35.7	7.3	14.9	0.8	1.1	1.3	0.6	100
Gilsonryggen Mb.	9.5	10.4	8.0	44.9	3.9	18.6	0.6	1.5	2.0	0.7	100

Table 5.4: Summarized bulk mineralogical values (XRD%) for the studied stratigraphical units in section N (1+2). Raw data in Appendix 5.

Formation&Member	10.0Å	7.0Å	3.6Å	4.3Å	3.2Å	3.2Å	3.0Å	2.9Å	2.8Å	2.7Å	Total
Grumantbyen Fm.	4.2	5.4	1.2	47.4	9.6	28.5	1.1	1.3	0.6	0.8	100.0
Marstranderbreen Mb.	8.0	6.6	2.3	33.9	11.5	27.6	6.5	1.0	1.8	0.8	100.0
Hollendardalen Fm. mudstone	16.9	29.8	5.4	30.9	3.0	9.1	0.9	1.6	1.4	0.9	100.0
Hollendardalen Fm. sandstone	10.8	19.9	4.3	43.6	4.1	12.3	0.9	1.3	1.9	0.8	100.0
Gilsonryggen Mb.	14.6	11.0	6.1	40.3	4.1	16.9	2.4	0.9	1.7	2.1	100.0

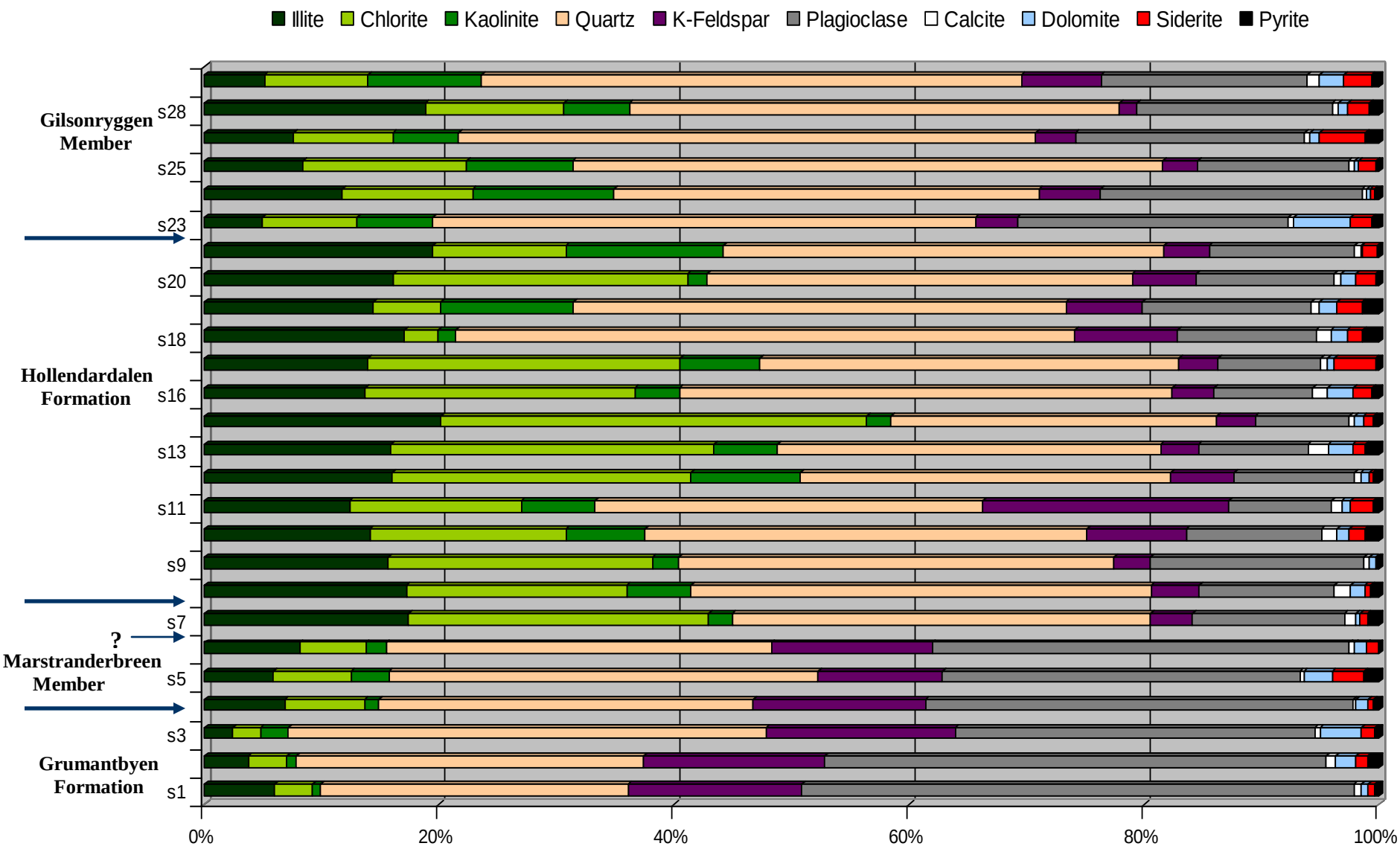

Figure 5-8: XRD% of bulk mineralogy in section N3 (for sample location in the log N3, see figure 4-1).

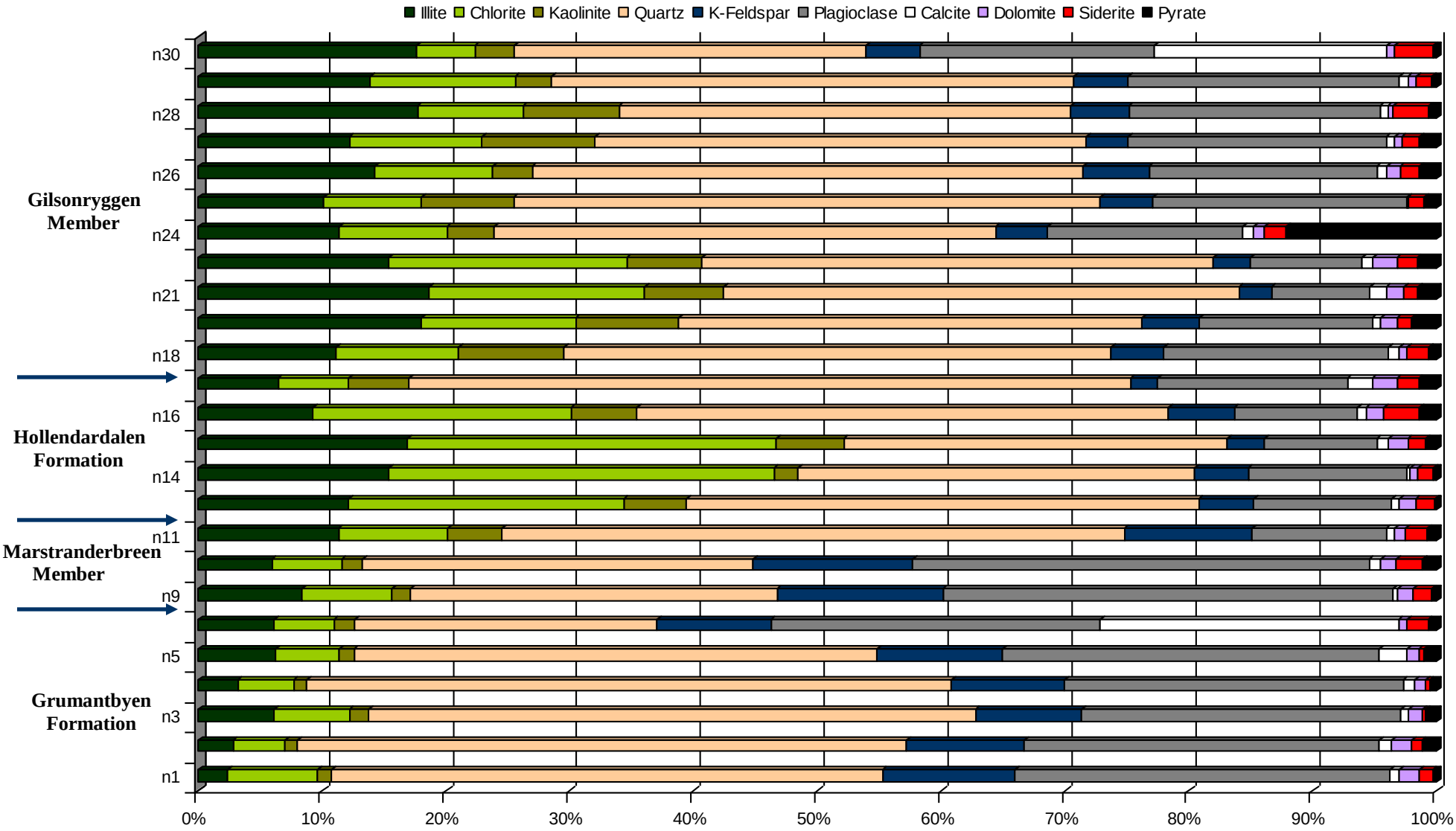

Figure 5-9: XRD% of bulk mineralogy in section N1+2 (for the sample location in the logN1+2, see figure 4-2).

Upper Grumantbyen Formation

Bulk X-ray diffraction analysis of the upper Grumantbyen Formation in section N3 shows high amounts of plagioclase (40 XRD%), followed by quartz (32.1 XRD%) and K-feldspar (15.4 XRD%). From the clay minerals, illite (4.1 XRD%) seems to have the highest concentration, followed by both chlorite and kaolinite (3 XRD%). Dolomite (2 XRD%) has the highest concentration among carbonate class of minerals. The sulfide class is represented by pyrite with 0.6 XRD% (Table 5-3, Appendix 4). In section N1+2 the highest amounts of minerals are given by quartz (47.4 XRD%) followed by plagioclase (28.5 XRD%) and clay minerals with more than 10%. Dolomite (1.3 XRD%) and calcite (1.1 XRD%) are the most common minerals from the carbonate class (Table 5-4, Appendix 5).

Marstranderbreen Member mudstone

The Marstranderbreen Member mudstone mineralogy from XRD estimations shows in section N3 the highest values for quartz (34.2 XRD%), followed by plagioclase (28.8 XRD%) and both chlorite and kaolinite (11.1 XRD%). Siderite (1.2 XRD%) and dolomite (1.2 XRD%) has the highest concentration from carbonate class. In section N1+2 the mineral XRD percentages are similar to those from section N3, only slight differences are observed. However, the calcite (6.5 XRD%) show much higher values (Tables 5-3, 5-4, Appendix 4, 5).

Hollendardalen Formation mudstone

Four samples (s13, s18, s19 and s20) were X-rayed from the mudstones of Hollendardalen Formation in section N3 (Table 5-3, Appendix 4). Except quartz (40.8 XRD%), the mineralogical composition is dominated by clay minerals with high amounts of illite (15.9 XRD%) and both chlorite and kaolinite (15.3 XRD%). Siderite (1.6 XRD%) and dolomite (1.5 XRD%) are in higher concentrations among the carbonate minerals. In section N1+2 (Table 5-4, Appendix 5) only one sample (n15) was X-rayed analyzed from mudstone facies of Hollendardalen Formation. The results show similarities with those from section N3 with a contrast in chlorite and kaolinite concentrations (29.8 XRD%).

Hollendardalen Formation sandstone

Nine samples (s8, s9, s10, s11, s12, s15, s16, s17, s22) from Hollendardalen Formation sandstone section N3 were used in bulk XRD analysis. The results show high amounts of clay minerals even in the sandstones of Hollendardalen with 18.7 XRD% chlorite and kaolinite, 14.4 XRD% illite and 5.4 XRD% kaolinite. SEM analyses in the Hollendardalen Formation thin sections indicate diagenetic kaolinite. Quartz constitutes 35.7 XRD%, while plagioclase and K-feldspar represent together more than 20 XRD% (Table 5-3, Appendix 4). The quartz concentration (43.6 XRD%) is higher in section N1+2 (Table 5-4, Appendix 5), while clay contents of chlorite and kaolinite (19.9 XRD%) and illite (10.8 XRD%) are comparable with those from section N3 (Table 5-3).

Gilsonryggen Member mudstone

The bulk X-ray mineralogical composition of Gilsonryggen Member mudstone in section N3 shows high proportions of quartz (44.9 XRD%) and plagioclase The clay minerals display high values, as are typical for shale lithologies (18.6 XRD%) (Table 5-3, Appendix 4). In section N1+2, illite (14.6 XRD%) has the highest values among the clay minerals, while quartz (40.3 XRD%) and plagioclase (16.9 XRD%) are the main constituents. Pyrite (2.1 XRD%) has higher values than in section N3 (0.7 XRD%) (Table 5-4, Appendix 5).

Related with possible paleoclimate and paleoenvironment discussions, ratios as 7Å/3.57Å (chlorite/kaolinite) or 4.26Å/3.24Å+3.19Å (quartz/feldspar) were investigated (Figure 5-10 and 5-11). The chlorite peak used in these ratios was the 7Å which contains both chlorite and kaolinite.

The identification of illite/smectite interstratification layer has been carried out by using the table for useful reflections for estimating percent illite in illite/EG-smectite proposed by Reynolds (1989). The results show 80% illite. The reflections near 6.5 $^{o}2\theta$ indicate R1 ordering (Reynolds, 1989).

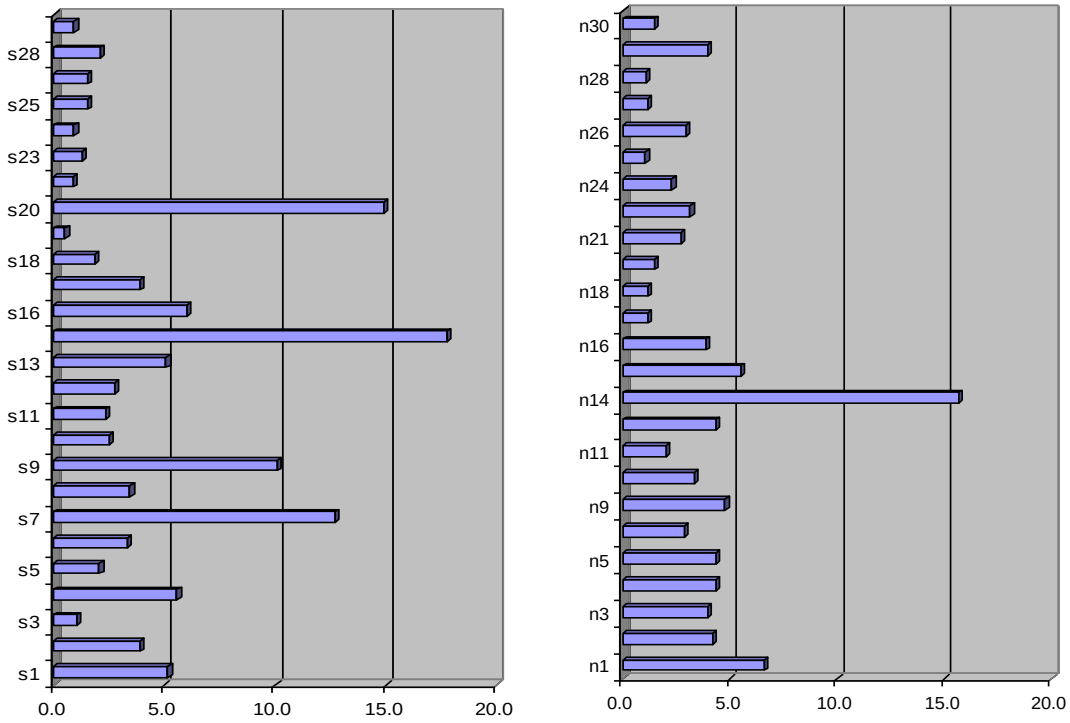

Figure 5-10: 7Å/3.57Å (chlorite/kaolinite) ratio in N3 (left) and N1+2 (right) sections. See figure 4-1 and 4- 2 for location of samples.

The 7Å/3.57Å (chlorite/kaolinite) ratio in N3 records the highest values in Hollendardalen Formation, in samples s15, s20 and s9. The Marstranderbreen Member registers the highest value of 7Å/3.57Å (chlorite/kaolinite) ratio in sample s7, in the upper part of unit. The Gilsonryggen Member presents generally low values of 7Å/3.57Å (chlorite/kaolinite) ratio in section N3 (Figures 5-10, 6-2, Appendix 4). In section N1+2, the 7Å/3.57Å (chlorite/kaolinite) ratio indicates the highest values in Hollendardalen Formation (15.7 in sample n14). However, it can be noticed a more constant distribution of 7Å/3.57Å (chlorite/kaolinite) ratio along section N1+2 compared to section N3. Grumantbyen Formation and Marstranderbreen Member register high values for chlorite, while the Gilsonryggen Member shows the opposite (Figures 5-10, 6-2, Appendix 5).

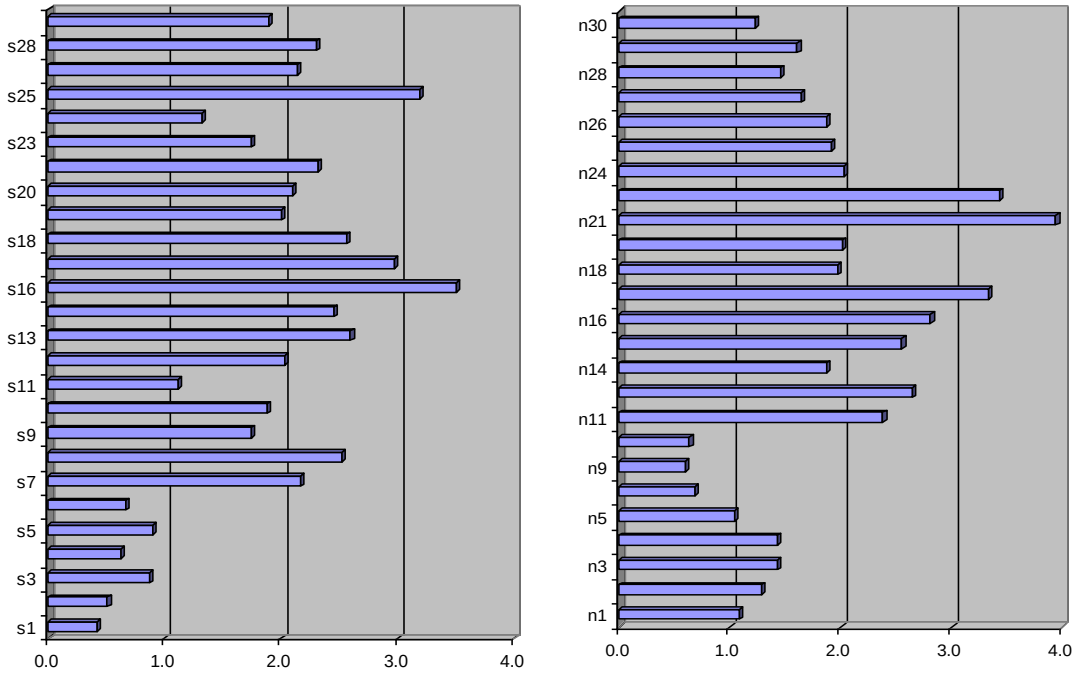

Figure 5-11: 4.25Å/(3.24Å+3.19Å) (quartz/feldspar) ratio in N3 (left) and N1+2 (right) sections. See figure 4-1 and 4- 2 for location of samples.

The 4.25Å/(3.24Å+3.19Å) (quartz/feldspar) ratio in N3 records the highest values in Hollendardalen Formation. The values indicated in Hollendardalen Formation a 4.25Å/(3.24Å+3.19Å) (quartz/feldspar) ratio average of 2.3 (Appendix 4). In Grumantbyen Formation and Marstranderbreen Member, the 4.25Å/(3.24Å+3.19Å) (quartz/feldspar) ratio indicates more feldspar than quartz. The Gilsonryggen Member presents generally higher values of quartz compare to feldspar (Figure 5-11, Appendix 4). In section N1+2, similar trends can be noticed. Hollendardalen Formation and Gilsonryggen Member show higher concentration of quartz compare to feldspar, while in Marstranderbreen Member, feldspar is more prominent. However, in contrast with section N3, the 4.25Å/(3.24Å+3.19Å) (quartz/feldspar) ratio is different in Grumantbyen Formation. Quartz (4.25Å) registers higher concentrations than feldspar (3.24Å+3.19Å).

5.3 CLAY SEPARATION

The methods in clay mineral separation and identification were explained in chapter 3.5.2.2. Seventeen samples were selected from sections N3 and section N1+2 for clay mineralogical analysis (Figure 5-13, Figure 5-14, Table 5-5). As mentioned in the introductory chapter, the reconstruction of paleoclimate at the Paleocene-Eocene time interval constitutes one of the major objectives of the pACE project. Based on this most of the samples (13) were selected in N3 and N1+2 sections from Gilsonryggen Member shale where the PETM (Paleocene-Eocene Thermal Maximum) is considered to be present. As a comparative mudstone unit the Marstranderbreen Member has also been the subject of clay mineralogical analysis (s4, s5, s6 and s7).

The following minerals have been identified in the ethylene glycolated runs: illite (10Å), smectite (17.1Å), chlorite (3.53Å), vermiculite (14.2Å) and kaolinite (3.57Å). The results are presented in figures 5-13, 5-14 and table 5-5.

In the case of chlorite, by checking the relative intensities 00l series in ethylene glycolated run it was observed that iron is probably the main constituent between the silicate and hydroxide octahedral sites. The identification of iron rich chlorite is showed in diffractograms by a weakening of the 001 and 003 reflections relative to the 002 and 004 reflections (Moore and Reynolds, 1989). The 14Å peak in the heated run high temperature (500^{o}C) show less intensities and became broader and diffuse. According to Moore and Reynolds (1989) this is an indication of Fe-chlorite (Figure 5-12). This observation is supported by chemical composition that has been checked under scanning electron microscope (SEM), where chamosite mineral has been identified.

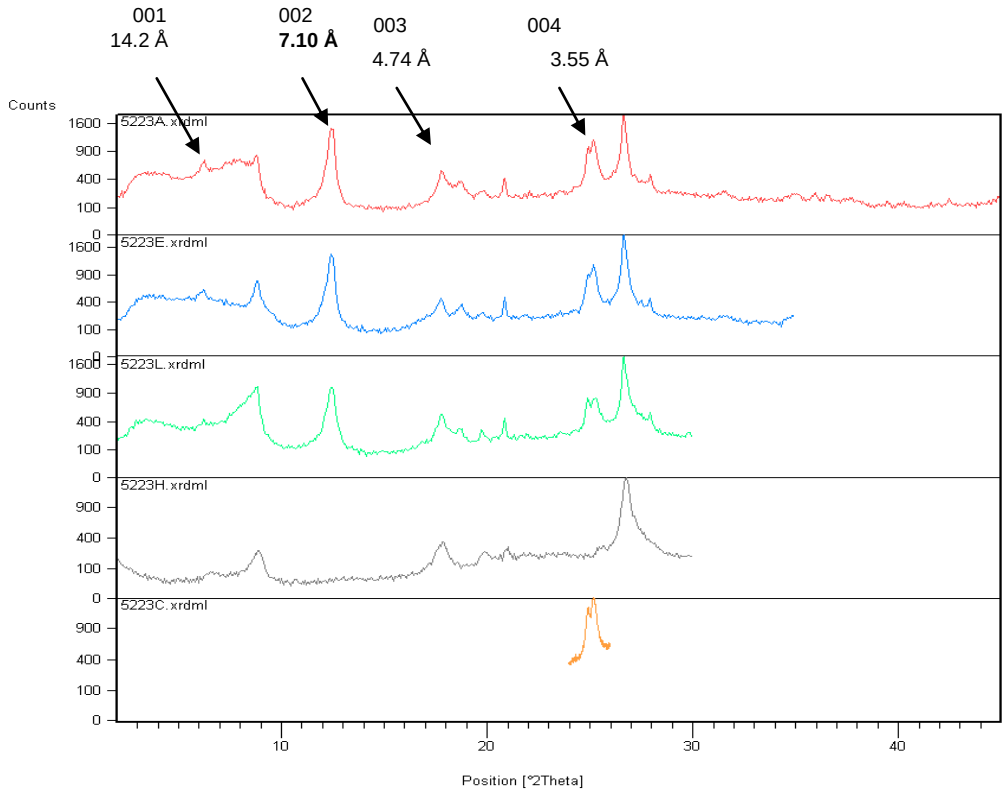

Figure 5-12: XRD diffractogram of s5 sample illustrating the presence of Fe-chlorite in Marstranderbreen Member (A - air dry, E - ethylene glycolated, L – low temperature, H – high temperature, C – slow scan).

The average calculated clay mineral compositions of the clay fractions in the two members (Marstranderbreen Member and Gilsonryggen Member) show the following results:

- clay mineral composition in Marstranderbreen Member is given mostly by chlorite (40.45 XRD%), kaolinite (28.49 XRD%) and illite (26.42 XRD%). Vermiculite (4.22 XRD%) and smectite (0.42 XRD%) have the lowest occurrence (Table 5-5, Figure 5-13, 5-14).
- clay mineral composition in Gilsonryggen Member calculated from both sections (N3 and N1+2) is formed from kaolinite (42 XRD%), chlorite (25.21 XRD%), illite (24.81 XRD%), vermiculite (4.89 XRD%) and smectite (3.08 XRD%) (table 5-5 Figure 5-13, 5-14).

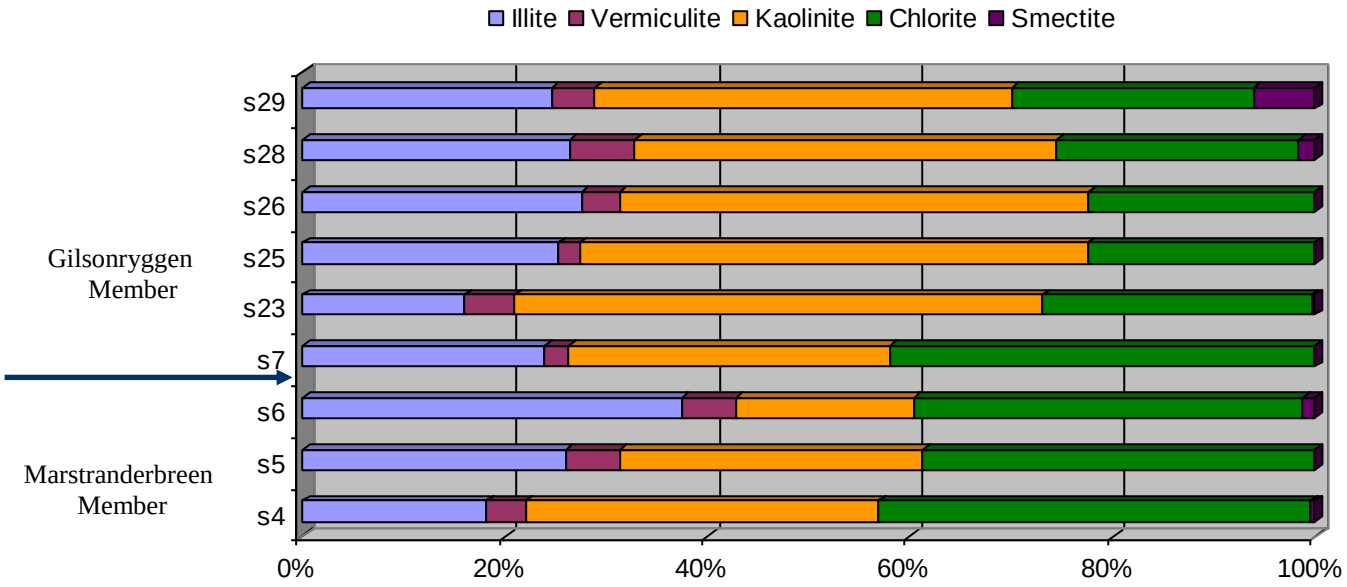

Figure 5-13: Clay mineral estimations (XRD%) plot in section N3 after ethylene glycolated run. s4, s5, s6 and s7 samples are located in Marstranderbreen Mb., while s23, s25, s26, s28 and s29 are located in Gilsonryggen Mb. See figure 4-1 for their location.

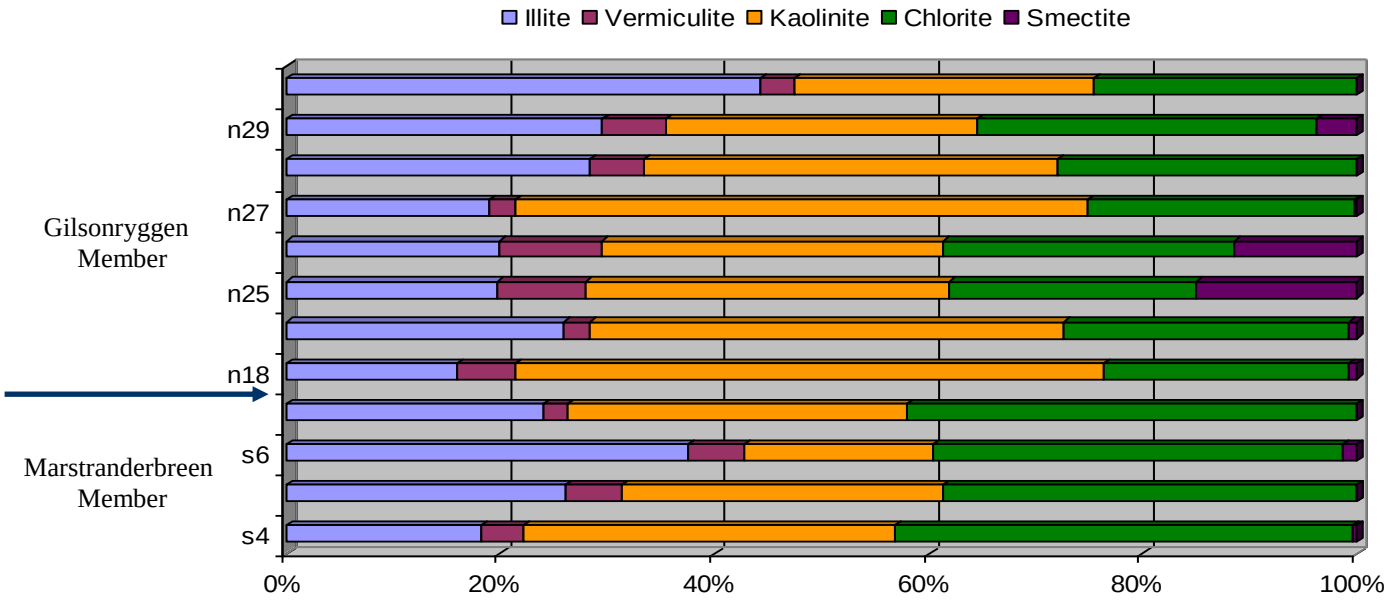

Figure 5-14: Clay mineral estimations (XRD%) plot in section N3 and N1+2 after ethylene glycolated run. s4, s5, s6 and s7 samples are located in Marstranderbreen Mb. in section N3, while n18, n24, n25, n26, n27, n28, n29 and n30 are located in Gilsonryggen Mb. in section N1+2. See figure 4-1 and 4-2 for their location.

By comparing the clay mineralogy composition of the two members (Marstranderbreen and Gilsonryggen) it can be noticed that Marstranderbreen Member contains more chlorite

(3.53Å) and less kaolinite (3.57Å) than Gilsonryggen Member. The vermiculite (14.2Å) and illite (10Å) mineral concentrations do not show any clear difference between the two members. Smectite registers higher concentrations in Gilsonryggen Member compared to Marstranderbreen Member in section N1+2, but generally, has low values in both members.

Table 5-5: Estimation of clay minerals (XRD%) after ethylene glycolated run of the clay fraction.

Member	Sample / Å	10 Å	14.2 Å	3.57 Å	3.53 Å	17.1 Å	Total
Marstrandbreen N3	s5	18.20	3.88	34.84	42.67	0.40	100
	s6	26.05	5.28	29.94	38.72	0.00	100
	s7	37.45	5.38	17.51	38.39	1.27	100
	s8	23.96	2.34	31.66	42.02	0.02	100
	Average	26.42	4.22	28.49	40.45	0.42	100
Gilsonryggen N3	s23	16.00	4.98	52.12	26.60	0.30	100
	s25	25.37	2.03	50.19	22.41	0.00	100
	s26	27.58	3.74	46.31	22.34	0.03	100
	s28	26.36	6.45	41.70	23.90	1.59	100
	s29	24.61	4.25	41.21	23.87	6.04	100
	Average	23.98	4.29	46.31	23.82	1.59	100
Gilsonryggen N1+2	n18	16.02	5.40	54.97	22.92	0.69	100
	n24	25.90	2.38	44.35	26.61	0.76	100
	n25	19.74	8.15	34.06	22.96	15.10	100
	n26	19.88	9.60	31.93	27.15	11.43	100
	n27	18.90	2.43	53.57	24.81	0.28	100
	n28	28.29	5.11	38.62	27.97	0.00	100
	n29	29.56	5.99	29.02	31.61	3.82	100
	n30	44.35	3.11	27.94	24.55	0.05	100
	Average	25.33	5.27	39.31	26.07	4.02	100

In both sections (N3 and N1+2), the calculated chlorite/kaolinite ratio indicates higher values in Marstranderbreen Member compared to Gilsonryggen Member. Furthermore, at the base of Gilsonryggen is observed in both sections (N3 and N1+2) the minimum values of chlorite/kaolinite (3.53Å/3.57Å) ratio. Thereafter, a slight increase of chlorite/kaolinite (3.53Å/3.57Å) is identified upwards in the Gilsonryggen Member in both sections (N3 and N1+2) (Figure 5-15 and Figure 5-16).

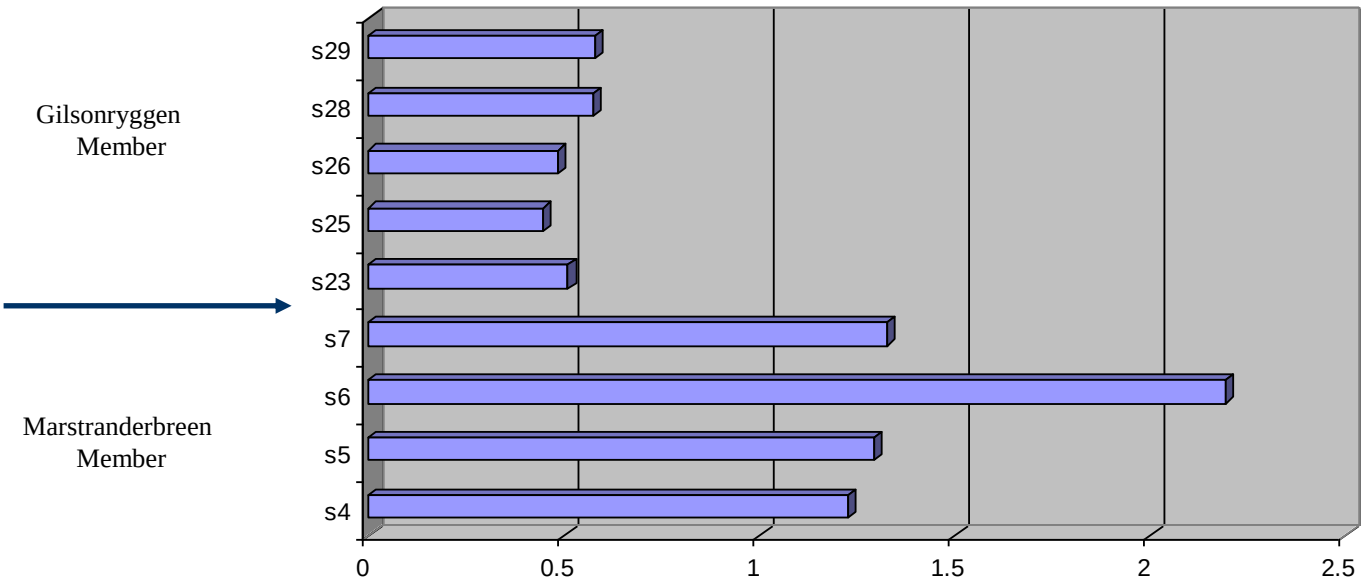

Figure 5-15: chlorite/kaolinite (3.53Å/3.57Å) ratio in section N3 from ethylene glycolated XRD%. See figure 4-1 for location of samples.

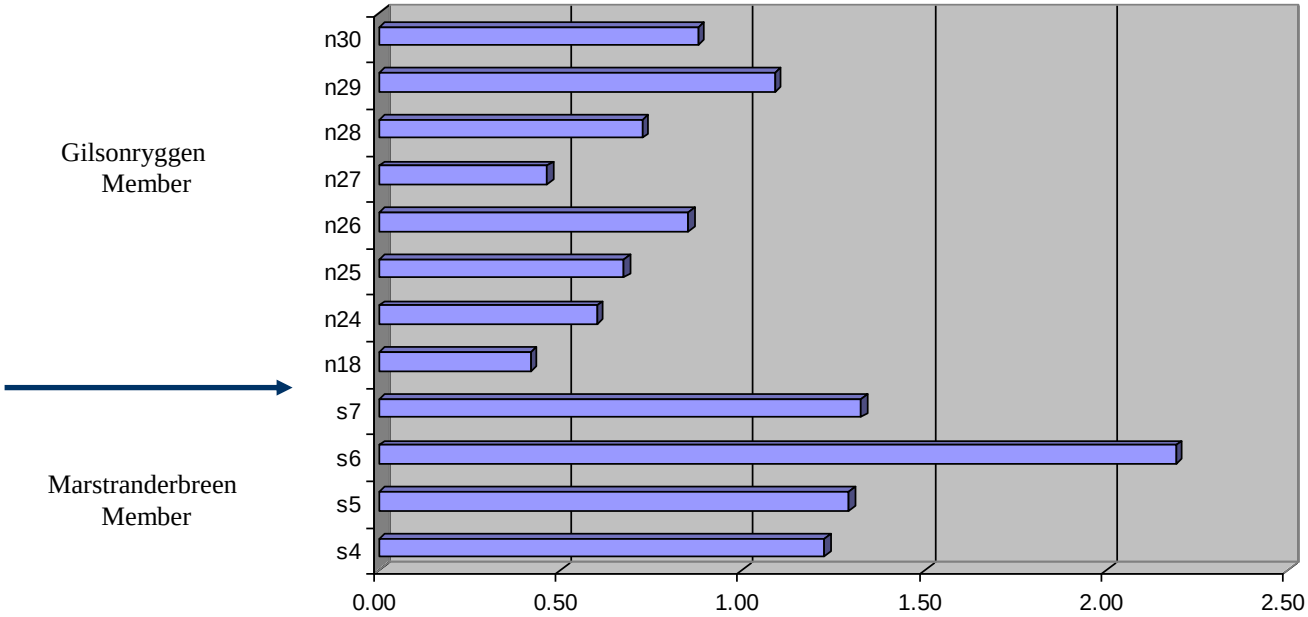

Figure 5-16: chlorite/kaolinite (3.53Å/3.57Å) ratio in section N3 (Marstranderbreen Member) and N1+2 (Gilsonryggen Member) from ethylene glycolated XRD%. See figure 4-1 and 4- 2 for location of samples.

5.4 NATURAL GAMMA RADIATION RESULTS

The natural gamma radiation in rocks essentially comes from three elemental sources: thorium, uranium and of radioactive isotope of potassium ^{40}K (Rider, 1991). The data measured along section N3 are presented in Appendix 6 and figure 5-17. From the gamma ray data a general increase in clay content from the Upper part of Grumantbyen Formation (240c/s) to the Gilsonryggen Member (301c/s) can be observed. It can be also noticed the high values of gamma ray in Hollendardalen sandstone (276c/s) in comparing with the underlying mudstone of Marstranderbreen Member (258c/s). Coarsening and fining-up cycles showing a variation in grain sizes and clay content can be distinguished along section N3 (Figure 5-17).

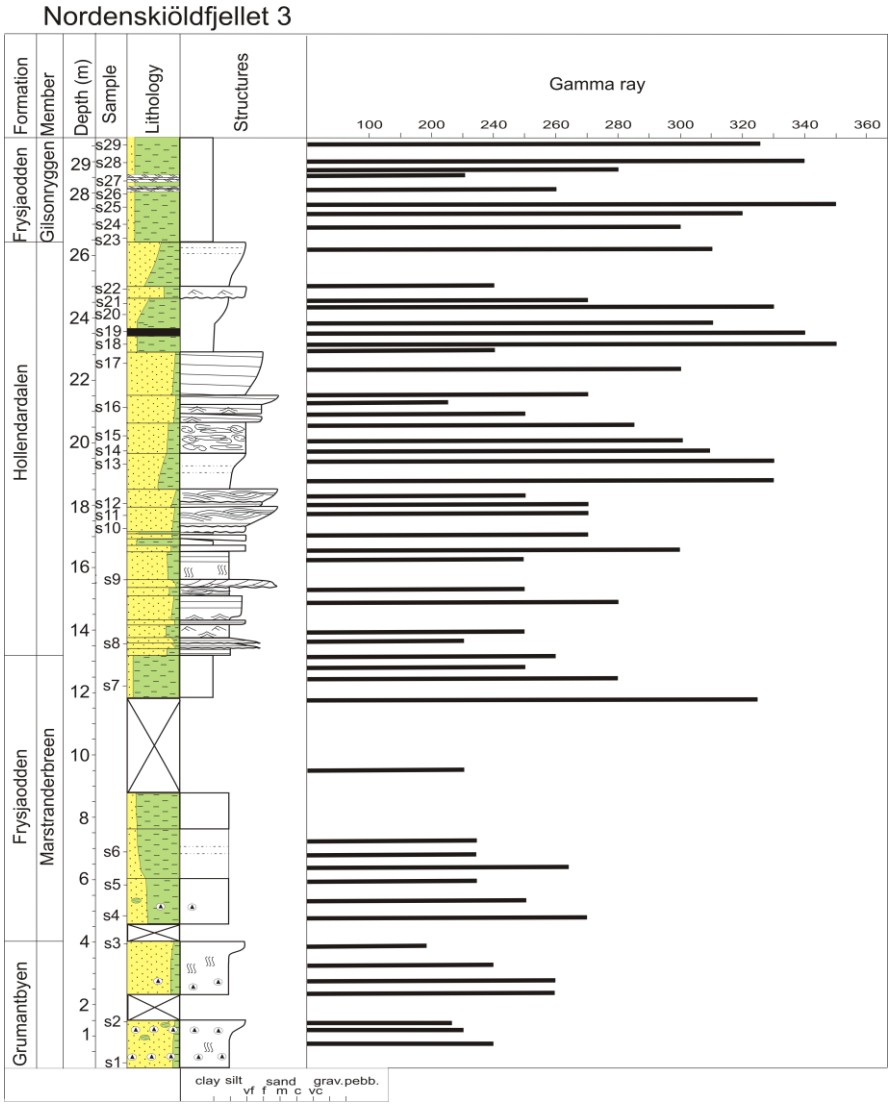

Figure 5-17: Natural gamma ray (counts/second) in section N3.

6. DISCUSSION OF DATA AND RECONSTRUCTION OF DEPOSITIONAL ENVIRONMENT

The discussion of data and reconstruction of depositional environments for the studied succession from upper Grumantbyen to upper Frysjaodden formations are carried out by integration of sedimentary log description (chapter 4), petrography (chapter 5), natural gamma ray data (chapter 5.2.3) and foraminiferal analysis (Rüther, 2007).

In the paleoclimate and paleoenvironment discussion of the studied sedimentary succession, a critical factor was to establish the clay mineral origins. SEM and thin sections analysis disclosed different origins of clay minerals in sections N3 and N1+2. Diagenetic kaolinite was identified in middle Hollendardalen Formation (Figure 5-5), while detrital illite was observed in basal Gilsonryggen (Figure 5-7). Detrital chlorite was observed in the thin sections of Hollendardalen Formation. This information are obviously insufficient to develop a quantitative data base of clay minerals origin in studied area. The origins may be distinguished by isotope dating (Chamley, 1989), but this procedure was not performed in the present study. Therefore, hypothesis of clay minerals provenance are more likely to be debated.

The composition of the clay minerals in the samples reflects the source material, but also the effect of burial diagenesis on the originally deposited clay assemblage along with more recent weathering of the outcrops (Shaw, 1987). The necessary clay mineral information can been gathered from the study area, since depositional environment was controlled by both tectonic and climatic events, as described in chapter 2. Thus, clay minerals might be originated from weathering, detrital and diagenetic processes. Recent weathering is probably minor in the present harsh Arctic climate. Kaolinite can be an early diagenetic result of feldspar and mica, and illite as a product of smectite transformation (Skeide, 1988). Kaolinite can be destroyed during burial, and may be transformed to illite at 3-4 km depth (Bjørlykke et. al., 1986). The illite presence in studied area is most likely clastic and not formed by diagenetic processes, since the estimated depth of Grumantbyen Formation is less than 1500m (Throndsen, 1982). Beside, illite identified in SEM analysis show detrital outlines. This presence of illite may be representative of colder, dry climates, dominated by physical weathering, but could also be derived from alteration of biotite during warmer and more humid conditions (Mallinson et al., 2003). The overall reduced amounts of biotite observed in the thin sections (Appendix 2 and 3) of the Frysjaodden and

Hollendardalen formations as well as the paleoclimate situation of Svalbard during Paleogene, suggest that illile might have formed at least partially from alteration of biotite. Illite could also be clastic, derived from sericitisation of feldspar.

Kaolinite is assumed to form in warm, humid climates on well-drained continental areas, since high precipitation accelerates leaching of parent rocks and support chemical weathering (Murru et al., 2002).

The occurrence of detrital chlorite and illite is rather related with higher latitudes, mainly as a result of enhanced physical erosion of magmatic and metamorphic rocks, while chemical alteration is limited (Brişan and Hosu, 2006). In this context the chlorite/kaolinite ratio can be applied for paleoclimate reconstructions. The recent high Arctic weathering process in Svalbard will result in predominantly mechanical weathering and consequently no serious change in the mineralogy originating from the geological formations. Fossil weathering, however, might have had a major impact on kaolinite formation. The climate of Paleocene-Eocene time interval was generally warmer than today with mean annual temperatures of 15 to 18° C (Schweitzer, 1980) and according to Gaucher (1981) the occurrence of kaolinite may be related with high precipitation and warm soil temperatures (minimum of 15^{o}C). The occurrence of PETM (Paleocene –Eocene Thermal Maximum) could have enhanced chemical weathering and precipitation of kaolinite in some soil profiles.

The primary accumulation of kaolinite in shallow seas, may indicate the proximity of shorelines since the kaolinite grains, being generally larger than the other clayminerals, commonly are deposited closer to the source (Chamley, 1989). Diagenetic chlorite is most often found as a dominant mineral in the zone of deep diagenesis (Skeide, 1988), deeply buried sediments to ranges of 3.5 to 4km (Temperature often >120^{o}C) (Bjørlykke and Aagard 1992). As it was specified, the burial depth of present studied formations is much less, and therefore the presence of chlorite is more likely to be dominated by a detrital origin. Smectite is a hydrated mineral and the rise in temperature and pressure during burial expels water from the interlayers (de Segnozac, 1970). Smectite will disappear at depth around 2-3 km (Dypvik, 1983). However, the very low smectite concentrations in the studied formations cannot be explained by inferring the burial depth. Hillenbrand and Ehrmann (2002) show that detrital smectite can form under a variety of conditions, but generally occurs as a weathering product of mafic to felsic rocks under cool temperatures and moderate precipitation conditions. This statement could better explain the

absence or low concentrations of smectite in N1 and N1+2 since the paleoclimate of the Paleogene period was rather warm and wet.

6.2 UPPER GRUMANTBYEN FORMATION

The upper Grumantbyen Formation is generally fining-up, composed of coarsening upward parasequences of highly bioturbated sandstones and siltstone. The high amount of glauconite in the formation suggests a marine environment with slow rates of clastic accumulation (Müller and Spielhagen, 1990). Glauconite enrichments are typical for low shoreface to shallow shelf environments (Boggs, 2006). Glauconite might be formed by alteration of illite and biotite or organic matter, particularly faecal pellets (Johnson and Reynolds, 1986). The presence of chert pebbles is interpreted by Dalland (1976) possibly to be the result of shoreline ice transportation. Marine algaes within and from littoral environments can lift and be a locally important medium that could have been responsible for the movement of gravel or pebbles (Gilbert, 1984). The chlorite, kaolinite and illite concentrations are reduced in Grumantbyen compared to Hollendardalen Formation (Figure 5-8, 5-9). Considering these clay minerals to be mainly detrital, a more distal source area may be suggested for Grumantbyen Formation compared to Hollendardalen Formation. The distribution is homogeneous with slightly oscillations. According to Robert and Charnley (1990) a worldwide modification of the environment, such as a global cooling or warming, extensive differential settling processes, or early diagenetic modifications of extra or intra-terrestrial materials might have determined a homogeneous and synchronous distributions in the clay mineral successions. The high chlorite/kaolinite ratios suggest a rather cold climate with clastic clay minerals mainly derived from mechanical weathering (Figure 5-10). The quartz/feldspar ratios (XRD%) (Figure 5-11) show high values of K-feldspar and plagioclase compare to quartz. This can be interpreted as unmature mineral compositions of Grumantbyen Formation sandstones, since quartz is more stable than feldspar during normal chemical weathering (Boggs, 2006). By analyzing the thin sections (Table 5-1, 5-2) of the Grumantbyen Formation the degree of sorting and roundness more noted to be generally low, indicating an unmature texture. Both degrees of sorting and roundness increase from immature to mature rocks (Boggs, 2006). The natural gamma ray data show clear evidence of coarsening upward succession with general low to moderate values recorded (Figure 5-17). The high amounts of feldspar observed in the mineralogical analysis

(Table 5-3, 5-4; Figure 5-8, 5-9; Appendix 2, 3, 4 and 5) and low content of illite, mica and organic matter suggest that potassium from feldspar is the main radioactive element (Rider, 1991). However, the presence of glauconite in sandstone may also render the radioactivity (Rider, 1991).

The lack of subaerial sedimentary structures, presence of glauconite and bioturbation and mineralogical analysis, indicate a shallow submerged marine deposition environment.

6.3 MARSTRANDERBREEN MEMBER

The Marstranderbreen Member is composed of moderate to non-bioturbated mudstone forming an overall general fining upward succession from basal siltstone to upper claystone, disposed in several coarsening-up parasequences. The change in bioturbation trend from vertical burrows at the base of formation to horizontal ones towards top is a clear indication of different depositional energy regimes (Reading, 1996). Vertical burrow are generally associated with higher energy environments, while horizontal ones suggest more quiet depositional conditions. The local compositional grain size variations observed in the thin sections support the idea of a dynamic energy system where possible turbiditic flows and/or various degrees of bioturbation are responsible for bedding and occasional presence of quartz clusters.

The presences of a conglomerate bed in section N1+2 (Figure 4-2) supports the idea of a dynamic depositional environment. The pebbles are poorly sorted and rounded indicating a fluid flow process (Boggs, 2006). The erosional surface present at the lower boundary support also this idea (Figure 4-11).

The presence of glauconite and of agglutinated foraminifera observed in thin sections is a clear indicator of marine depositional environments. Foraminiferal diversities show low values with Fisher Alpha index fluctuating between 2.5 to 3.5 and Shannon Weaver index ranging from 1.7 to 2.1 (Rüther, 2007). This reflects a rather restricted than normal marine environment. The gamma radiations values (Figure 5-17) are comparable to the underlying Grumantbyen Formation, with large differences at the top of unit, where the presence of a maximum flooding surface is suspected (Rüther, 2007).

The mineralogical composition of Marstranderbreen Member from both thin sections and XRD% estimations, displays similarities with the composition of the Grumantbyen Formation. The size of the clay fraction, however, is very different and with higher concentrations in the

mudstones of the Marstranderbreen unit (Appendix 2, 3). The amounts of K-feldspar and plagioclase concentrations, as seen in the XRD% of bulk samples, are similar in the two units (Figures 5-8 and 5-9). The chlorite/kaolinite (3.53Å/3.57Å) and quartz/feldspar (4.25Å/(3.24Å+3.19Å)) ratios (Figures 5-15, 5-16 and 5-11) have comparative values to those from Grumantbyen Formation, favorable in both cases to chlorite and feldspar respectively. This information indicates similar paleoclimates conditions and/or similar sources of sediments for both Grumantbyen and Marstranderbreen sedimentary units.

According to Steel et al. (1981) Hollendardalen and Frysjaodden formations represent the first deposits reflecting a change in the tectonic regime from transtensional to transpressional regime along the sheared Western Spitsbergen margin. Concurrently, a change in sediment infill from an eastern to western source occurred. This change in tectonic regime can explain the differences in formation thicknesses between the two sections, related to an early stage of the Spitsbergen orogeny. However, from mineralogical data in both thin sections and XRD no clear evidence of different feeding sources can be observed in the Marstranderbreen Member. A possible transitional regime from transtension to transpression may better characterize Marstranderbreen Member, the lower member of Frysjaodden Formation. Furthermore, these observations better fit with foreland-basin scenario proposed by Bruhn and Steel (2003), where deposition was controlled by the position and height of a thrust-load-generated peripheral bulge with landward-stepping and basinward-stepping parts of an eastward-migrating basin.

Bruhn and Steel (2003) suggest at basin scale the maximum flooding surface for lower Frysjaodden Formation. The microfossil assemblages support this idea. (Rüther, 2007). From sedimentary logs data, petrography (thin sections and XRD), microfossils and natural gamma ray data the Marstranderbreen Member mainly represent offshore shelf deposits accumulated in a restricted basin environment during a transgressive cycle. Mineralogical analyses suggest a distal sediment source area.

6.3 HOLLENDARDALEN FORMATION

Based on lithological variations, the Hollendardalen Formation can be divided in three distinct parts: lower Hollendardalen (13.2-20.7m in log N3), mid Hollendardalen (20.7-26.4m in log N3) and upper Hollendardalen (22.9-24.6m in log N3). This is comparable with section N1+2 (Figure 6-2).

The lower part of the Hollendardalen Formation comprises silt and sand sediments of planar parallel lamination, wave and ripple cross bedding, through cross beds, hummocky cross stratified sandstone and soft sediment deformations displayed in a general coarsening upward successions. The two sand units of fining upward developments located at the base of succession, resemble deposits of the upper flow regime of turbidity currents and may correspond to a B interval in Bouma sequence (Boggs, 2006). A hyperpycnal flow process seems to represent the most probably mechanism in generation of the deposits (Reading, 1996). These processes can be found on gentle slopes in offshore transitional settings. Densities current are created by density differences within water masses (Boggs, 2006). There are several reasons that might create such density differences. For instance, a terrestrial cold water stream can gravitationally transport sediments basinwards. Nearshore, evaporation may generate dense brines that flow seaward along the bottom as an underflow (Boggs, 2006).

The two storm beds located at levels 17.5 and 18.5m (log N3) are rich in plant debris and fragments, which are interpreted to represent reworked shoreface deposits incorporated in the offshore transition zone, since the HCS preservation in the shoreface environment is unlikely (Reading, 1996). The deposition of very fine sandstones with soft sediment deformation on top of the storm beds indicates that the transition (regression) from offshore transition to shallower water, probably shoreface, occurred relatively fast.

The mid Hollendardalen consists of low angle cross stratified sandstone and occasional wave ripple lamination. These facies are common in foreshore environments (Reading 1996).

The upper Hollendardalen comprises both mudstone and sandstone beds. The mudstone is characterized by a coal layer and suspected to represent a maximum regressive surface (Rüther, 2007). The presence of a coal seam in section N3 indicates a high groundwater table, a prerequisite for establishing a coastal marsh environment (Nagy, 2005). In section N1+2 the presence of root structures at a stratigraphical comparable level supports the terrestrial origin of deposits. These sedimentological features might disclose a possible delta top or coastal delta

setting (Reading, 1996). However, no evidence of distributary channels, crevasse splays or levees has been observed in both sections (N3 and N1+2) in Hollendardalen Formation. Therefore, another hypothesis about the origin of these terrestrial dominated deposits can be inferred. A barrier island or coastal beach setting may better characterize these deposits. According to Reading (1996), beach-ridge strandplains are wave-dominated, sand-rich shorelines composed of both strandplain and a beach shoreface. The sand is distributed in this environment both by a number of small rivers and from the shelf along the coast by longshore drift. The Hollendardalen Formation was deposited during a fall in sea level (Rüther, 2007). This observation corroborated with the lack of terrestrial influx in sediment supply fits better with coastal, beach depositional model. According to Reading (1996), for the formation of beach-ridge strandplains, a fall in sea level is required when no river feeding system is present. During a sea level drop, the self sediments are eroded and redeposited as a series of progradating beach ridge. The marine scenario might be trace by association with the framboidal pyrite presence in sample s18, located just bellow the coal seam (Figure 6-2). Periods with active sulphate-reducing bacteria and partly aneorobic conditions at a certain sediment depth and probably carbonate and sulphate-rich waters, is normally responsible for generation of framboidal pyrite (Iordanidis, 2003). This indicates a marine influence in the basin and suggests that the possible coastal beach was not isolated from the marine environment during peat accumulation.

The overlying sandstones of section N3 can be interpreted as transgressive sands deposited during a rise in relative sea level. The presence of an undulating erosional base at level 24.6m in N3 may represent a transgressive surface and the sequence boundary between regressive and transgressive system tracts (Rüther, 2007).

From the above discussion the zones of deposition in Hollendardalen Formation can be interpreted to develop from offshore transition at the base of the formation to shoreface and foreshore towards top. The distributive processes involved in sediment dispersal and accumulation in this shallow marine environment is under discussion. According to Banks (1973) there are three main types of energy source in the offshore to shallow marine zone:

- wave generated and storms;
- semipermanent currents;
- tidal currents

Evidence of wave activity is reflected in the wave ripples of sections N1+2 and N3. However, their scarce occurrence and the small scale of the wave ripples may suggest that wave activity was not the major force in sediment transport.

The action of storm waves is not so easily dismissed. The presence of the two hummocky cross stratified sandstones is clear evidence of their occurrence and influence. Although storms acting at the shoreline, are capable of transporting sediment into offshore areas (Boggs, 2006). Most probably, at least, two big storm periods affected the shoreline, generated the large seaward backflow of water including terrestrial materials like pieces of woods or plant debris. Since storms often will transport sediment away from the shore, the groove casts measured at the based of second upper storm bed indicate an offshore direction as being towards the south.

Semipermanent currents may be longshore or coastal currents, have most likely due to the general setting been responsible for sediment transportation in the studied area. Their occurrence would be likely in the shallowest part of the basin.

Tidal currents are periodical flows which can be recognized by their bipolarity of paleocurrent distributions. No bipolarity data have been noticed in the data, and a major tidal influence is unlikely (Table 4-1, Figure 6-1).

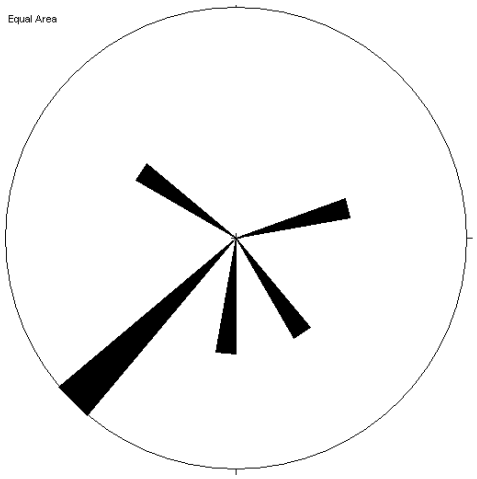

Figure 6-1: Paleocurrent direction measured in Hollendardalen Formation and plotted by using StereoWinFull120 software.

Nevertheless, Banks (1973) suggests that a random distribution of paleocurrents could be due to rotary tidal flow, to changing patterns of flow during the deposition of one unit, or possibly to the strong influence of storms.

It can be concluded that the lower and middle part of Hollendardalen Formation was probably deposited in a marine environment dominated by storms, waves, coastal currents and with only a minor tidal influence.

Petrographical data of the Hollendardalen Formation show important differences and similarities when compared to the underlying Marstranderbreen Member and Grumantbyen Formation. Both plagioclase and K-feldspar are strongly reduced in Hollendardalen while the amount of illite, chlorite and kaolinite is higher (Figure 5-8, 5-9). The chlorite/kaolinite (7Å/3.57Å) ratio resulted from bulk XRD%, shows similarities with the underlying units. Chlorite is dominant, but with higher concentrations in Hollendardalen Formation (Figure 5-10). This might be an indicator of a nearby source area different from that of Grumantbyen Formation (Müller, 1990). A possible scenario can be related to coastal current, storm or wave activities which have eroded the mudstone beds (deposited in a possible lagoonal or backshore environment), and the resultant sediments were transported basinward. This may explain the high clay content in Hollendardalen sandstone Formation.

High contents of illite, chlorite and kaolinite is typical for clastic sedimentary environments with a medium to high dynamics (Chamley, 1989). This is the case in the clay mineral composition of Hollendardalen Formation, where illite and chlorite are the main clay minerals constituents, followed by kaolinite (table 5-5). The high amounts of illite and chlorite reflect a decrease in intensity of hydrolysis, thus an enhancement of mechanical alteration. This is specific for high latitudes environments characterized by generally cold climates (Velde, 1995). In this context the low amounts of kaolinite encountered in Hollendardalen Formation is not surprising, since the paleogeographic position of the Tertiary basin was higher than 65^{o} north latitude in the Paleocene-Eocene time interval.

The quartz/feldspar (4.25Å/(3.24Å+3.19Å)) ratio is in the favor of quartz and this is in contrast with the underlying units of Marstranderbreen Member and Grumantbyen Formation. This can be explained both by a change in degree of weathering or by a change in provenance.

In the SEM analysis, as it has been seen the kaolinite is mainly of authigenic origin. The mode of occurrence is partially interstitial and partially as grain-shape aggregates of clay. Its origin is probably linked to crystallization of introduced minerals from solution or deposition of mineral from colloidal suspensions in the case of interstitial one. Alteration of present minerals (K-feldspar) is the most probable source for kaolinite grain shape aggregates (Shelton, 1964).

The natural gamma radiation in Hollendardalen Formation supports the high clay mineral content records in thin sections and XRD analysis. The values of natural gamma ray radiation disclose the relationship between grain size and shale content (Rider, 1991). The high values recorded in Holledardalen sandstones Formation might thus be explained by the overall fine to very fine grain sizes of sand.

The diversity of foraminifera in Hollendardalen Formation shown by Fisher Alpha index is very low (1.4), and the same is the case with Shannon Weaver index (1.7). This information indicates that deposition of Hollendardalen was, at least in some places, under extremely restricted conditions (Rüther 2007). This is basically available for Hollendardalen Formation mudstones where the samples were collected for micropaleontology analysis.

6.4 GILSONRYGGEN MEMBER

In both sections N3 and N1+2 the sedimentological contact between Hollendardalen Formation sandstone and overlying Gilsonryggen Member shale is sharp. This abrupt transition indicates an erosional phase or a rapid transgression (Rüther 2007). The presence of thin siderite beds in both sections at the base of Gilsonryggen Member (first 5 meters) is associated with occurrence of maximum flooding surface. The maximum flooding surface separates the transgressive systems tract from highstand system tract (Emery and Myers, 1996). It is commonly characterized by extensive condensation and the widest landward extent of the marine condensed facies. Condensation or slow net deposition allows more time for diagenetic reactions to proceed, so condensed sections are commonly enriched in normally rare authigenic minerals such as glauconite, phosphate, pyrite, and siderite. High values in natural gamma ray are also common (Emery, and Myers, 1996).

From the foraminifera analysis, the Fisher alpha and Shanon Weaver diversity index, the most marine condition in the studied section are found in the Gilsonryggen Member shales (Rüther, 2007). The diversity increases upwards in Gilsonryggen Member from values of 3-4 for Fisher Alpha index to 1.8-2 for Shanon Weaver index. The natural gamma ray radiation is normally high, which is common for shale deposits. The reduced amount of mica observed in the thin sections may denote long periods of chemical weathering (Carroll, 1970). This is also supported by the relative high quarts/feldspar ratio, where quartz mineral is dominating (Figure 5-11).

Clay mineral separation analysis has been carried out for the Gilsonryggen Member in both field sections (chapter 5). The average values of the clay mineral composition in the two sections (Table 5-5, Figure 5-15, 5-16) show a consistency which show similar depositional environments and diagenetic mechanisms in section N3 and N1+2. However, the smectite contents in section N1+2 are about 2.5 times larger than in section N3. This can be explained by the samples that were used in section N1+2 were located in the vicinity of bentonite beds, a "contamination" effect. The bentonite beds are fine-grained and probably derived from volcanic activity. An aeolian transport of the volcanic ash is inferred.

In section N3 the few samples analyzed were only collected from basal Gilsonryggen Member where bentonites are absent. By checking the clay matrix composition under SEM, it was observed that detrital illite is composed of irregular flakes and forms the main clay mineralogical constituent along the lower part of Gilsonryggen Member. This is an important observation referring to the PETM discussion.

A special attention with respect to PETM was directed to the variation in the chlorite/kaolinite (7Å/3.57Å) ratio (Figure 5-12, 5-13, 6-3). Even if the samples collected in the two sections do not correspond to exactly the same stratigraphical levels, a comparable chlorite/kaolinite ratio can be noticed (0.51 in section N3 and 0.66 in section N1+2). In both sections the lowest chlorite/kaolinite ratio was observed at the base of Gilsonryggen Member in sample s25 and n18 respectively (Figure 5-12, 5-13, 6-3). In section N3, due to short section sampled, the chlorite/kaolinite ratios display comparative values at the base of Gilsonryggen, while in the section N1+2 a general upward increase of kaolinite compare to chlorite is noticed. This is a clear evidence of an important event.

The presence of nearby located siderite beds indicating a maximum flooding surface should be considered in the PETM discussion. As was specified in the chapter 2.4.2, sea surface water temperature increased with 5-8^{o}C during PETM event. This can be related to basic physics properties of the water which experience an increase in volume directly proportional to temperature. Therefore, the presence of maximum flooding surface might be a climatic consequence. By considering the origin of these two minerals as being clastic, erosional products (as discussed at the beginning of this chapter), then probably chemical weathering developed in a warmer climate may explain a higher concentration of kaolinite along the base of Gilsonryggen Member compared to underlying formations (Figures 5-10, 6-3). Based on these observations and

on the assumption that in section N3 kaolinite is also reduced upwards it can be inferred that the Paleocene-Eocene Thermal Maximum (PETM) is most probably located at the base of Gilsonryggen Member, only 2-4 meters above of underlying Hollendardalen sandstone Formation.

The total average low amount of smectite (XRD%) in the Gilsonryggen Member can be explained by its possible transformation firstly in halloysite and then further to kaolinite in a moist climate (Carroll, 1970). The burial depth estimated by Throndsen (1982), based on vitrinite reflectance studies of coal and dispersed organic matter in Nordenskiöldfjellet area, indicates about 1700m burial for the Grumatbyen Formation. This value can be utilized for the all studied sections since the total thickness is less than 75m. The temperature and depth where smectite starts to degrade coincides with the temperature range of initial quartz precipitation (Bjørlykke and Aagard, 1992). This is controlled by silica concentration in the pore water, as silica being the controlling factor for smectite dissolution. Hower (1981) showed that 80% illite from smectite transformation occurs usually at about 5km depth of burial with temperature higher than 120^{o}C. In this case, the burial depth seems to be too shallow compared to the smectite / illite data. However, Reynolds (1989) quoted few examples from all over the world where smectite-to-illite transition occurs at shallower depths or lower temperatures. A complex reaction, depending on several factors might have controlled the diagenetic change from smectite to illite than temperature and depth might be involved. However, as it was observed in SEM analysis, illite is mostly clastic, formed probably from weathering. Therefore, reworking of older rock formations can be more responsible for illite occurrence than from diagenesis.

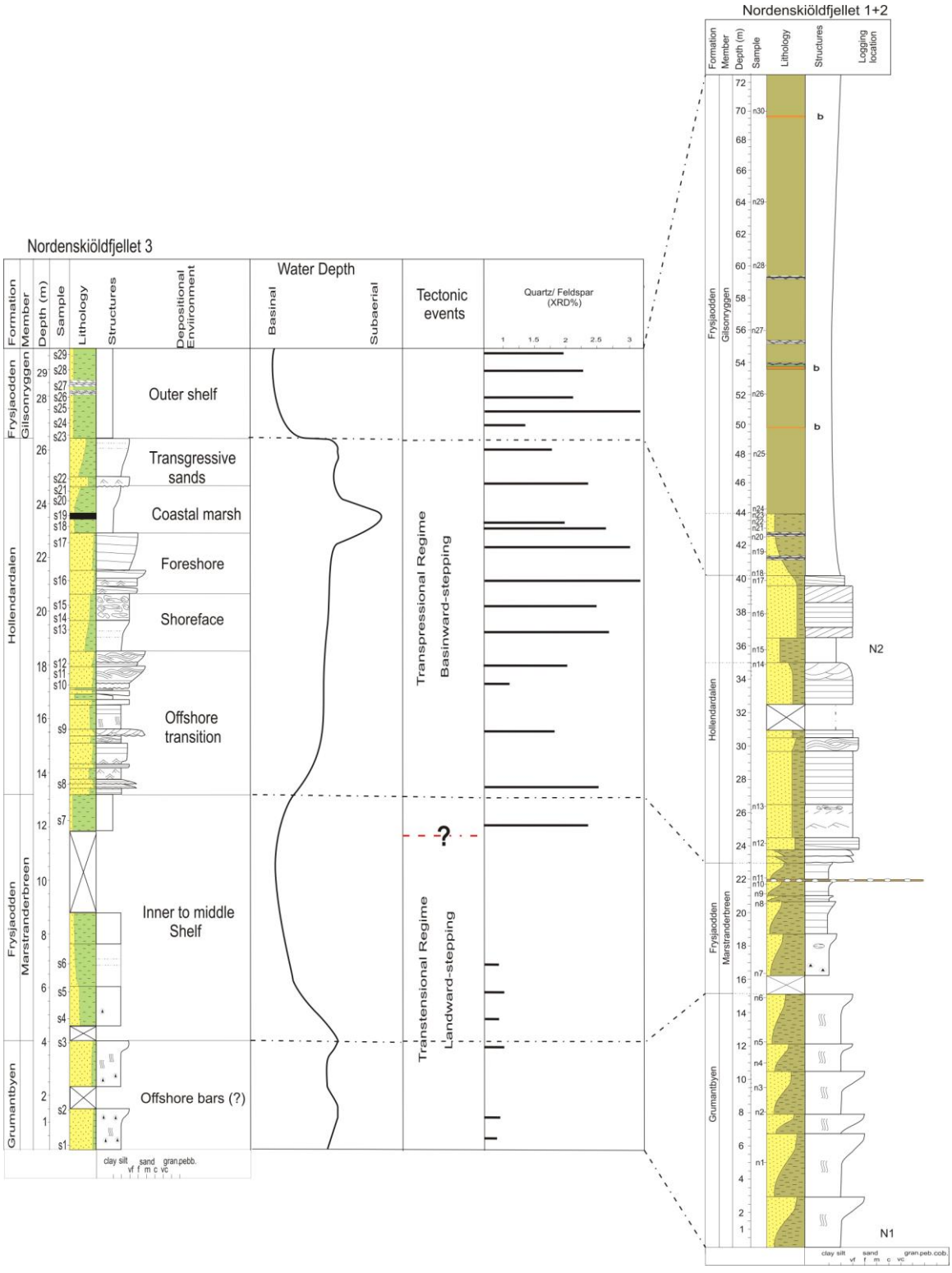

Figure 6-2: Suggested depositional environment, paleowater depth, tectonical regime, quartz/feldspar ratio and correlation of the two logs (N3-left and N1+2-right).

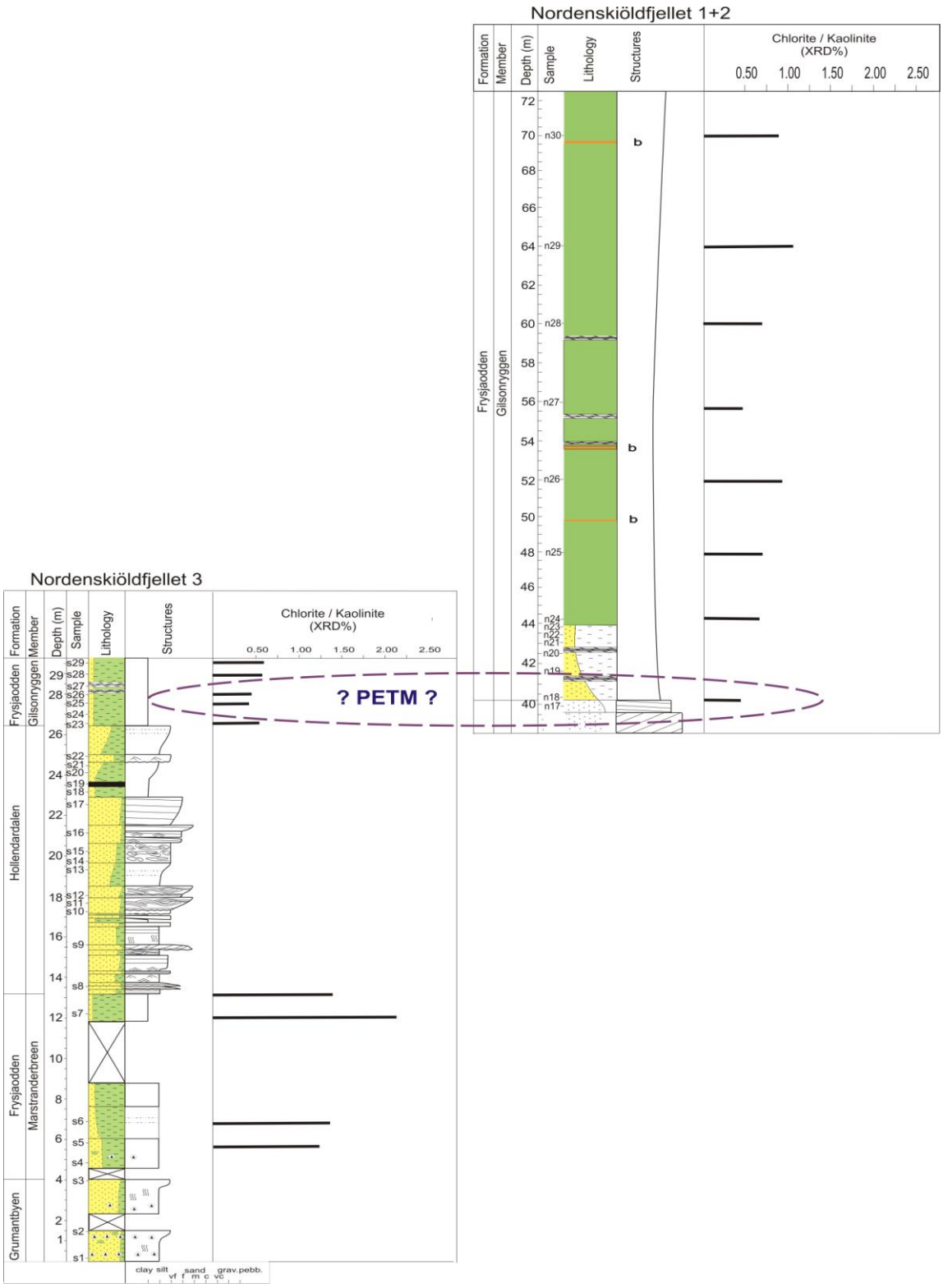

Figure 6-3: Chlorite (3.53Å)/kaolinite (3.57Å) ratio from XRD% clay mineral separations pointing to possible PETM presence.

7 CONCLUSIONS

Results from sedimentary field logging, mineralogical analysis (XRD and thin sections), natural gamma ray and foraminiferal assemblages provide a basis for the reconstruction of depositional environments of the Grumantbyen (upper part), Frysjaodden and Hollendardalen Formations. The following conclusion can be outlined:

1. The upper part of the Grumantbyen Formation represents a massive marine sandstone unit, rich in glauconite, plagioclase and K-feldspar deposited during a general retrogradational regime. It was deposited as coarsening upwards sequences of highly bioturbated sandstones. The presence of chert pebble horizons may suggest both ice rafting and marine algae as transport agent. Chlorite/kaolinite and quartz/feldspar ratio suggest a colder climate interval and distal provenance of sediments. The lack of subaerial sedimentary structures observed in the field corroborated to results from mineralogical analysis, indicate a shallow marine deposition environment, entirely submerged.

2. The Marstranderbreen Member consists of siltstones and claystone disposed in a general fining upward succession. The member represents offshore shelf deposits accumulated during a gradual increase in sea level. The maximum flooding surface in Marstranderbreen Member, determinated by presence of high glauconite concentrations, foraminiferal species diversity, abundance and lithology is located in the upper part of the succession. The mineralogical composition shows similarities with underlying Grumantbyen Formation while the overlying Hollendardalen Formation is more different in composition. This reflects similar sediment sources for both Grumantbyen Formation and Marstranderbreen Member compared to Hollendardalen Formation. Based on mineralogical results, the tectonic inversion regime from transtension to transpression, or from landward-stepping to basin-stepping occurred at the transition between Martranderbreen Member and Hollendardalen Formation. A particular thing is the boundary between Marstranderbreen Member and Hollendardalen Formation where a mismatch between the lithology and the mineralogy is observed. Based on mineralogical results, the boarder between the two units is 1.5-2m below the lithological one.

3. Hollendardalen Formation is interpreted as an offshore transition to shoreface, and foreshore deposits, mainly characterized by marine depositional processes. No clear evidence of a fluvial terrestrial feeder system has been observed. It was deposited during a general lowering of sea level with a maximum regressional surface at the level of the coal seam which is interpreted as part of a beach-ridge strandplain. The upper most part of the Hollendardalen Formation comprises transgressive sands deposited at the initiation of a new transgressive episode.

5. Gilsonryggen Member represents a typical marine shale succession, probably accumulated from pelagic rain. The maximum flooding surface is marked by the presence of siderite beds and foraminiferal fauna at the base of succession. It comprises bentonite beds in the middle and upper part. The clay mineralogy analyses pointed out the PETM occurrence at 2-4 meters above Hollendardalen Formation.

REFERENCES:

Banks N. L. 1973. *Tide-dominated offshore sedimentation, Lower Cambrian, north Norway,* Sedimentology 20, 213-228

Bjørlykke, K., Aagard, P., Dypvik, H., Hastings, D.S. and Harper, A.S. 1986. *Diagenesis and reservoir properties of Jurassic sandstone from the Haltenbanken area, off-shore mid-Norway,* in: Habitat of hydrocarbons on the Norwegian Continental Shelf, Norwegian petroleum Society, No. 2, Graham and Trotman publication, p. 275-286.

Bjørlykke, K. and Aagaard, P. 1992. *Clay Minerals in North Sea Sandstones*. In Houseknecht, D.W. and Pittman, E.D. (eds.), Origin, Diagenesis, and Petrophysics of Clay Minerals in Sandstones, SEPM Special Publication 47, 65-80.

Boggs, S. Jr. 2006 *Principles of Sedimentology and Stratigraphy,* (Fourth Edition), by Prentice Hall ISBN-13 978 0131547285.

Brişan-Bican, N. and Hosu, A. 2006 *Clay mineral association in the salt formation of the Transylvanian basin and its paleoenvironmental significance.* Studia Universitatis Babeş-Bolyai, Geologia, 51 (1-2), 35 – 41.

Bruhn, R. and Steel, R. 2003. *High-resolution sequence stratigraphy of a clastic foredeep succession (Paleocene, Spitsbergen): An example of peripheral-bulge-controlled depositional architecture.* Journal of Sedimentary Research 73 (5), 745-755.

Carroll, D., 1970. *Clay minerals: A guide to their X-ray identification*. Geological Society of America, INC., Boulder, Colorado.

Chamley, H., 1989. *Clay Sedimentology*. Springer, Heidelberg, 620 pp.

Cramer, B. S., and Kent D. V. 2005. Bolide summer: *The Paleocene/Eocene thermal maximum as a response to an extraterrestrial trigger*, Palaeogeogr. Palaeoclimatol. Palaeoecol., 224, 144–166.

Dalland, A. 1976. *Erratic clasts in the Lower Tertiary deposits of Svalbards - evidence of transport by winter ice*. Årbok - Norsk Polarinstitutt 1976, 151.165.

Dallmann, W.K., Midbø, P.S., Nøttvedt, A., Steel, R.J. 1999. *Tertiary lithostratigraphy*. *In*: Dallmann, W.K. (Ed.), Lithostratigraphic Lexicon of Svalbard. Norsk Polarinstitutt, Tromsø, 215– 263.

Dallmann, W.K., Kjærnet, T., Nøttvedt A. 2001. *Geomorphological and quaternary geological map of Svalbard 1:100 000*. Norwegian Polar Institute, Tromsø.

De Segonzac, G. D. 1970. *The transformation of clay minerals during diagenesis and low grade metamorphism* – a review: Sedimentology, 15, p.281-346.

Dickens, G. R., J. R. O'Neil, D. K. Rea, and R. M. Owen 1995, *Dissociation of oceanic methane hydrate as a cause of the carbon isotope excursion at the end of the Paleocene*, Paleoceanography, 10, 965–971.

Dypvik, H. 1983. *Clay mineral transformation in tertiary and Mesozoic sediments from the North Sea*: AAPG Bulletin 67: 1, p. 160-165.

Emery, D., Myers, K.J., 1996. Sequence Stratigraphy. Blackwell, Oxford, 297 pp.

Farley, K.A.; Eltgroth, S.F. 2003. *An alternative age model for the Paleocene--Eocene thermal maximum using extraterrestrial ^{3}He.* Earth and Planetary Science Letters 208 (3-4): 135-148. doi:10.1016/S0012-821X(03)00017-7.

Gaucher, G., 1981. *Les facteurs de la pe´dogenese*. G. Lelotte, Dison, Belgium, 730 pp.

Gilbert, R. 1984 The Movement of Gravel by the Alga Fucus Vesiculosus (L.) on an Arctic Intertidal Flat, Journal of Sedimentary Petrology Vol. 54, No. 2, Pages 463-468.

Harland, W.B. 1969. *Contribution of Spitsbergen to understanding of the tectonic evolution of the North Atlantic region in North Atlantic*, Geology and Continental Drift. AAPG Mem., 12, 817–851.

Hillenbrand, C.-D., Ehrmann, W., 2002. *Distribution of clay minerals in drift sediments on the continental rise west of the Antarctic Peninsula*, ODP Leg 178, Sites 1095 and 1096. In: Barker, P.F., Camerlaenghi, A., Acton, G.D., Ramsay, A.T.S. (Eds.), Proceedings of the Ocean Drilling Program. Scientific Results 178, pp. 1 –29.

Hinz, K., H.-U. Schlüter, A.C. Grant, S.P. Srivastava, D. Umpleby, and Wood, J. 1979. *Geophysical transects of the Labrador Sea: Labrador to Southwest Greenland*, Tectophysics, 59, 151-183.

Hower, J., 1981. Shale diagenesis. In: Clays and the Resource Geologist. I.J. Langstaffe (ed.). Mineralogical Association of Canada, Short Course Handbook, 7, 60-80.

Iordanidis, A., Georgakopoulos, A. 2003. *Pliocene lignites from Apofysis mine, Amynteo basin, Northwestern Greece: petrographical characteristics and depositional environment*. International Journal of Coal Geology 54, 57– 68.

Johnsson, M. J. and Reynolds, R. C. 1986. *Clay mineralogy of shale-limestone rhythmites in the Scaglia Rossa (Turonian-Eocene),* Italian Apennines. J. Sediment. Petrol., 56: 501-509.

Katz, M. E., Pak, D. K., Dickens, G. R., & Miller, K. G. 1999. *The Source and Fate of Massive Carbon Input During the Late Paleocene Thermal Maximum*. Science 286 (November): 1531-3.

Kelly, D. C., T. J. Bralower, J. C. Zachos, I. Premoli Silva, and E. Thomas 1996, *Rapid diversification of planktonic foraminifera in the tropical Pacific (ODP Site 865) during the late Paleocene thermal maximum*, Geology, 24, 423–426.

Koch, P. L., J. C. Zachos, and P. D. Gingerich 1992, *Correlation between isotope records in marine and continental carbon reservoirs near the Palaeocene/Eocene boundary*, Nature, 358, 319– 322.

Kurtz, A., Kump, L.R., Arthur, M.A., Zachos, J.C., and Paytan, A., 2003. *Early Cenozoic decoupling of the global carbon and cycles*. Paleoceanography, 18 (1090, doi:10.1029/2003PA000908).

Livšic, J.J. 1967. *Tertiary deposits in the western part of the Archipelago of Svalbard*. *In* Sokolov, V.N. (ed). Materialy po stratigrafii Špicbergena. Leningrad: NIIGA, 185-204.

Livšic, J.J. 1974. Paleogene deposits and the platform structure of Svalbard. *Norsk Polarinstitutt Skrifter* 159, 1-50.

Major, H. and Nagy, J. 1964. *Adventdalen. Geologisk kart*. Norsk Polarinstitutt.

Major, H. and Nagy, J. 1972. Geology of the Adventdalen map area. *Norsk Polarinstitutt Skrifter* 138, 1-58.

Mallinson, J. D., Flower, B., Hine, A., Brooks, G., Garza, M. R. 2003. *Paleoclimate implications of high latitude precession-scale mineralogic fluctuations during early Oligocene Antarctic glaciation*: the Great Australian Bight record, Global and Planetary Change 39, 257–269

Mehra, O. P. and Jackson, M.L. 1960. Iron oxide removal from soils and clays by a dithionite-citrate system buffered with sodium bicarbonate: in *Clays and Clay Minerals, Proc.7th Natl. Conf., Washington, D.C., 1958,* Ada Swineford, ed., Pergamon Press, New York, 317-327. Stumm, W. and Morgan, J. J. (1981) *Aquatic Chemistry*

Moore, M. D. and Reynolds, JR., 1989. *X-ray Diffraction and the identification and analysis of clay minerals*, Oxford University Press.

Moran, K., Backman, J., Brinkhuis, H., Clemens, S.C., Cronin, T., Dickens, G.R., Eynaud, F., Gattacceca, J., Jakobsson, M., Jordan, R.W., Kaminski, M., King, J., Koc, N., Krylov, A., Martinez, N., Matthiessen, J., McInroy, D., Moore, T.C., Onodera, J., O'Regan, M., Palike, H., Rea, B., Rio, D., Sakamoto, T., Smith, D.C., Stein, R., St John, K., Suto, I., Suzuki, N., Takahashi, K., Watanabe, M., Yamamoto, M., Farrell, J., Frank, M., Kubik, P., Jokat, W. and Kristoffersen, Y. 2006. *The Cenozoic palaeoenvironment of the Arctic Ocean*. Nature 441 (7093), 601-605.

Müller, R.D., Spielhagen, R.F., 1990. *Evolution of the Central Tertiary Basin of Spitsbergen*: towards a synthesis of sediment and plate tectonic history. Palaeogeography, Palaeoclimatology, Palaeoecology 80, 153– 172.

Murru, M., Ferrara, C., Da Pelo, S., Ibba, A. 2002. *The Palaeocene–Middle Eocene deposits of Sardinia (Italy) and their palaeoclimatic significance.* Dipartimento di Scienze della Terra, Via Trentino 51, 09127 Cagliari, Italy.

Myhre, A. M., Eldholm, O. and Sundvor, E. 1982. *The margin between Senja and Spitsbergen Fracture Zones*: Implications from plate tectonics *Tectonophysics* 89, 33-50.

Nagy, J., Kaminski, M.A., Kuhnt, W. and Bremer, M.A. 2000. *Agglutinated Foraminifera from Neritic to Bathyal Facies in the Palaeogene of Spitsbergen and the Barents Sea*. *In* Hart, M.B., Kaminski, M.A. and Smart, C.W. (eds). Proceedings of the Fifth International Workshop on Agglutinated Foraminifera: Grzybowski Foundation Special Publication, 7, 333-361.

Nagy, J. 2005. Delta-influenced foraminiferal facies and sequence stratigraphy of Paleocene deposits in Spitsbergen. *Palaeogeography Palaeoclimatology Palaeoecology* 222 (1-2), 161-179.

Pagani, M., K. Caldeira, D. Archer, and J. C. Zachos 2006, *An ancient carbon mystery*, Science, 314, 1556– 1557.

Panchuk, K., Ridgwell, A. and Kump L.R. 2008. *Sedimentary response to Paleocene-Eocene Thermal Maximum carbon release: A model-data comparison,* Geology Vol. 36**,** 315-318.

Reading, H.G. 1996. *Sedimentary environments: processes, facies, and stratigraphy*. 3rd ed, Oxford: Blackwell Science Ltd.

Rüther, C. D. 2007. *Delta influenced Paleogene depositional environments of the Frysjaodden and Hollendardalen formations*, University of Oslo (Unpublished Master Thesis).

Rider, M.H. 1991. *The geological interpretation of well logs*. –Rev. ed., Whittles Publishing, Caithness 57-122.

Robert, C. and Charnley, H., 1990. *Paleoenvironmenta! significance of clay mineral associations at the Cretaceous-Tertiary passage.* Palaeogeogr., Palaeoclimato!., Palaeoeco!., 79: 205-219.

Röhl, U. T. Westerhold, T. J. Bralower, and J. C. Zachos 2007. *On the duration of the Paleocene-Eocene thermal maximum (PETM),* Geochem. Geophys. Geosyst., 8, 12002, doi:10.1029/2007GC001784.

Schweitzer, H.-J. 1980. *Environment and climate in the Early Tertiary of Spitsbergen*. Palaeogeography Palaeoclimatology Palaeoecology 30, 297-311.

Shaw, H. F. 1987.Clays and their effects in source and reservoir rocks. Short course, 17-19 June 1987, Department of Geology, Imperial Collage of science and technology, London, 50 pp.

Shelton, J. W.1964. *Authigenic kaolinite in sandstone,* Journal of Sedimentary Research; SEPM Society for Sedimentary Geology, v. 34; no. 1; p. 102-111.

Skeide, M. 1988. *A sedimentological and mineralogical study of the lower cretaceous deposits in the Viking Graben, Northern North Sea*. University of Oslo. (Unpublished Candidate Scient Thesis).

Sluijs, A. Röhl, U., Schouten, S., Brumsack, H. J. Sangiorgi, F., Damsté S. S. J., and Brinkhuis H. 2008. *Arctic late Paleocene–early Eocene paleoenvironments with special emphasis on the Paleocene-Eocene thermal maximum (Lomonosov Ridge, Integrated Ocean Drilling Program Expedition 302).* Paleoceanography, Vol. 23, PA1S11 doi:10.1029/2007PA001495.

Smith, F. A., Wing, S. L., Freeman, K. H. 2007. *Magnitude of the carbon isotope excursion at the Paleocene–Eocene thermal maximum: The role of plant community change*. Earth and Planetary Science Letters 262, 50–65.

Spencer, A.M., Home, P.C. and Berglund, L.T. 1984. *Tertiary structural development of the western Barents Shelf,* Tromso to Svalbard. In: Petroleum Geology of the North European Margin (Ed. A.M. Spencer), Norwegian Petroleum Society, Graham and Trotman, London 199–209.

Steel, R.J., Dalland, A., Kalgraf, K., Larsen, V., 1981. *The central Tertiary basin of Spitsbergen—sedimentary development in a sheared margin basin*. In: Kerr, J.W., Fergusson, A.J. (Eds.), Geology of the North Atlantic Borderlands, Memoir Canadian
Society of Petroleum Geologists, vol. 7, 647– 664.

Steel, R.J., Gjelberg, J., Helland-Hansen, W., Kleinsphen, K., Noettvedt, A., Rye Larsen, M., 1985. *The Tertiary strike-slip basins and orogenic belt of Spitsbergen.* In: Biddle, K.T., Christie-Blick, N. (Eds.), Strike-Slip Deformation, Basin Formation and Sedimentation, Special Publication Society of Economic Paleontologists and Mineralogists, vol. 37, 339– 359.

Storey, M., Duncan, R.A., Swisher III, C.C. 2007. *Paleocene-Eocene Thermal Maximum and the Opening of the Northeast Atlantic*. Science 316 (5824): 587. doi:10.1126/science.1135274.

Talwani, M. and Eldholm, O. 1977. *Evolution of the Norwegian- Greenland Sea* Bull. Geol. Sot. Am. 88,969-999

Thomas, E., and N. J. Shackleton 1996, *The Palaeocene-Eocene benthic foraminiferal extinction and stable isotope anomalies, in Correlation of the Early Paleogene in Northwestern Europe*, edited by R.W. O. B. Knox et al., Geol. Soc. Spec. Publ., 101, 401–441.

Thomas, D.J.; Zachos, J.C.; Bralower, T.J.; Thomas, E.; Bohaty, S. 2002. Warming the fuel for the fire: *Evidence for the thermal dissociation of methane hydrate during the Paleocene-Eocene thermal maximum*. Geology 30 (12): 1067-1070. doi:10.1130/0091-7613(2002)030.

Thorez, J 1976, *Practical identification of clay minerals*, Editions G. Lelotte, Dison (Belgique).

Throndsen, T. 1982: *Vitrinite reflectance studies of coals and dispersed organic matter in Tertiary deposits in the Adventdalen area*, Svalbard. Polar Research 2, 77-91.

Velde, B. 1995, Composition and mineralogy of clay minerals, In *Origin and mineralogy of clays* (Velde, B., Ed.) Springer-Verlag, New York, 8-42.

Worsley, D.W., Aga, O.J., 1986. *Evolution of An Arctic Archipelago*. The Geological History of Svalbard. Statoil, Stavanger. (121 pp.).

Zachos, J.C., Lohmann, K.C., Walker, J.C.G. and Wise, S.W. 1993. Abrupt climate change and transient climates during the Paleogene: A marine perspective. *Journal of Geology* 101, 191-213.

Zachos, J. C., M. Pagani, L. Sloan, E. Thomas, and K. Billups. 2001, *Trends, rhythms, and aberrations in global climate 65 Ma to Present*, Science, 292, 686–693.

Zachos, J.C., Bohaty, S.M., John, C.M., McCarren, H., Kelly, D.C. and Nielsen, T. 2007. The Palaeocene-Eocene carbon isotope excursion: constraints from individual shell planktonic foraminifer records. *Philosophical Transactions of the Royal Society a-Mathematical Physical and Engineering Sciences* 365 (1856), 1829-1842.

APPENDIX 1: LOGGING SHEET

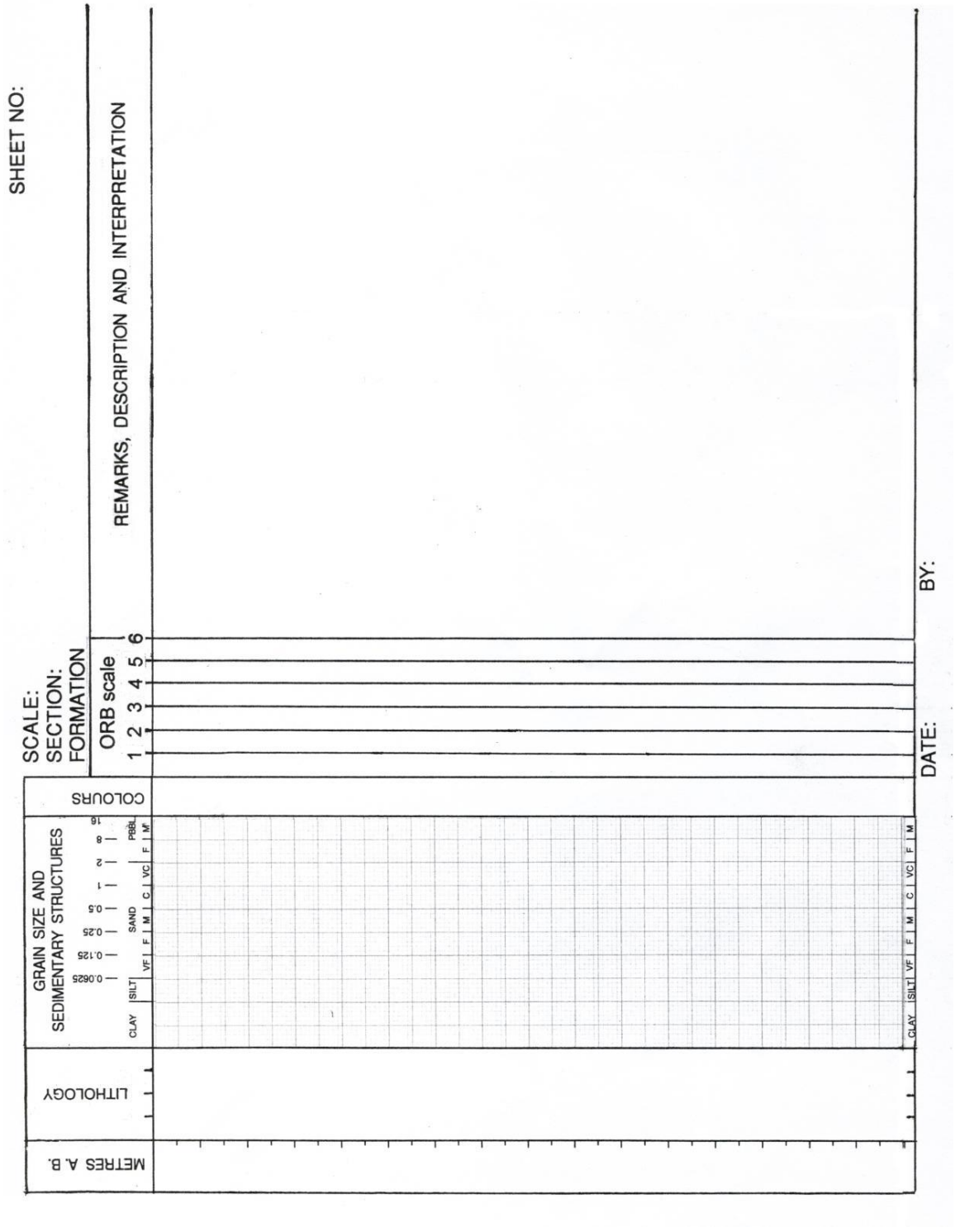

APPENDIX 2: MINERAL COUNTING (THIN SECTIONS) IN SECTION N3

Formation	Sample	Monocr. Qz	Polycr. Qz	Chert	Fds.	Muscovite	Biotite	OM	Fe Oxide	Pyrite	Clay Matrix	Chlorite	Glauconite	Forams	Total
		%	%	%	%	%	%	%	%	%	%	%	%	%	%
Grumantbyen	s1	42.5	4.75	1.25	7.25	0.00	0.00	3.50	13.00	0.00	27.75	0.00	0.00	0	100
Grumantbyen	s3	73.3	2.50	0.50	6.50	2.50	1.00	3.00	2.50	0.00	5.00	0.75	2.50	0	100
average		**57.88**	**3.63**	**0.88**	**6.88**	**2.50**	**1.00**	**3.25**	**7.75**	**0.00**	**16.38**	**0.75**	**2.50**	**0**	**100**
Marstranderbreen	s4	55.75	12.25	0.00	6.25	0.75	1.75	8.25	2.75	0.25	9.25	0.00	2.75	0	100
Marstranderbreen	s5	35.50	10.50	4.25	6.25	1.50	2.75	5.75	2.25	0.25	26.75	1.00	3.25	0	100
Marstranderbreen	s6	44.25	10.25	5.50	7.00	1.75	0.75	2.50	0.75	1.00	24.50	0.50	1.25	0	100
Marstranderbreen	s7	20.50	0.00	0.00	0.00	0.00	0.00	8.50	1.50	0.00	69.50	0.00	0.00	0	100
average		**39.00**	**11.00**	**4.88**	**6.50**	**1.33**	**1.75**	**6.25**	**1.81**	**0.50**	**32.50**	**0.75**	**2.42**	**0**	**100**
Hollendardalen	s8	31.25	6.00	5.75	7.00	0.50	1.00	3.00	0.50	0.00	45.00	0.00	0.00	0	100
Hollendardalen	s9	23.50	8.00	1.50	3.75	1.75	2.00	7.25	2.00	0.25	50.00	0.00	0.00	0	100
Hollendardalen	s10	30.50	7.75	11.50	2.75	0.00	1.50	5.25	1.25	0.75	37.25	1.50	0.00	0	100
Hollendardalen	s11	37.50	7.00	20.25	0.00	0.25	3.75	1.50	1.00	0.00	27.75	1.00	0.00	0	100
Hollendardalen	s12	38.25	5.25	13.25	1.50	0.25	1.75	4.00	1.00	0.00	34.50	0.25	0.00	0	100
Hollendardalen	s13	20.00	7.50	8.00	2.00	1.25	2.00	14.00	0.00	0.00	44.50	0.75	0.00	0	100
Hollendardalen	s15	31.25	3.25	4.25	1.00	1.00	1.75	8.25	0.25	0.25	48.50	0.25	0.00	0	100
Hollendardalen	s16	10.75	6.50	4.50	3.50	0.25	3.50	2.50	23.25	0.00	44.75	0.25	0.25	0	100
Hollendardalen	s17	43.00	9.75	8.75	2.75	0.25	0.50	3.25	0.50	0.00	30.50	0.75	0.00	0	100
Hollendardalen	s18	25.00	0.00	0.25	4.50	0.75	0.25	54.25	2.00	0.50	12.50	0.00	0.00	0	100
Hollendardalen	s19	10.00	0.00	0.00	0.00	0.00	0.00	81.50	6.00	0.00	2.50	0.00	0.00	0	100
Hollendardalen	s20	21.25	0.50	0.00	1.00	0.00	0.25	5.75	9.25	0.00	62.00	0.00	0.00	0	100
Hollendardalen	s21	32.00	7.00	3.50	0.75	0.75	3.50	3.75	8.25	0.00	39.25	1.25	0.00	0	100
average		**27.25**	**6.23**	**7.41**	**2.77**	**0.70**	**1.81**	**14.94**	**4.60**	**0.44**	**36.85**	**0.75**	**0.25**	**0**	**100**
Gilsonryggen	s24	27.00	4.00	0.00	3.50	2.50	2.00	8.25	10.50	0.00	41.75	0.00	0.50	0	100
Gilsonryggen	s28	17.50	0.25	0.00	0.50	1.50	0.00	1.50	0.00	0.00	78.25	0.00	0.00	0.5	100
average		**22.25**	**2.13**	**0.00**	**2.00**	**2.00**	**2.00**	**4.88**	**10.50**	**0.00**	**60.00**	**0.00**	**0.50**	**0.5**	**100**

Monocr. Qz. – monocrystalline quartz
Polycr. Qz – polycrystalline quartz
Fds. – feldspar
OM – organic matter
Fe Oxide – iron oxide

APPENDIX 3: MINERAL COUNTING (THIN SECTIONS) IN SECTION N1+2

Formation	Sample	Monocr. Qz	Polycr. Qz	Chert	Fds.	Muscovite	Biotite	OM	Fe Oxide	Pyrite	Clay Matrix	Chlorite	Glauconite	Forams	Total
		%	%	%	%	%	%	%	%	%	%	%	%	%	%
Grumantbyen	n1	27.75	7.50	1.00	16.00	1.50	0.00	2.00	0.00	0.50	43.50	0.00	0.00	0.3	100
Grumantbyen	n4	23.25	3.25	0.50	9.00	0.25	0.50	3.00	7.75	0.75	51.75	0.00	0.00	0	100
average		**25.50**	**5.38**	**0.75**	**12.50**	**0.88**	**0.50**	**2.50**	**7.75**	**0.63**	**47.63**	**0.00**	**0.00**	**0.3**	**100**
Mastranderbreen	n8	50.75	2.50	0.00	3.25	1.25	0.50	2.50	12.00	0.00	25.75	0.25	1.25	0	100
Mastranderbreen	n9	47.50	20.75	1.00	5.00	0.25	0.50	3.00	3.50	0.50	16.25	1.50	0.25	0	100
Mastranderbreen	n10	55.25	2.50	0.00	9.75	0.75	0.75	2.75	7.50	0.00	18.50	1.00	1.25	0	100
Mastranderbreen	n11	49.50	4.75	9.00	4.75	0.00	0.00	2.25	0.75	0.00	28.50	0.50	0.00	0	100
average		**50.75**	**7.63**	**5.00**	**5.69**	**0.75**	**0.58**	**2.63**	**5.94**	**0.50**	**22.25**	**0.81**	**0.92**	**0**	**100**
Hollendardalen	n13	36.00	10.00	3.25	1.75	0.25	2.75	2.75	3.75	0.75	38.50	0.00	0.00	0.3	100
Hollendardalen	n14	23.00	11.25	1.50	1.00	0.75	0.25	9.75	1.75	0.25	50.00	0.00	0.25	0.3	100
Hollendardalen	n15	7.25	0.00	0.00	0.25	0.25	1.25	6.75	0.00	0.00	84.00	0.25	0.00	0	100
Hollendardalen	n16	34.00	11.75	14.25	1.25	0.00	0.50	0.50	0.50	0.00	37.25	0.00	0.00	0	100
Hollendardalen	n17	41.50	12.00	11.50	2.50	0.00	0.00	1.50	0.25	0.00	30.25	0.50	0.00	0	100
average		**28.35**	**11.25**	**7.63**	**1.35**	**0.42**	**1.19**	**4.25**	**1.56**	**0.50**	**48.00**	**0.38**	**0.25**	**0.3**	**100**
Gilsonryggen	n18	12.50	10.00	1.50	1.50	0.25	1.75	3.75	0.50	0.00	67.75	0.50	0.00	0	100
Gilsonryggen	n20	16.50	0.00	0.00	0.00	0.00	0.25	11.75	1.75	0.00	68.50	1.00	0.25	0	100
Gilsonryggen	n22	23.50	0.00	0.00	0.00	0.00	0.50	8.25	1.00	2.50	64.25	0.00	0.00	0	100
average		**17.50**	**10.00**	**1.50**	**1.50**	**0.25**	**0.83**	**7.92**	**1.08**	**2.50**	**66.83**	**0.75**	**0.25**	**0**	**100**

Monocr. Qz. – monocrystalline quartz
Polycr. Qz – polycrystalline quartz
Fds. – feldspar
OM – organic matter
Fe Oxide – iron oxide

APPENDIX 4: MINERAL ESTIMATION (XRD%) FROM BULK IN SECTION N3

Mineral	Illite	Chlorite	Kaolinite	Quartz	K-Feldspar	Plagioclase	Calcite	Dolomite	Siderite	Pyrite	Sum
Sample / d-spacing	**10.0Å**	**7.0 Å**	**3.58Å**	**4.26 Å**	**3.24 Å**	**3.19 Å**	**3.03 Å**	**2.89 Å**	**2.79 Å**	**2.71 Å**	
s1	6.0	3.2	0.6	26.2	14.8	47.0	0.6	0.6	0.5	0.4	**100.0**
s2	3.7	3.3	0.8	29.6	15.4	42.7	0.7	1.7	1.0	1.0	**100.0**
s3	2.4	2.4	2.3	40.7	16.1	30.6	0.5	3.5	1.2	0.3	**100.0**
s4	6.9	6.8	1.2	31.9	14.6	36.4	0.2	1.0	0.5	0.5	**100.0**
s5	5.9	6.6	3.2	36.5	10.6	30.4	0.3	2.4	2.7	1.3	**100.0**
s6	8.1	5.6	1.7	32.8	13.7	35.5	0.5	1.1	1.0	0.0	**100.0**
s7	17.4	25.5	2.0	35.6	3.6	12.9	1.0	0.3	0.6	1.0	**100.0**
s8	17.2	18.7	5.5	39.2	4.0	11.5	1.4	1.2	0.5	0.7	**100.0**
s9	15.7	22.5	2.2	37.0	3.1	18.2	0.4	0.6	0.0	0.3	**100.0**
s10	14.1	16.7	6.7	37.6	8.5	11.5	1.3	1.0	1.3	1.2	**100.0**
s11	12.4	14.6	6.2	33.1	20.9	8.8	0.8	0.8	1.9	0.5	**100.0**
s12	16.0	25.5	9.3	31.5	5.4	10.2	0.5	0.8	0.3	0.5	**100.0**
s13	15.9	27.5	5.4	32.6	3.2	9.3	1.7	2.1	1.1	1.1	**100.0**
s15	20.2	36.2	2.0	27.7	3.3	8.0	0.5	0.8	0.8	0.5	**100.0**
s16	13.7	22.9	3.8	41.9	3.6	8.4	1.3	2.2	1.6	0.6	**100.0**
s17	13.9	26.6	6.8	35.7	3.3	8.7	0.6	0.6	3.5	0.3	**100.0**
s18	17.0	2.9	1.5	52.7	8.8	11.8	1.3	1.4	1.3	1.4	**100.0**
s19	14.4	5.7	11.3	41.9	6.5	14.4	0.7	1.4	2.2	1.4	**100.0**
s20	16.1	25.0	1.7	36.1	5.5	11.7	0.6	1.2	1.7	0.3	**100.0**
s22	19.5	11.3	13.4	37.4	3.9	12.3	0.6	0.1	1.3	0.1	**100.0**
s23	4.9	8.1	6.4	46.2	3.6	23.0	0.5	4.8	1.9	0.6	**100.0**
s24	11.8	11.1	12.1	36.1	5.3	22.2	0.4	0.3	0.3	0.4	**100.0**
s25	8.4	13.9	9.0	50.2	2.9	12.9	0.5	0.4	1.5	0.2	**100.0**
s26	7.6	8.5	5.5	49.1	3.4	19.5	0.4	0.9	3.9	1.2	**100.0**
s28	18.9	11.8	5.6	41.7	1.5	16.6	0.5	0.8	1.8	0.8	**100.0**
s29	5.1	8.8	9.7	46.0	6.8	17.5	1.0	2.0	2.4	0.7	**100.0**

APPENDIX 5: MINERAL ESTIMATION (XRD%) FROM BULK IN SECTION N1+2

Mineral	Illite	Chlorite	Kaolinite	Quartz	K-Feldspar	Plagioclase	Calcite	Dolomite	Siderite	Pyrite	Sum
Sample /d-spacing	**10.0Å**	**7.0 Å**	**3.58Å**	**4.26 Å**	**3.24 Å**	**3.19 Å**	**3.03 Å**	**2.89 Å**	**2.79 Å**	**2.71 Å**	
n1	2.4	7.2	1.1	44.5	10.7	30.3	0.7	1.7	1.0	0.3	100.0
n2	2.8	4.2	1.0	49.1	9.5	28.6	1.0	1.6	0.8	1.2	100.0
n3	6.1	6.1	1.6	49.0	8.6	25.8	0.7	1.1	0.3	0.9	100.0
n4	3.2	4.5	1.0	52.1	9.1	27.3	0.9	0.9	0.3	0.6	100.0
n5	6.2	5.2	1.2	42.2	10.1	30.4	2.3	0.9	0.5	1.0	100.0
n8	6.2	4.8	1.7	24.4	9.2	26.6	24.1	0.7	1.7	0.7	100.0
n9	8.4	7.2	1.5	29.6	13.4	36.3	0.4	1.2	1.5	0.4	100.0
n10	6.0	5.6	1.7	31.5	12.9	36.8	0.9	1.2	2.1	1.2	100.0
n11	11.4	8.8	4.4	50.3	10.3	10.8	0.7	0.9	1.7	0.8	100.0
n13	12.2	22.2	5.1	41.3	4.5	11.2	0.6	1.3	1.6	0.1	100.0
n14	15.4	31.1	2.0	32.0	4.3	12.7	0.3	0.6	1.2	0.3	100.0
n15	16.9	29.8	5.4	30.9	3.0	9.1	0.9	1.6	1.4	0.9	100.0
n16	9.3	20.8	5.4	42.8	5.4	9.9	0.7	1.4	2.9	1.4	100.0
n17	6.5	5.7	4.8	58.3	2.2	15.3	2.0	2.0	1.8	1.4	100.0
n18	11.1	9.9	8.6	44.1	4.2	18.2	0.8	0.7	1.7	0.7	100.0
n19	18.1	12.4	8.3	37.4	4.6	14.0	0.7	1.4	1.2	2.0	100.0
n21	18.7	17.4	6.3	41.6	2.6	7.9	1.3	1.5	1.1	1.5	100.0
n22	15.4	19.2	6.1	41.3	3.0	9.0	0.8	2.0	1.6	1.6	100.0
n24	11.4	8.7	3.8	40.5	4.2	15.8	0.9	0.8	1.8	12.2	100.0
n25	10.1	7.9	7.5	47.3	4.3	20.5	0.0	0.1	1.3	1.0	100.0
n26	14.3	9.5	3.2	44.5	5.3	18.4	0.8	1.1	1.6	1.4	100.0
n27	12.2	10.7	9.1	39.7	3.4	20.8	0.7	0.5	1.4	1.4	100.0
n28	17.7	8.5	7.8	36.4	4.7	20.3	0.7	0.4	2.9	0.6	100.0
n29	13.9	11.7	2.9	42.2	4.4	21.8	0.7	0.7	1.3	0.4	100.0
n30	17.7	4.7	3.2	28.4	4.3	18.9	18.8	0.6	3.1	0.3	100.0

APPENDIX 6: NATURAL GAMMA RAY VALUES (COUNTS/SECOND) IN SECTION N3

Formation / Member	Depth (m)	Natural gamma radiation (c/s)
Gilsonryggen	27	300
	27.2	320
	27.4	320
	27.6	350
	28.2	260
	28.3	260
	28.5	230
	28.7	280
	29	340
	29.2	327
	29.5	325
Hollendardalen	13.3	230
	13.6	230
	14	250
	14.9	280
	15.3	240
	15.6	250
	15.8	250
	16.4	250
	16.6	300
	17	270
	17.7	270
	17.9	265
	18.2	250
	18.7	330
	19.4	330
	19.6	310
	19.8	310
	20	300
	20.6	285
	20.8	230
	21.4	225
	21.6	270
	22.3	300
	22.8	240
	23	240
	12.3	350
	23.7	340
	23.9	310
	24.3	330
	24.6	270
	25	240
	26	310

Formation / Member	Depth (m)	Natural gamma radiation (c/s)
Marstranderbreen	4.7	270
	4.9	270
	5.3	250
	6	235
	6.4	265
	6.7	235
	7.3	235
	9.5	230
	11.9	325
	12.5	280
	12.7	250
	12.9	255
	13.1	260
Grumatbyen	0.05	280
	0.6	240
	1.1	230
	1.5	221
	2.4	260
	2.6	260
	3.2	240
	3.9	190

ACKNOWLEDGEMENTS

This Master's thesis was carried out at the Department of Geology, University of Oslo, under the kind supervision of the professors Henning Dypvik and Jenö Nagy.

First and foremost, a big thank you to Henning Dypvik, who has been more than a supervisor. Thanks for the exciting and challenging tasks, for the educational and encouraging discussions, for his really high promptitude in addressing all of my questions and problems. His thoughts, suggestions, ideas and recommendations have always been offered in a friendly and most of all a motivating manner.

I would like to also thank Jenö Nagy for the interesting and constructive discussions and for his readiness to help me at all times.

Worldwide University Networks (WUN) is acknowledged for the financial support needed in the Svalbard fieldwork. Special thanks to Tim White for the fruitful discussions during and after the field trip. Big thanks to Denise Rüther for our teamwork during the field trip and for her kindness and pleasant company.

Big thanks to Berit Løken Berg and Tulio Benites for their support in lab work, their kindness and patience.

Furthermore, I would like to express my thankfulness to all my classmates for the most enjoyable and fascinating study and work atmosphere that I ever experienced. A special thank you to my good friend and classmate Ehimen Ebohimen Williams for the nice time spent together in the Department of Geology and not only.

Mika Harju and Minttu Koskinen, my best neigbhours and friends that I ever have in Oslo, are thanked for their lovely company, positive attitude and encouragements.

Lastly, I wish to express my sincerest and most profound gratitude to my family and friends for their love and help and for always encouraging me and providing moral support throughout this thesis. Special thanks to my brother, Marius Burcă, I could have not done this Master's Program without his help.